AD-A036 402 MASSACHUSETTS INST OF TECH CAMBRIDGE GAS TURBINE LAB F/G 21/5
STUDIES ON TRANSONIC TURBINES WITH FILM-COOLED BLADES.(U)
JUN 76 H O DEMUREN, N ADAMS, F HAJJAR N00014-67-A-0204-0079
UNCLASSIFIED TR-76-1 NL

1 OF 2
ADA036402

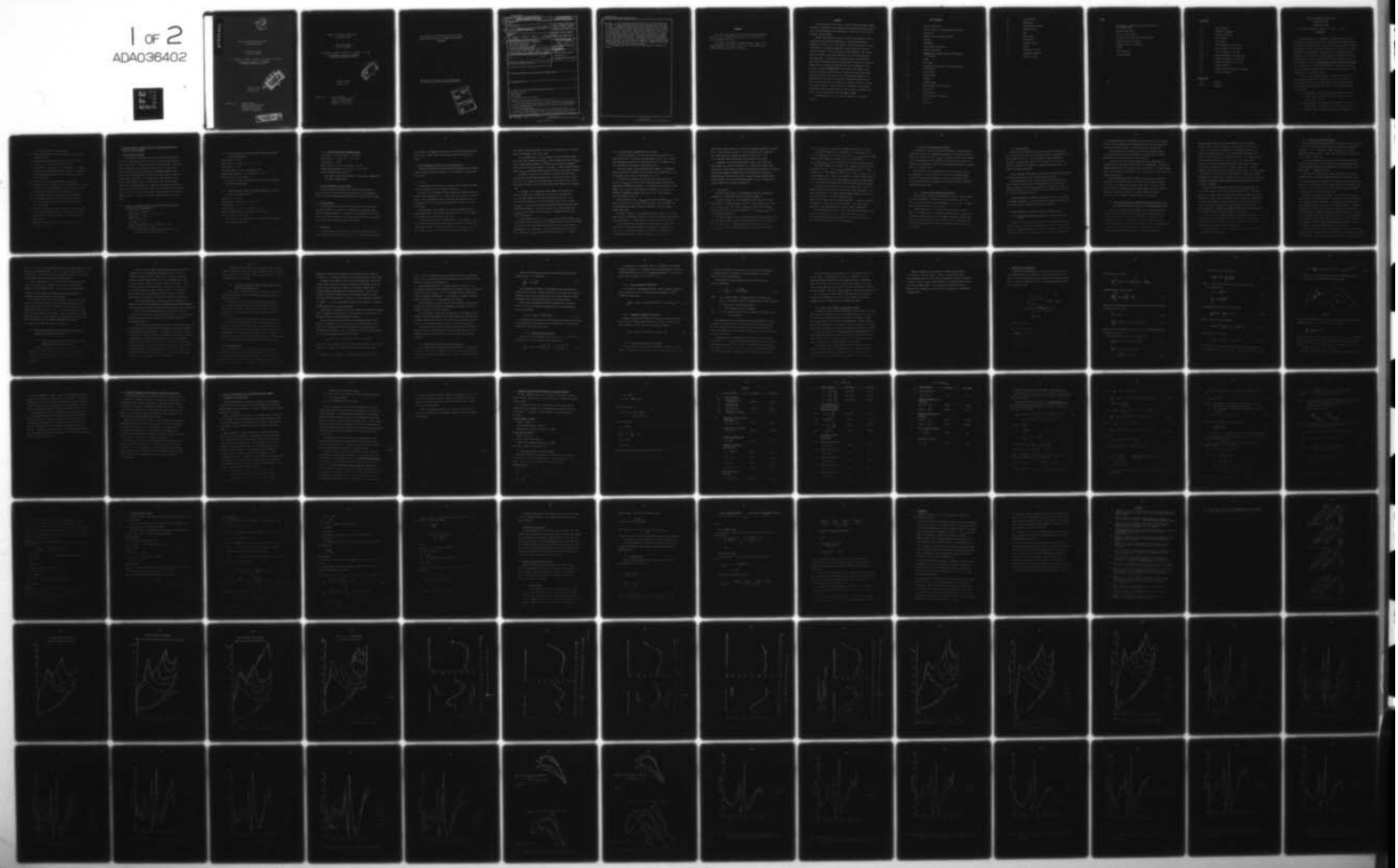

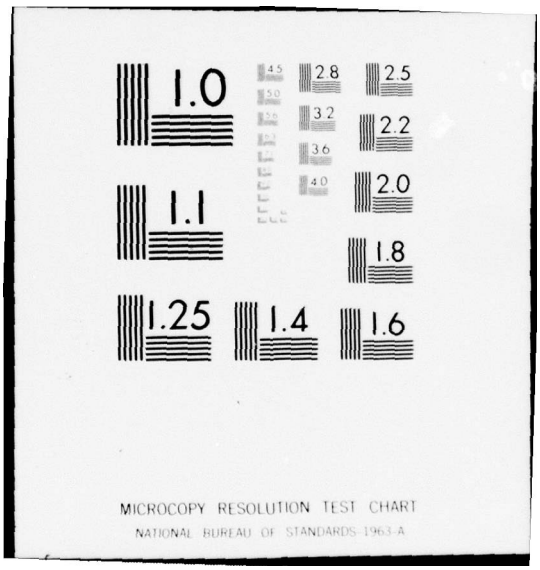
1.0
1.1
1.25
1.4
1.6
1.8
2.0
2.2
2.5
2.8
3.2
3.6
4.0
4.5
5.0
MICROCOPY RESOLUTION TEST CHART
NATIONAL BUREAU OF STANDARDS-1963-A

12

Studies on Transonic Turbines with Film-Cooled Blades

A Third Annual Report
7/1/75 - 6/30/76

H. O. Demuren, N. Adams, F. Hajjar, O. M. Amana, J. F. Louis
Massachusetts Institute of Technology
Cambridge, Massachusetts 02139

Technical Report
November 1976

Submitted to: Power Programs
Material Sciences Division
Office of Naval Research
Department of the Navy
Arlington, Virginia 22217

Studies on Transonic Turbines with Film-Cooled Blades

A Third Annual Report
7/1/75 - 6/30/76

H. O. Demuren, N. Adams, F. Hajjar, O. M. Amana, J. F. Louis

Massachusetts Institute of Technology
Cambridge, Massachusetts 02139

Technical Report
November 1976

Submitted to:

Power Programs
Material Sciences Division
Office of Naval Research
Department of the Navy
Arlington, Virginia 22217

This research was sponsored by the Office of Naval Research under Contract No. N00014-67-A-204-0079, NR 094-370

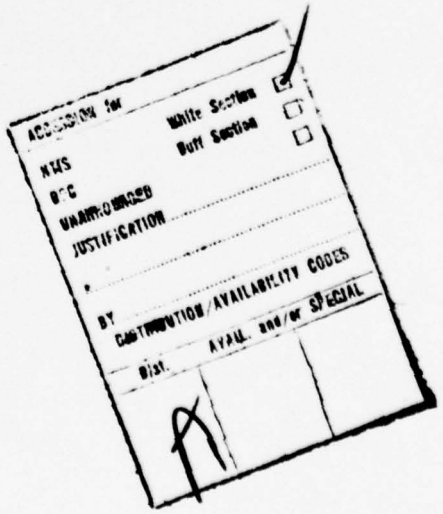

Unclassified

SECURITY CLASSIFICATION OF THIS PAGE (When Data Entered)

REPORT DOCUMENTATION PAGE

READ INSTRUCTIONS BEFORE COMPLETING FORM

1. REPORT NUMBER: TR-76-1	2. GOVT ACCESSION NO.
3. RECIPIENT'S CATALOG NUMBER	
4. TITLE (and Subtitle): Studies on Transonic Turbines with Film-Cooled Blades: A Third Annual Report	5. TYPE OF REPORT & PERIOD COVERED: Technical Report - Annual Report. 7/1/75-6/30/76.
	6. PERFORMING ORG. REPORT NUMBER
7. AUTHOR(s): H. O. Demuren, N. Adams, F. Hajjar, O. M. Amana, Jean F. Louis	8. CONTRACT OR GRANT NUMBER(s): N00014-67-A-0204-0079
9. PERFORMING ORGANIZATION NAME AND ADDRESS: Massachusetts Institute of Technology, Gas Turbine Laboratory, Cambridge, Massachusetts 02139	10. PROGRAM ELEMENT, PROJECT, TASK AREA & WORK UNIT NUMBERS: 12 109p.
11. CONTROLLING OFFICE NAME AND ADDRESS: Director, Power Programs, Material Sciences Division, Office of Naval Research, Dept. of the Navy, 800 No. Quincy St., Arlington, Virginia 22217	12. REPORT DATE: 11 June 1976
	13. NUMBER OF PAGES: 99
14. MONITORING AGENCY NAME & ADDRESS (if different from Controlling Office): 9 Annual Technical Rept. no. 3, 1 Jul 75-30 Jun 76,	15. SECURITY CLASS. (of this report): Unclassified
	15a. DECLASSIFICATION/DOWNGRADING SCHEDULE

16. DISTRIBUTION STATEMENT (of this Report)

Approved for public release; distribution limited

17. DISTRIBUTION STATEMENT (of the abstract entered in Block 20, if different from Report)

18. SUPPLEMENTARY NOTES

19. KEY WORDS (Continue on reverse side if necessary and identify by block number)

Transonic turbines
Heat transfer
Film cooling
Flow around blade trailing edge

20. ABSTRACT (Continue on reverse side if necessary and identify by block number)

In the third year of the contract, further advances were made towards the goal of gathering the heat transfer and aerodynamics flow data necessary for a good understanding of the performance of film-cooled, highly-loaded, transonic turbine blading.

The MIT cascade blowdown facility now fully operational was used in evaluating the heat transfer performance of the four blade profiles designed in the first year of the program. The results show that the level of turbulence is an important parameter in determining heat transfer in transonic

next page

DD FORM 1 JAN 73 1473 EDITION OF 1 NOV 65 IS OBSOLETE

Unclassified

SECURITY CLASSIFICATION OF THIS PAGE (When Data Entered)

145850

cont.

cascades. It also shows that the heat transfer to the trailing edge of the blades is very high being about 75% of the heat transfer to the leading edge. A comparison of the Nusselt number calculated from heat transfer measurements with the Nusselt number obtained by a prediction method using the pressure distribution shows good correspondence. The variation of average Stanton number over a range of Mach numbers shows that the reference blade has the most superior heat transfer performance. Preliminary data has been obtained on the off-design performance of the blades and full scale tests are underway. Comparative studies show that about 21% less heat needs to be taken out by internal cooling if one stage of a transonic turbine is used to replace two moderately loaded subsonic stages which produce the same output, have the same inlet stagnation conditions, have the same mass flow and the same tip speed.

This demonstrates one of the potential advantages of transonic turbines.

FOREWORD

This report was prepared by the M.I.T. Gas Turbine Laboratory under Contract No. N00014-76-C-0253 and covers the third year of activities under this contract.

The principal investigator is Professor Jean F. Louis. The contract monitor is Mr. James R. Patton, Jr., Power Program, Office of Naval Research, Department of the Navy.

ABSTRACT

In the third year of the contract, further advances were made towards the goal of gathering the heat transfer and aerodynamics flow data necessary for a good understanding of the performance of film-cooled, highly-loaded, transonic turbine blading.

The MIT cascade blowdown facility now fully operational was used in evaluating the heat transfer performance of the four blade profiles designed in the first year of the program. The results show that the level of turbulence is an important parameter in determining heat transfer in transonic cascades. It also shows that the heat transfer to the trailing edge of the blades is very high being about 75% of the heat transfer to the leading edge. A comparison of the Nusselt number calculated from heat transfer measurements with the Nusselt number obtained by a prediction method using the pressure distribution shows good correspondence. The variation of average Stanton number over a range of Mach numbers shows that the reference blade has the most superior heat transfer performance. Preliminary data has been obtained on the off-design performance of the blades and full scale tests are underway. Comparative studies show that about 21% less heat needs to be taken out by internal cooling if one stage of a transonic turbine is used to replace two moderately loaded subsonic stages which produce the same output, have the same inlet stagnation conditions, have the same mass flow and the same tip speed.

This demonstrates one of the potential advantages of transonic turbines.

LIST OF SYMBOLS

A	Cross sectional area
a	Ratio of coolant to mainstream mass flow rates
c	Blade chord
C_p	Specific heat at constant pressure
d	Diameter
g	Blade space
h	Heat Transfer Coefficient
k	Thermal Conductivity
k_o	Momentum ratio between coolant and mainstream $(\rho u^2)_c/(\rho u^2)_h$
	Length
M	Mach number
m	Mass flux ratio between coolant and mainstream $(\rho u)_e/(\rho u)_g$
$\dot{m}$	Mass flow rate
Nu	Nusselt number
P	Pressure
Pr	Prandtle number
$\dot{q}''$	Heat transfer rate per unit area
R	Gas coolant
Re	Reynolds number
Re_{xtr}	Reynolds number at transition
S	Entropy
s	Blade pitch

St	Stanton number
T	Temperature
te	Trailing edge thickness
Tu	Turbulence level
t	Time
U	Blade speed
V	Flow velocity
W	Relative velocity
w	Losses
x	Coordinate direction
y	Coordinate direction
z	Number of blades

Greek

α	Blade angles in absolute coordinate in relation to to axial direction
β	Relative blade angles
γ	Ratio of specific heats
η	Efficiency (also film cooling effectiveness)
μ	Dynamic viscosity coefficient
ν	Kinematic viscosity coefficient
ρ	density
ϕ	Flow coefficient
ψ	Load coefficient

Subscripts

$( )_x$	Axial component
$( )_\theta$	Tangential component
$( )_o$	Stagnation parameter
$( )_w$	Wall parameter
$( )_g$	Gas parameter
$( )_1$	Static parameter at nozzle inlet
$( )_2$	Static parameter at rotor inlet
$( )_3$	Static parameter at rotor exit
$( )_{01}$	Stagnation parameter at nozzle inlet
$( )_{02}$	Stagnation parameter at rotor inlet
$( )_{03}$	Stagnation parameter at rotor exit
$( )_e$	Coolant parameter
$( )_d$	Parameter based on leading edge diameter
$( )_{is}$	Isentropic condition

Superscripts

$( )^{ab}$	Absolute
$( )^{rel}$	relative

STUDIES ON TRANSONIC TURBINES WITH FILM-COOLED BLADES

A THIRD ANNUAL REPORT

H. O. Demuren, N. Adams, F. Hajjar, O. M. Amana, J. F. Louis

Introduction

The increasing interest in Transonic turbines shown over the last few years is a reflection of the need to increase the work output obtained per unit of cooled-blade surface. Much of the increase in turbine efficiency obtained over the last two decades has been due to our ability to increase the turbine inlet temperature through the use of more efficient cooling techniques. As more and more coolant mass flow is obtained from the compressor, however, a point is reached when the losses introduced by the use of coolant mass flow more than offset the increase in efficiency attainable by an increase in the turbine inlet temperature. At this point, the need arises to optimize the work output per unit of cooled-blade surface. This requires the use of transonic blading.

The goal of these studies has been to gather the necessary heat transfer and aerodynamic data which would be of use to the designer of high performance, film-cooled, highly-loaded transonic turbine blading. In the first and second years of the contract, the following key tasks were performed:

(a) The gathering of the film cooling effectiveness data in the transonic range $1.5<M<1.4$ using the shock tunnel for both slot and holes injection.

(b) The gathering of heat transfer and aerodynamics data at the trailing edge of a transonic blade, and the use of this data to formulate a model for the heat transfer and aerodynamic flow

at the trailing edge of transonic blades.

(c) The design, manufacture and commissioning of the MIT cascade blowdown facility.

(d) The design and aerodynamic testing of four transonic blade profiles in a conventional wind tunnel at VKI.

(e) An estimation of the coolant flow requirements of a transonic turbine and a comparison between the coolant flow requirements of the transonic turbine with that of a subsonic turbine of equal work output.

In the third year, the following tasks were accomplished:

(1) Aerodynamic and heat transfer tests were performed for the four transonic blade profiles designed in the first contract year, at zero angle of incidence in the blowdown facility.

(2) The instrumentation in the blowdown facility was updated.

(3) A preliminary evaluation of the off-design performance of the reference blade profile has been carried out and full tests are underway.

(4) The design and manufacture of the equipment for the experiment to measure the effects of periodic unsteadiness on the aerodynamic and heat transfer performance of turbine blades has been completed.

(5) Comparative studies between Transonic and Subsonic Turbines have been carried out.

I. AERODYNAMIC AND HEAT TRANSFER TESTING OF THE FOUR TRANSONIC BLADE PROFILES AT ZERO INCIDENCE

1.1 Blade and Cascade Geometry

The conventional transonic blade profile is usually designed with a straight suction surface with the throat at the trailing edge [11], as shown in Figure 1(a). This was chosen as the reference blade. The other three blade profiles are variations of this profile to a large extent. Thus, the blade shown in Figure 1(b) has an unguided expansion on the suction side. The expansion fan, which is developed, helps to weaken the trailing edge shock system. As a result of the added expansion, the trailing edge dimension comes out smaller than that of the reference blade; and so it became necessary to design the blade shown in Figure 1(c), which has the same profile as the reference blade, but with a thin trailing edge. The last profile Figure 1(d) shows a longer blade with a convergent-divergent nozzle. A summary of the blade and cascade geometry is given below.

1.1.1 Reference Convergent Transonic Blade with Straight Suction Back and Thick Trailing Edge (Blade 1)

Blade chord c = 66.0 mm
Blade spacing g = 49.5, i.e., g/c = 0.75
Stagger angle γ = 51°
Inlet flow angle β_1 = 60°
Exit angle β_2 = 25°
Trailing-edge thickness te = 2.8 mm, te/c - 0.0424
Number of blades in the cascade = 6
with Blade 3 suction side and Blade 4 pressure side instrumented with static-pressure taps.

1.1.2 Wholly Convergent Blade with Straight Suction Back but Thin Trailing Edge (Blade 2)

Blade chord c = 64.2 mm

Blade spacing g = 48.15 mm, i.e., g/c = 0.75

Stagger angle γ = 51°

Inlet flow angle β_1 = 60°, exit angle β_2 = 25°

Trailing-edge thickness, te = 1.3 mm, te/c = 0.02025

Number of blades in the cascade = 6

with Blade 3 suction side and Blade 4 pressure side instrumented with static-pressure taps.

1.1.3 Transonic Turbine Blade with Unguided Expansion on the Suction Side (Plug Nozzle) (Blade 3)

Blade chord c = 66.0 mm

Blade spacing g = 49.5 mm, i.e., c/g = 0.75

Stagger angle γ = 51°

Inlet flow angle β_1 = 60°, exit angle β_2 = 25°

Trailing-edge thickness, te = 1.46 mm, te/c = 0.0221

Number of blades in the cascade = 6

with Blade 3 suction side and Blade 4 pressure side instrumented with static-pressure taps.

1.1.4 Blade With Convergent-Divergent Channel

Blade chord c = 76.0 mm; Throat O = 18.30 mm

Blade spacing g = 49.6 mm, i.e., g/c = 0.64

Stagger angle γ = 46.5°

Inlet flow angle β_1 = 60°, Exit angle β_2 = 25°

Trailing-edge thickness, te = 1.14, i.e., te/c = 0.015

Number of blades in the cascade = 6

with Blade 3 suction side and Blade 4 pressure side instrumented with static pressure taps.

1.2 Blade Instrumentation for VKI tunnel:

The blade velocity distribution was measured at the mid-span by pressure taps on the pressure side and suction side of two neighboring blades such that the instrumented blade surfaces formed the blade passage.

1.3 Inlet Flow Field

The Mach number distribution at the cascade inlet was derived from wall static pressure in a plane "0.1c" ahead of the leading-edge plane. Inlet Mach number variation as a function of exit Mach number was measured and the inlet-angle variation in the transverse direction was also measured. No influence on the outlet Mach number was observed.

1.4 Cascade Flow

The blade velocity is expressed by the local Mach number calculated from the local static pressure on the blade and the total pressure upstream

of the cascade. Measurements were taken on the suction and pressure sides of the blade. The Mach number distributions are plotted in Figures 2 through 5.

1.5 Blade Performance as measured in the VKI Wind Tunnel:

The blade performance was evaluated from the downstream wake traverses behind the blades at an axial distance of "0.3c" behind the trailing edge in all cases.

1.5.1 Losses

The variation of blade losses as a function of the outlet Mach number for all the blades is plotted in Figures 6 through 9.

For Blade 1, the convergent reference blade with straight suction back, for exit Mach number up to M_2 = 0.7 blade losses, ran up to 8%. This high level of loss was apparently caused by trailing edge thickness (te/c = 4% as compared to te/c = 2.025% in the second blade, and te/c = 2.2% in the third blade).

Local supersonic zones, lambda ("λ") shocks and diffusion losses cause a sudden rise in the level of the losses from $M_2 > 0.7$ with maximum loss of about 11% occurring at about M_2 = 0.85.

The decrease in the level of losses from M_2 = 0.85 to around $M_{2\ design}$ = 1.3 is linked with the fact that the shocks became more oblique and flow reattachment occurred. The new increase of ω for $M_2 > M_{2\ design}$ up to the limit loading M_{2limit} = 1.59, is due to the increasing strength of the

left-running trailing edge shock which caused the boundary layer to separate without reattachment on the suction side.

Losses recorded for $M_2 > M_{2\ limit}$ depend on the total pressure losses due to the blade boundary layer $(\Delta P_0)_{B.L.}$, the trailing-edge shocks $(\Delta P_0)_{shock}$, and the mixing process between the trailing edge plane and the measuring plane as well as the outlet velocity. The $(\Delta P_0)_{B.L.}$ remains roughly constant, while $(\Delta P_0)_{shock}$ and mixing losses increase as the exit Mach number increases.

For Blade 2, (Figure 7), the convergent blade with straight suction back and thin trailing-edge thickness (te/c = 2.025%) for exit Mach number up to M_2 = 0.75, losses were decreasing until they reached a value of 4.7%. This again is probably due to flow acceleration and thinning of the boundary layer.

As in Blade 1, local supersonic zones, lambda ("λ") shocks, and diffusion losses cause a sudden rise in the level of the losses for $M_2 > 0.75$ with maximum loss of about 6% occurring at about M_2 = 0.95. The losses then decrease as in the first blade from M_2 = 0.95 to around $M_{2\ design}$ = 1.3 as the shock becomes oblique and possible flow reattachment occurs after separation. The pattern in which the losses decrease from $M_{2\ design}$ is very similar to that of Blade 1 (straight suction back with thick trailing edge).

The new increase in ω for $M_2 > M_{2\ design}$ up to the limit-loading $M_{2\ limit}$ is due both to mixing losses and to the increasing strength of the left-running trailing edge shock, which causes the boundary layer to separate without reattachment on the suction side. The very sharp increase in the level of the losses after $M_{2\ design}$ is similar to that of Blade 1; at around

M_2 = 1.5 each reaching a comparable level of losses.

For Blade 3 (Figure 8), the plug nozzle blade with expansion on the suction side (te/c = 2.21%), for exit Mach numbers up to M_2 = 0.7, losses were decreasing and reached their minimum value of 5.5%, probably due to flow acceleration and thinning of the boundary layer.

As in other blades, local supersonic zones, lambda ("λ") shocks and flow diffusion cause a sudden rise in the level of the losses for $M_2 > 0.7$, with maximum loss of about 7.5% occurring at M_2 = 0.9.

The losses then decrease as in the first and second blades from M_2 = 0.9 to $M_{2design}$ = 1.3 as the shock becomes oblique and possible flow reattachment occurs after separation. The decrease is fairly sharp, unlike Blades 1 and 2, and the losses flatten out between M_2 = 1.2 and M_2 = 1.4 providing a reasonable operating zone with (ω = 5%). This region of loss lies between 5% and 5.3%.

Losses increase for $M_2 > M_{2design}$ up to the limit-loading M_{2limit} = 1.67, but not as steep as in the first and second blades. This is probably due to the comparatively smaller increase of strength of the left-running trailing edge shock.

For Blade 4 (Figure 9), the convergent-divergent blade, (te/c = 1.5%), losses were first decreasing apparently due to flow acceleration and thinning of the boundary layer. Losses reached a low value of 6.5% at M_2 = 0.75

As the pressure ratio increased, local sonic bubbles, lambda ("λ") shocks, and flow diffusion increased the loss level to a maximum of 8.25% at M_2 = 0.86. Losses then decreased, as in Blades 1, 2 and 3, but at a very sharp rate (from M_2 = 0.86 to around $M_{2design}$ = 1.3) as the

shock became oblique (weaker), and as flow reattachment occurred after separation. A very low level of losses, 3.5%, was recorded at the design exit Mach number region and remained low (below 4% between M_2 = 1.2 to 1.5), providing a good working range of low-loss exit Mach number.

A comparison of the loss curves (Figure 4.19a) shows clearly that each profile has a superior performance in a different Mach number range and presents a unique potential when cooling problems and problems of structural integrity are carefully examined along with optimization of efficiency. Remembering also that lower blade chord c means increased secondary losses tends to suggest a more broadly based assessment of losses to determine an optimum profile for a particular application.

1.5.2 Outlet Angles

The outlet angles shown on the performance curves were measured with reference to the tangential direction (Figures 6 through 9).

For Blade 1 (Figure 6), the convergent reference blade with straight suction back, β_2 decreased slightly from 25.5° to 24° between M_2 = 0.6 and M_2 = 1.3 ($\beta_{2\ design}$ = 25°). For $M_2 > M_{2design}$, the exit angle increases slowly up to M_2 = 1.4 in a linear fashion. At $M_2 = M_{2limit\ loading}$ = 1.59, the deviation was about 10°.

For Blade 2 (Figure 7), the convergent blade with straight suction back but thin trailing edge, β_2 decreased slightly from 25.5° to 23.5° between M_2 = 0.5 and M_2 = 1.1. A gradual increase was noticed from M_2 = 1.1 to $M_{2\ design}$ = 1.3 when β_2 increased back to 25°, the design exit angle.

For $M_2 > M_{2\ design}$, the exit angle increased very sharply as in Blade 1.

For Blade 3 (Figure 8), the plug nozzle, β_2 decreased from 28° to $\beta_2 = 24.5°$ between $M_2 = 0.6$ and $M_2 = 1.3$. For $M_2 > M_{2\ design}$, the exit angle increased very sharply as in Blades 1 and 2 in a linear form. At $M_2 = M_{2\ limit\ loading} = 1.67$ the deviation of about 10° was again recorded.

For Blade 4 (Figure 9), the exit angle β_2 changes very little for all the ranges of the M_2 up to $M_{2\ design}$, fluctuating by about 0.5° from a mean of 24.5°. (The design exit angle is 25°.) After $M_{2\ design}$ (M = 1.3), a sharp increase in the value of the deviation is noticed, already amounting to a 2° deviation at $M_2 = 1.47$, which suggests a possible large deviation of the exit angle at higher exit Mach numbers similar to the other blades.

As shown in Figure 10, there are noticeable differences in the exit angle behavior for each blade in the Mach number range investigated. The striking difference is the rather large deviation in Blade 3, close to 3°, at low Mach numbers. This is not surprising since Blade 3 is the plug nozzle with unguided expansion. At these low subsonic Mach numbers it acts as an inefficient diffuser. This deviation then disappears as the design supersonic exit Mach number is approached.

Another striking point is that a very sharp and high deviation is noted in all the cases at $M_2 > 1.4$, i.e., just a little over $M_{2\ design}$. This is associated with the over-expansion at the trailing edge corner and the effect is even seen on the wake inclination.

1.5.3 Effect of Reynolds Number Variation

In addition to the normal test series performed at Reynolds numbers between 10^5 and 10^6, the reference blade (Blade 1) was tested at constant inlet total pressure of $P_{01} = P_{atmisp} + 1000$ mmHg, constant Reynolds number of 10^6 (corresponding to the highest total pressure for the highest Mach number in the normal test series), while the downstream pressure was varied with a back pressure valve.

The results of these tests showed that the Reynolds number effect was negligible in the test range of 10^5 to 10^6. No noticeable change was seen on the pressure distribution. Both the peak position and its value remained practically unchanged, and the pattern of the shock-system remained exactly the same.

1.5.4 Effect of Blade Solidity on Performance

Tests were also carried out to determine the effect of stage solidity on cascade performance. Reference Blade 1 was tested at $g/c = 0.81$ and $g/c = 0.695$ (former tests were conducted at $g/c = 0.75$). In addition Blade 3 (plug) was tested at $g/c = 0.695$.

Careful examination of the blade velocity distribution (compare Figure 2 and Figure 11) and the schlieren photographs show a change in the locations and inclinations of the left-running shocks for the same values of M_{ts}. Also, as the blade spacing increased, the shock got weaker and some flow separations resulting in the shock-boundary-layer interactions were avoided.

1.5.5 Downstream Wake

Analysis of the downstream wake using the downstream traverse taken at 0.3c behind the blades and schlieren photos shows an interesting effect of Mach number on the wake. As M_2 increases the flow nonuniformity increases. A characteristic effect is the increase in the wake depth during the transition from subsonic to supersonic exit Mach number. The width of the wake changes also.

For the different blade profiles, the effect of trailing edge thickness can also be seen clearly in the relative width of the wake.

Careful examination of the schlieren photos of the wake flow shows that it consists, under certain flow conditions, of von Karman vortex streaks. Because of the long exposure time of the camera, an estimate of the shedding frequency of the vortices can not be made from the evaluation of the present schlieren pictures.

Further experiments are planned in conjunction with VKI to determine the shedding frequencies by directly measuring the pulsating wake pressure with a high-frequency-response Kulite pressure transducer.

1.6 Cascade Performance as measured in the MIT Blowdown Facility:

1.6.1 Blade Pressure Distribution as Measured in the MIT Blowdown Facility

Plots of the blade pressure (Mach number) distributions are shown in Figures 12 and 13. A very fast expansion takes place on the suction side with the Mach number reaching its first peak, at a location where the first surface roughness (bump) is located on the blade. The flow decelerates

a bit and quickly starts to accelerate again, until it hits the left-running shock, from the neighboring blade, downstream of which the flow decelerates and later accelerates towards the trailing edge on the suction side.

As the pressure ratio increases, the shock moves downwards towards the blade trailing edge and this represents a typical pattern of pressure distribution on the suction side for all the blades.

On the pressure side, a rapid acceleration occurs downstream of the stagnation point, then quickly stops close to the leading edge. The flow then gradually accelerates to its maximum value, which occurs at the blade trailing edge. Once the flow is choked there is very little change in the pressure side pressure distribution.

All the blade profiles tested featured the same typical variation in Mach number (pressure) distribution, differing only in absolute values of the peaks due to strength and locations of the shocks hitting the suction sides. Since all the blades showed the same tendency to peak at nearly the same place on the suction surface, it would seem logical to attribute this peak to the geometry (large curvature) of the blade.

1.6.2 Comparison Between Blade Pressure Distributions Obtained at the MIT Blowdown Cascade Facility and the VKI High Speed Wind Tunnel

A detailed comparison was made between the Mach number distribution around the blade obtained in the MIT hot blowdown cascade facility with that obtained in the VKI high speed windtunnel (see Figures 2 through 5 and Figures 12 and 13). On the whole, the overall pattern of the Mach number distribution was similar. Fast acceleration from the stagnation point the suction side leads to the first peak of Mach number. But the location and absolute value (magnitude) of the peak was different.

The peak shifted forward in the tests conducted on the hot blowdown cascade facility. There are several possible reasons for this. First, it must be recalled that the experiment in the windtunnel at VKI was a cold flow investigation (T_g/T_b = 1) with a low level of turbulence 0.7%. whereas experiments on the MIT cascade facility were hot flow experiments (inlet stagnation temperature of 450°K, T_g/T_b = 1.5), with a high turbulence level (10%). Schlieren photos taken at VKI showed a distinct region with a separation bubble on the blade suction side. A combined effect of large blade curvature and surface roughness (bump) could have triggered this separation while the distinct region served to generate the necessary turbulence in the shear layer to reattach the flow. Also, the high freestream turbulence could allow a quick turbulent flow reattachment and thus create an earlier transition.

Another possible reason could be that there are fewer pressure taps on the blade tested at the MIT hot blowdown cascade facility. There were twenty five pressure taps and twenty five heat transfer gauges evenly distributed all around a single instrumented blade as compared to instrumenting two blades (that formed the central channel) with thirty six pressure taps on the suction side and twenty two on the pressure side in the tests in the VKI windtunnel. Thus at MIT, pressure taps were not as closely located and the exact location of the peak could have been missed.

But on the whole the overall pattern of the pressure distribution was the same. The correct peaks of the Mach number before, at and after the shock could not be exactly located but the distribution still shows the existence and movement of the shocks correctly.

A good agreement is seen on the pressure side with gradual Mach number increase up to the trailing edge.

1.6.3 Blade Heat Transfer Distribution

The blade heat transfer distributions are plotted in Figures 14 through 19. Plots of the local Nusselt number Nu as a function of the relative coordinate $\bar{X} = X/c$; and plots of $Nu/Re^{0.8}$ versus $\bar{X}$ are all shown. (Additional curves of $Nu/Re^{0.5}$ versus $\bar{X}$ and $Nu/Re^{0.66}$ versus $\bar{X}$ were drawn for the blades. (Figure 20.)

To aid the understanding of the curves for heat transfer and static pressure distributions, a typical pattern of heat transfer and of dimensionless pressure coefficient have been drawn on polar diagrams around the blade surface (Figures 21 and 22).

On the whole the external flow pressure distribution and level of turbulence have, as expected, greatly influenced the boundary layer flow which in turn practically dictates the heat transfer structure on the blade surface. It is remarkable to see a similar effect of shock boundary layer interaction on both the pressure and heat transfer distributions around the blade, may be seen in these figures also.

Generally the pattern is as follows. On the suction side from the leading edge, the pressure distribution indicates a very fast acceleration to a minimum pressure, a condition very favorable for the formation of a laminar boundary layer, and thus the Nusselt number decreases. Transition from laminar to turbulent flow then caused a jump in the Nusselt number. The Nusselt number thereafter fluctuates up and down similar to the behavior of the pressure distribution in this area, until it hits the left-running shock coming from the trailing edge of the neighboring blade. Downstream of the shock, the Nusselt number drops significantly and later starts to increase as the flow accelerates toward the trailing edge.

On the pressure side, from the leading edge the pressure distribution indicates again a rapid acceleration conducive to the maintenance of a laminar boundary layer, and as a result, the Nusselt number falls. Transition occurs

at s/c = 0.3, and the Nusselt number increases all the way towards the trailing edge due to the rapid decrease in pressure up to the trailing edge on the pressure side. This increase in the Nusselt number is caused by the thinning of the boundary layer due to favorable pressure gradient.

It must be mentioned that a high level of heat transfer was recorded close to the trailing edge, amounting to about 75% of the mean value measured at the leading-edge region. It was also noticed that zones with variation in heat transfer rate generally coincide with zones with variation in pressure distribution (Mach number).

In all cases, straight lines have been used to connect all the data points. Because of the relative distances between the data points, the true picture of the heat transfer distribution, in particular the exact values and locations of the peak, may not be exactly the same as shown. The heat transfer gauge (3/32" diameter) itself is averaging over a certain area, across which the Nusselt number could have varied very significantly. Thus the so-called local heat transfer distribution is in fact an average over a certain small area in that region.

1.6.4 Comparison Between Experimental Heat Transfer Data and an Available NASA Theoretical Prediction

1.6.4.1 Theoretical Prediction Based on Hot Blowdown Cascade Blade Pressure Distribution (as Input)

A comparison between the experimental results and values obtained by available theoretical method is shown in Figures 23 through 28. A modified NASA Compressible Laminar and Turbulent Boundary Layer Program [1] is used to predict the heat transfer distribution.

As input into the program, the experimental pressure distribution obtained from the hot blowdown cascade tests was used. The curves (Figures 23 through 28) did not agree point by point but on the whole the general pattern was the same, and it was an agreement good enough for such a complex quantity as the heat transfer coefficient. There are obvious reasons for the differences in the curves. Surface curvature, surface roughness, initial turbulence level of the freestream and shock boundary layer interactions are not taken into account in NASA program except insofar as they affect the pressure distribution.

On the experimental side, the physical size of the gauge (3/32" diameter x 0.020" thick aluminum discs) necessitates an average measurement over a certain surface area, across which the heat transfer could have varied.

The most obvious discrepancy between the two results occurred as a result of two different locations for the transition point. The experimental data showed an earlier transition to turbulent flow than the theoretical prediction.

There are several possible reasons for this. The theoretical prediction, as mentioned earlier, does not take into account the freestream turbulence, and also assumes an adiabatic wall. The experiment on the other hand has a high level of freestream turbulence which tends to destabilize the laminar boundary layer and forces an early transition, while the heat transfer across the boundary layer to the blade acts at the same time to stabilize the boundary layer by dissipating the energy of turbulence. This will tend to delay transition. The net effect when coupled with the effect of the blade surface roughness (the blades in fact do have bumps in this region of interest) could have caused the early transition.

On the pressure side however, the experimental data on the heat transfer suggests that instead of having a transition point, a transition region could in fact have existed, This is possible under the favorable pressure gradient in this region.

1.6.4.2 Theoretical Prediction Using VKI Wind Tunnel Cold Flow Blade Pressure Distribution

Another series of theoretical predictions were done, this time using the experimental pressure distribution obtained from cold flow VKI wind tunnel tests.

The three curves of heat transfer distribution (experimental data, theoretical prediction based on the high turbulence hot flow blade pressure distribution, and theoretical prediction using the low turbulence cold flow pressure distribution) are shown in Figures 29 through 31.

The prediction based on low turbulence cold flow is very similar to that based on high-turbulence, hot-flow except for the location of the suction side transition point. There are also differences in the absolute value and location of peaks but apart form this, there is very good agreement. The low-turbulence, cold-flow has the most delayed transition as expected. This is definitely the effect of the difference in the freestream turbulence on the transition of the boundary layer.

1.6.5 Transition Point

Several investigations [2, 3, 4 and 5] have shown that the main flow level of turbulence exerts considerable influence on the stability of a laminar boundary layer and on heat transfer. Effect of turbulence on losses in turbine cascades is shown in the structure of the boundary layer. Friction losses and intensity of heat exchange can alter markedly, of course,

depending on whether the flow regime in the boundary layer is laminar or turbulent. It is therefore essential to know the true location of transition.

Normally, in the absence of high scale surface roughness, flow in the boundary layer changes from laminar to turbulent either through instability resulting from the growth in thickness of the laminar boundary layer or through turbulent reattachment after laminar separation. Studies on the behavior of turbulent boundary layers in accelerating flows [6, 7] have shown that when the acceleration is severe enough and acceleration parameter $K = \frac{\partial}{U_e^2}\frac{dU_e}{dx} > 3 \times 10^{-6}$, the originally turbulent layer undergoes a reversion towards laminar just as in this experiment.

Unfortunately, quantitative data on the influence of freestream turbulence level on transition, heat transfer [2, 3] and losses are scanty and the few references that are available substantially differ.

Zysina-Molozhen [4] and others have been studying the effect of turbulence on transition in the boundary layer of gas turbine blades. They came up with an empirical formula for calculating the Reynolds number at the beginning of transition R_{extr}, as a function of the level of turbulence T_u, wall to gas temperature ratio and Mach number:

$$R_{extr} = 0.71 \times 10 \ (1 + 3M_0^{1.7}) \ T_u^{-1.76} \ \psi^{-2.3}(1 + 38M_1^{0.6})$$

where M_1 is the Mach number of the flow at the maximum velocity region before transition; M_0 is the Mach number of the flow at cascade inlet; and $\psi = T_w/T_g$.

Plotting R_{extr} [4] versus T_u (turbulence level) for typical values

of M_1 M_0 and ψ has shown that R_{extr} decreases rapidly when T_u increases from 1.5% to 3%, indicating that the transition point moves forward and then remains at a relatively fixed position.

Zysina-Molozhen and Kunst [4] noticed, however, that for $T_u > 4.5\%$, the dependence alters and some stabilization is observed in R_{extr}, which having reached the value of $R_{extr} = 1.2 \times 10^5$, noticeably ceases to decline with a further increase in turbulence. It is as though it reaches the maximum possible displacement of the transitional point upstream.

But the quantity R_{extr} cannot truly be a good measure of the transition point since it takes no account of acceleration of the flow. Re_θ would probably have been a much better measure.

In the experiment, transition is controlled by the streamwise pressure history (turbulent reattachment after laminar separation). The rapid rise in Nusselt number which occurs at $x/c = 0.20$ on the suction surface and $x/c = 0.35$ on the pressure surface is taken as evidence of transition.

Knowing the exact location of transition and forcing the theoretical program to start to calculate turbulent boundary layer from there would probably greatly improve the quality of the theoretical heat transfer prediction.

1.6.6 Heat Transfer at the Blade Leading Edge Region

It has been shown by numerous investigators that with increasing flow turbulence, heat transfer is intensified over the entire leading surfaces of cylinders or spheres, particularly in the vicinity of the frontal stagnation point.

Kestin [2] and others have correlated heat transfer in the frontal stagnation point of a cylinder as

$$\frac{Nu}{\sqrt{Re}} = f(T_u \sqrt{Re}) \tag{1.1}$$

This relationship is based on the assumption that heat transfer is intensified in this case by eddies generated in the boundary layer near the stagnation point by flow turbulence, with the distance between the eddies (wavelength) being inversely proportional to the Reynolds number.

Dyban et al. [8] suggest from general consideration of similarity theory, the use of the turbulent Reynolds number ($T_u \cdot Re$) and correlate data by the expression

$$Nu_{T_u} = \varepsilon_{T_u} Nu_{T_u=0} = f(Re_{T_u}) Nu_{T_u=0} \tag{1.2}$$

A comparison is made between the experimental heat transfer data obtained at the leading edge with predictions based on empirical and semi-empirical formulation of other works listed below.

1.6.6.1 Kestin and Wood Correlation

Kestin and Wood [2] formulated that in the range $0 < (T_u \, Re^{1/2}) < 40$, heat transfer at the leading edge could be expressed as

$$\frac{Nu}{Re^{0.5}} = 0.945 + 3.48 \left(\frac{T_u \cdot Re^{1/2}}{100} \right) - 3.99 \left(\frac{T_u \cdot Re^{1/2}}{100} \right)^2 \tag{1.3}$$

In Equation (3) the turbulence level T_u is expressed as an absolute fraction (as opposed to a percentage), and the Reynolds number is based on leading-edge diameter and inlet flow stagnation parameters. All the tests were carried out between $16.3 \leq T_u \cdot Re^{1/2} < 27.6$.

1.6.6.2 Smith and Kuethe's Correlation

On the basis of a semi-empirical theory, Smith and Kuethe [9] were the first to suggest the use of a single correlation parameter $T_u \cdot Re^{1/2}$. According to their theory

$$\frac{Nu}{Re^{1/2}} = 0.3762 + 0.0138\ T_u(Re\times10^{-3})^{1/2} - 1.32\cdot10^{-6}(T_u \cdot Re^{1/2})^2 \qquad (1.4)$$

1.6.6.3 Mujumdar and Douglas's Correlation

Mujumdar and Douglas [10] observed that a better correlation could be made in terms of turbulent Reynolds number, $Re_T(=T_u \cdot Re)$, instead of the single parameter $T_u \cdot Re^{1/2}$, and gave the following correlation

$$\frac{Nu}{Re^{1/2}} = 0.981 + 1.017\cdot10^{-4}\ Re_T + 2.74\times10^{-9}\ Re_T^2 \qquad (1.5)$$

1.6.6.4 Dyban, Epik and Kozlova's Correlation

Judging from the results of their wide range of experimental investigations on heat transfer in the vicinity of the front stagnation point of

a cylinder in traverse flow, Dyban et al. [8] concluded that freestream turbulence affects heat transfer in that critical point in the same manner as does the Reynolds number.

Using turbulent Reynolds number $T_u' \cdot Re$, they came out with the empirical formulation

$$\varepsilon_o = \frac{Nu_o}{Nu_{T_u=0}} = 1 + \frac{0.8\ T_u' \cdot Re}{1500 + T_u' \cdot Re} \tag{1.6}$$

where Nu_o is Nusselt number at stagnation point in turbulent flow

$Nu_{T_u=0}$ is the Nusselt number at stagnation point in zero turbulence

ε_o is the ratio of the two values above

is the percentage level of turbulence

and Re is the Reynolds number based on leading-edge diameter and inlet flow conditions.

When experimental data are compared with these formulations, as shown in Figure 32, the results show that the measured Nu_o at the blade leading edge were consistently lower by as much as 30% than the predicted values in all cases except for the Smith-Kuethe correlation in which the differences decrease to less than 7%.

There is, however, some question about the Smith-Kuethe correlation for $T_u \cdot Re^{1/2} > 20$. As Kuethe himself has indicated, the theory would require modifications for $T_u \cdot Re^{1/2} > 20$. Since the experiments reported here were in the range $16.3 \leq T_u \cdot Re^{1/2} \leq 27.6$, the agreement between the experimental data and the Smith-Kuethe correlation should be veiwed with reservation.

There is no doubt that the measured Nu_d was consistently lower than its true value. An explanation for this is the possibility that the leading-edge gauge could not have been placed exactly at the stagnation point and, even if it were, it was averaging heat transfer over an area in the leading edge zone, where there is a very sharp gradient of pressure and heat transfer. The ratio of gauge diameter to leading edge diameter = 0.5.

It is therefore not unreasonable to indicate that the maximum heat transfer at the leading edge may not have been recorded but, instead, averaged out over a certain area of the leading edge region.

1.6.7 Effect of Mach Number on Blade Nusselt Number

An attempt was made to correlate the effect of Mach number on the blade heat transfer. Variations of Nu/Re^n, for various values of n (n = 0.5, 0.66, 0.8 and 1.0) were investigated and some are shown in Figures 17 through 20. Stanton number as a function of the dimensionless chordwise location x/c was also investigated. Unfortunately, the shock movement on the suction side makes it impossible to arrive at a meaningful quantitative correlation.

A plot of mean $Nu/Re^{0.5}$, obtained from the area measurements of the heat transfer distribution curves, for the entire blade surface is plotted as a function of exit Mach number in Figure 33. The plot shows that the mean heat transfer to the blade increases with Mach number.

A comparison is also made between the measured blade mean Nusselt number with several available experimental data. As shown in Figure 34 our experimental data lie in the upper region (high values) which is expected as a result of the high level of turbulence at which we operated.

Finally a comparison of the mean heat transfer (Stanton number) as a function of exit Mach number is made of all the blades tested. This comparison (Figure 35) shows that the average heat transfer coefficient of Blades 1 and 3 is about the same whereas the convergent-divergent blade has a higher Stanton number. This high value of the Stanton number is probably due to the higher level of ρu over the surface of the convergent-divergent blade.

II. UPDATING THE INSTRUMENTATION

In updating the instrumentation, a look was taken at the effect of the temperature difference between the copper slug and the rest of the surface of the blade which results in the pulsing of the thermal boundary layer. In order to estimate this effect, an approximate integral method was used as shown below:

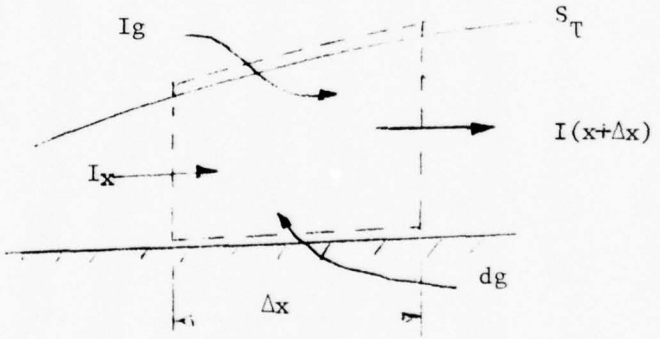

Figure (a)

$$I_x + \Delta x = I_x + I_\delta + dq$$

$$\text{i.e. } I_x + \Delta x - I_x = I_\delta + dq$$

$$\text{i.e. } \left(\frac{d}{dx} I_x\right) \Delta x = I_\delta + dq \qquad (2.1)$$

$$I_x = \int_0^{\delta_T} \rho V_x c_p T \, dy$$

Thus Equation (2.1) becomes

$$\frac{d}{dx}\int_0^{\delta_T} \rho V_x c_p T\, dy - c_p T_\infty \frac{d}{dx}\int_0^{\delta_T} \rho V_x\, dy = -k\left(\frac{\partial T}{\partial y}\right)_{y=0}$$

Assuming constant ρ and c_p we have

$$\frac{d}{dx}\left[\int_0^{\delta_T} V_x(T_\infty - T)\, dy\right] = \alpha\left(\frac{\partial T}{\partial y}\right)_0 \tag{2.2}$$

Assume that the momentum and temperature profiles are similar and use the 7th power profile to obtain

$$\frac{V_x}{V} = (y/\delta)^{1/7} \tag{2.3}$$

$$\frac{T - T_0}{T_\infty - T_0} = (y/\delta_T)^{1/7} = (y/\delta)^{1/7} \cdot (\delta/\delta_T)^{1/7} = \theta \tag{2.4}$$

where T_0 is the wall temperature and δ and δ_T are the momentum and thermal boundary layers respectively.

Using Equations (2.3) and (2.4) in (2.2) gives

$$\frac{1}{72}\frac{d}{dx}\left[(\delta_T/\delta)^{\delta/7}\, \delta\, V_\infty (T_\infty - T_0)\right] = \alpha\left(\frac{\partial T}{\partial y}\right)_0 \tag{2.5}$$

$$\left(\frac{\partial T}{\partial Y}\right)_0 = (T_\infty - T_0)(\delta/\delta_T)^{1/7}\, \frac{\partial}{\partial y}\left(\frac{V_x}{V_\infty}\right)$$

$$= \frac{(T_\infty - T_0)}{V_\infty}(\delta/\delta_T)^{1/7}\, \frac{\tau_0}{\mu} \tag{2.6}$$

Equation (2.6) into (2.5) gives

$$\frac{1}{72}\frac{d}{dx}(\xi^{\delta/7}\delta) = \frac{\tau_0}{\rho V_\infty^2}\frac{1}{\xi^{1/7}}\frac{1}{Pr} \tag{2.7}$$

where $\xi = \delta_T/\delta$ and τ_0 is the friction coefficient at wall.

For turbulent flow:

$$\delta/x = 0.37\left(\frac{V_\infty x}{\nu}\right)^{-1/5} \tag{2.8}$$

$$\frac{\tau_0}{\rho V_\infty^2} = 0.0225\left(\frac{V_\infty \delta}{\nu}\right)^{-1/4} \tag{2.9}$$

Using Equations (2.8) and (2.9) in (2.7) gives

$$\frac{d}{dx}(\xi^{8/7}x^{4/5}) = \frac{5.62}{Pr}x^{-1/5}\xi^{-1/7} \tag{2.10}$$

Equation (2.10) may be rearranged as

$$(\xi^{8/7}x^{4/5})^{1/8}\frac{d}{dx}(\xi^{8/7}x^{4/5}) = \frac{5.62}{Pr}x^{-1/10} \tag{2.11}$$

Solving Equation (2.11) gives

$$\xi = \frac{\delta T}{\delta} = 4.56\ Pr^{-7/9}[1 - (x_0/x)^{9/10}]^{7/9} \tag{2.12}$$

where x_0 is an unstarted heating length which represents the distance from the leading edge to the gauge in question. Equation (2.12) in (2.6) gives

$$Nu_x = \left(\frac{\dot{q}'' x}{\Delta T K}\right) = 0.0233\ Rex^{0.8}\ Pr^{0.111}\left[1 - (x_0/x)^{0.9}\right]^{-0.111} \qquad (2.13)$$

Equation (2.13) gives the correct power for the Reynolds number for $x_0 = 0$ but gives a lower dependence on Prandtl number.

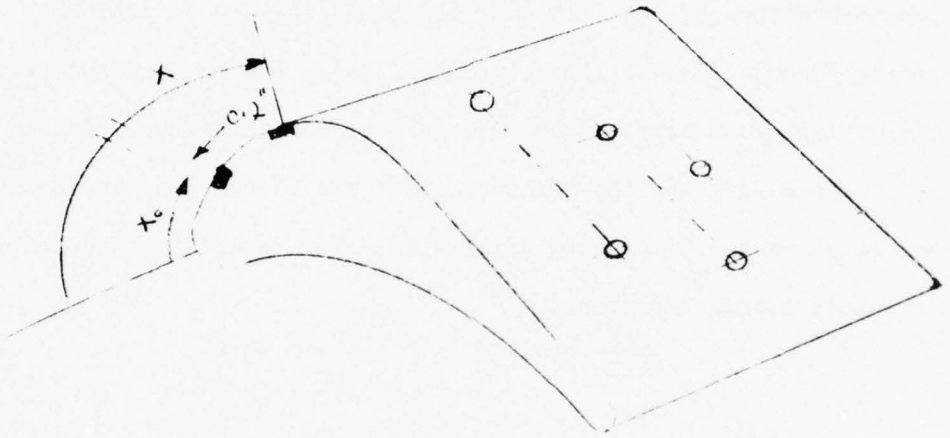

Figure (b)

Thus if it is required to find the effect of the first gauge on the second gauge then $x_{0_1} = 0.25"$; $x = 0.5"$; $x_{0_2} = 0.35"$. Hence,

$$\frac{\dot{q}''}{\dot{q}''} = \frac{\Delta T}{T_\infty - T_0}\left[R_1 - R_2\right]$$

where $\Delta\dot{q}$ is the error in recorded heat transfer, and $R = \left[1 - (x_0/x)^{0.9}\right]^{0.111}$ and ΔT is the temperature difference between the metal slug and the blade surface (Figure 36). For the conditions of the experiment at $t = 1$ sec., $\Delta T = 47°F$ and $T_\infty - T_0 = 270°F$. Then $\Delta\dot{q}/\dot{q} = 0.0113$.

The effect of the first gauge on the third gauge is even smaller (0.15%).

Thus it was recommended to stagger the heat transfer gauges as shown in Figure (b) in order to keep these effects to less than 1%. The obvious weaknesses of the analysis include the assumption of constant density and the fact that the effects of curvature have not been taken into account. However, staggering the gauges is expected to keep the errors very low.

The photograph of the new meliumeuted blades are shown in figure 37. The static pressure tubes are embedded further inside the blade so that less distortion of the flow over the blade surface is produced. The bridges for matching the heat transfer gauges and the pressure taps with the oscillograph have also been made a permanent feature of the facility. The master for the manufacture of the blades was smoothened so that the lumps on the blade were eliminated. The resultant blade profile had a slightly slower expansion.

III. OFF-DESIGN PERFORMANCE OF THE REFERENCE TRANSONIC BLADE PROFILE:

The off-design performance of transonic blades is of great importance to the designer. Thus, in this section of the study, an investigation of the aerodynamic and heat transfer performance of the reference blade profile figure 1(a) was carried out at angles of incidence other than 0. The tests have not yet been completed, but some preliminary results at one exit Mach number of 1.14 has been obtained. Thus, while no final conclusion will be drawn, some preliminary comments will be made.

Figure 38 (a), (b), and (c) show the isotropic Mach number distribution obtained for angles of incidence equal to zero, +5° and +10° respectively for an exit Mach number of 1.14. The movement of the stagnation point is apparent, and it appears as if the transition point extends into a transition zone which seems to get larger with increasing angle of incidence. The Mach number at transition also appears to be higher.

Figures 39(a), (b), and (c) show the Nusselt number distribution for angles of incidence equal to zero, +5° and +10° respectively for an exit Mach number of 1.14. A comparison of the distributions shows the movement of the stagnation point. These results are preliminary and further testing which is underway is required before any trends can be recognized and conclusions drawn.

IV. EFFECT OF UNSTEADINESS ON THE AERODYNAMIC AND HEAT TRANSFER PERFORMANCE OF TURBINE BLADES

Flows in gas turbines are necessarily unsteady. The unsteadiness arises from factors such as blade passage, the propagation of azimuthal nonuniformities and the propagation of periodic disturbances which originate upstream of the turbine.

These disturbances are likely to have a marked effect on the flow field, the base flow and the trailing edge shock system behavior as well as on the heat transfer. The aerodynamic flow around the trailing edge of the blade is of great interest because of its effect on blade row losses.

When a transonic cascade is operated at conditions other than limit loading, the left running trailing edge shock of the first blade usually interacts with the boundary layer of the suction side of the adjacent blade and this interaction could result in local or full flow separation, which has a great influence on aerodynamic losses. Since the rotor typically operates at a high angular velocity with many individual blades, a stator could see in the neighborhood of 10^5 fluctuations per minute. The purpose of this experimental investigation is to examine the effects of the high frequency periodic unsteadiness on the performance of the given turbine blade. The experiment is being designed to investigate the following phenomena:

(i) the aerodynamic and heat transfer properties in the neighborhood of the oscillating shock-boundary layer interaction on the suction side of the adjacent blade;

(ii) the effect of the periodic unsteady disturbances on the

potential flow in the blade passage;

(iii) the effect of the disturbances on the base pressure behind the stationary blade;

(iv) the accumulated losses in the wake.

The above experiment is to be conducted utilizing the MIT linear cascade tunnel which is attached to the hot blowdown facility in the Gas Turbine Laboratory. In the experimental investigation, a disturbance generated by rotating a small elliptical body downstream of the cascade blade will be used to simulate periodic unsteady effects. Blade, cascade wall, and traversing rake instrumentation will be used in measuring the aerodynamic and heat transfer properties for different operating conditions. A traversing probe will be used downstream of the cascade to measure cascade losses.

The experiment should help provide a basic understanding of the losses which are inherent in all gas turbine generators which utilize transonic rotating machinery. It should also better help to understand the cooling requirements for this type of turbine blading.

A small air turbine was chosen to provide the required flexibility of rotating the elliptical piece downstream of the turbine cascade. The air turbine has a variable speed of from 0 to 100,000RPM while operating off the shop air. The company which was given the contract for the air turbine is the Barbour Stockwell Company of Cambridge, Massachusetts. The air turbine was supposed to be delivered in May but during the acceptance tests problems occured with the bearings of the turbine above 90,000 RPM and delivery was not possible in May. It was later decided to run the turbine below 90,000 RPM and so the air turbine will be delivered within

two weeks of the time of writing. Meanwhile, components of the air turbine control system consisting of a magnetic pickup attached to the air turbine, an electrically operated throttle valve and the air cleaning system have been installed.

Work is also underway in the area of an analytical study of the effect of unsteadiness on the aerodynamic and heat transfer performance of the blades.

V. COMPARATIVE STUDIES BETWEEN TRANSONIC AND SUBSONIC TURBINES:

For this comparative study, let us consider a case where one highly loaded transonic turbine stage is used to replace two conventional subsonic turbine stages.

It is assumed that the mass flow rate $\dot{m}g$, turbine inlet stagnation temperature T_{01} and pressure P_{01}, work-output and tip speed are the same in both cases. In addition, the axial velocity is assumed constant in both cases.

For the Transonic Turbine:-

Number of stages = 1

Stage Stagnation Pressure Ratio = 4

Turbine Inlet Stagnation Temperature = 1800°K

For the Subsonic Turbine:-

Number of stages = 2

1st Stage:- Stage Pressure Ratio = 2

Turbine Inlet Stagnation Temperature = 1800°K

2nd Stage:- Stagnation Pressure Ratio = 2

5.1 Gasdynamic Analysis of the two Turbines

Gasdynamic analysis of the Transonic Turbine Stage has been carried out and the results given in Table Number 1. A similar analysis is now carried out here for the two stages of the Subsonic Turbines.

Turbine 1st Stage:-

$$T_{01} = 1800°$$

$$\frac{P_{01}}{P_{03}} = 2$$

$$\frac{T_{01}}{T_{03}} = \left(\frac{P_{01}}{P_{03}}\right)^{\frac{\gamma-1}{\gamma}\eta} = 1.155$$

$\therefore\ T_{03} = 1560°K$

$\Delta T_o = 1800 - 1560°K = 240°K$

Specific Work Output

$$\Delta W = \bar{c}p \cdot \Delta T_0 = \left(\frac{\gamma}{\gamma-1}\right) \frac{R}{M} \Delta T_0$$

$$= 299154.93\ m^2/sec^2$$

For the 2nd stage,

$T_{01} = 1560°K$

$$\frac{P_{01}}{P_{03}} = 2, \quad \frac{T_{01}}{T_{03}} = 1.155$$

$T_{03} = 1350°K$

$\Delta T_0 = 210°K$

The detailed multi-stage analysis is shown in Table II.

Table II

	Stage Parameter	1st Stage	2nd Stage
1.	Design Parameters		
(a)	Turbine Inlet Total Temperature	1800°K	1560°K
(b)	Stage Stagnation Pressure Ratio	2	2
(c)	Blade Speed (U)	550 m/s	550 m.s
(d)	Target Total to total polytropic efficiency	0.9	0.9
2.	Stagnation Temperature Drop Across Stage		
	$\Delta T_0 = T_{01} - T_{03}$	240°K	210°K
3.	Stage Specific Work Output		
	$\Delta W = \bar{C}_p \Delta T_0$	299154.9	260887.6
4.	Change in Tangential Vel		
	$\Delta Cy = \frac{\Delta W}{\mu}$	543.92	474.34
5.	Tangential Components of the Velocities		
	$W_{y3} = (\frac{\Delta Cy + \mu}{2})$	546.47	512.17
	$C_{y3} = W_{y3} - U$	-3.53	-37.83
	$W_{y2} = C_{y3}$	-3.53	-37.83
	$C_{y2} = W_{y2} + U$	-3.53	-37.83
6.	Rotor Inlet and Exit Velocities		
	$C_2 = \sqrt{C_x^2 + C_{y2}^2}$	657.16 m/s	628 m/s

Table II (continued)

Stage Parameter		1st Stage	2nd Stage
	$W_2 = \sqrt{W_x^2 + W_{y2}^2}$	365.02 m/s	367 m/s
	$C_3 = \sqrt{C_w^2 + C_{y3}^2}$	365.02 m/s	367 m/s
	$W_3 = \sqrt{W_x^2 + W_{y3}^2}$	657.16 m/s	628 m/s
7.	Static Temperatures & Acoustic Velocities at Rotor Inlet and Exit		
(a)	$T_2 = T_{02} - \frac{C_2^2}{2Cp}$	1626.19°K	1401.27°K
(b)	$a_2 = \sqrt{\gamma \frac{R}{m} T_2}$	778.51	722.67
(c)	$T_3 = T_{03} - \frac{C_3^2}{2Cp}$	1506.37	1295.79
(d)	$a_3 = \sqrt{\gamma \frac{R}{m} T_3}$	749.28	694.94
8.	Mach Number at Rotor Inlet & Exit		
(a)	Absolute Inlet Mach No.		
	$M_{c2} = C_2/A_2$	0.84	0.87
(b)	Relative Inlet Mach No.		
	$M_{w2} = W_2/a_2$	0.47	0.51
(c)	Axial Inlet Mach No.		
	$M_{cx2} = C_x/a_2$	0.47	0.51
(d)	Absolute Exit Mach No.		
	$M_{c3} = c_3/a_3$	0.49	0.53
(e)	Relative Exit Mach No.		
	$M_{w3} = W_3/a_3$	0.88	0.90

Table II (continued)

Stage Parameter	1st Stage	2nd Stage
(f) Axial Exit Mach No.		
$M_{cx3} = c_x/a_3$	0.49	0.53
9. Stagnation Temperature at Rotor Inlet		
Absolute T_{02}^{ab}	1800°K	1560°K
Relative T_{02}^{rel}	1679.81	1455.48°K
10. Stagnation Temperature at Rotor Exit		
Absolute T_{03}^{ab}	1560°K	1350°K
Relative T_{03}^{rel}	1679.81	1455.48°K
11. Stage Loading Coefficient		
$\psi = \frac{\bar{c}_p \Delta T_o}{\mu^2}$	0.99	0.86
12. Stage Flow Coefficient		
$\phi = \frac{C_x}{\mu}$	0.66	0.66

5.2 Estimate of the Coolant Flow Requirements Using Film Cooling

As mentioned above in Section 5.1, film cooling of varying degrees of sophisitication offers a more practical solution for high-temperature turbine blade cooling.

Film-cooling effectiveness data on flat plates gathered at M.I.T. Gas Turbine Laboratory, which incorporates the effect of geometry on film-cooling effectiveness, shows that for double row of holes, with injection angle of 20°, gives

$$\eta_{isoth} = 156.17 \left(\pi^{*1.41} \cdot \frac{4}{\pi}\right)^{-.24} \left(m^{-1.35}\ \theta^{-0.68}\right)^{-.24} \left(\frac{x}{D} \cdot \frac{y_1}{D}\right)^{-.24} \qquad (5.1)$$

$$= 156.17 \left(\pi^{*1.41} \cdot \frac{4}{\pi}\right)^{-.24} \left(K_0^{-1.35}\right) \left(\frac{x}{D} \cdot \frac{y_1}{D}\right)^{-.24}$$

where $m = \dfrac{\rho U_c}{\rho U_q}$;

$$= \frac{T_{c\ exit}}{T_q}$$

$$K_0^2 = \frac{\rho U_c^2}{\rho U_g^2} \quad ; \quad K_0 = m\sqrt{\theta} = \frac{M_c}{M_g}$$

The main flow $\dot{m}_g = (\rho UA)_g = \rho_g U_g\, sh \cos\beta_{th}\, h.$

Coolant flow $\dot{m}_c = 2.48 \dfrac{C}{x} \cdot \dfrac{\pi D^2}{4} \cdot \dfrac{h_1}{y_1}\, \rho_c U_c$

Here the perimeter of the blade profile is taken as 2.48C, which is equal to the perimeter of the reference blade.

$$\therefore \frac{\dot{m}_g}{\dot{m}_c} = \frac{4}{2.48\pi} \cdot \frac{S}{C} \cdot \cos\beta\ \frac{\rho U_{g\ throat}}{\rho U_c} \cdot \frac{x}{d} \cdot \frac{y_1}{d} \qquad (5.2)$$

Combining equations 5.1 and 5.2, we get the following expressions:

For $\eta_{iso} < 62\%$, i.e., $A_2 < 45$

$$\frac{\dot{m}_c}{\dot{m}_g} = 1.944\,\eta^{4.17}\ \frac{m'}{m}^{-0.35}\ \Theta^{-0.68}\ (s/c\cos\beta)^{-1} \qquad (5.3)$$

where $m' = \dfrac{\rho U_c}{\rho U_{q\ throat}}$

For $33.4\% < \eta_{isoth} < 62\%$; i.e., $45 \quad A_2 \quad 180$

$$\frac{\dot{m}_c}{\dot{m}_g} = 0.833\ ^{2.273}\ \frac{m'}{m}\ m^{-0.35}\ \ ^{-0.68}\ (\frac{s}{c}\ \cos\beta)^{-1} \qquad (5.4)$$

For $\eta_{isoth} < 33\%$, i.e., $A_2 > 180$

$$\frac{\dot{m}_c}{\dot{m}_g} = 0.380\eta^{1.538}\ \ \frac{m'}{m}\ .\ m^{-0.35}\ \Theta^{-0.68}\ (\frac{s}{c}\ \cos\beta)^{-1} \qquad (5.5)$$

where

$$A_2 = \eta^{*1.41}\ m^{-1.35}\ \Theta^{-0.68}\ \frac{x}{Seg}\ .$$

With $\dfrac{x}{Seq} = \dfrac{4}{\pi} \cdot \dfrac{x}{d} \cdot \dfrac{y_1}{d}$ for double row of holes,

$$\frac{m'}{m} = \frac{\dfrac{\rho U_c}{\rho U_{g\ throat}}}{\dfrac{\rho U_c}{U_{g\ injection}}} = \frac{(U_g)_{injection}}{(U_q)_{throat}} = \frac{A^*}{A_{inject}} = 0.63$$

for the reference Blade 1.

Equation 5.3, which represents high values of $\eta_{isothermal}$ is used in this analysis.

According to the definition of film-cooling isothermal effectiveness,

$$\eta_{isoth} = \frac{q' - q''}{q'} \tag{5.6}$$

where q - heat transfer to the blade in the absence of film cooling

q' - heat transfer to the blade with film cooling

q'' - $(1 - \eta_{isothermal})$ - and this must be handled by the internal cooling,

$$\text{i.e., } q'' = \dot{m}_c \, \bar{C}p_c \, (T_{c.exit} - T_{c.m}) \tag{5.7}$$

Let us define an internal cooling effectiveness:

$$\varepsilon = \frac{T_{c\ exit} - T_{c.in}}{T_{blade} - T_{c}.in} \tag{5.8}$$

varies from 0.0 to 1, higher values of generally 0.5 are of interest. ε is a strong function of the type of internal cooling; its configuration coolant flow Reynold number, etc.

Tc_{in}, $T_{c\ exit}$ - coolant inlet and exit temperatures respecitvely combining equation 5.7 and 5.8 results in:

$$q'' = \dot{m}_c \cdot \bar{C}_{pc} \cdot \varepsilon \, (T_{blade} - T_{c.in})$$

$$\dot{m}_c = \frac{q''}{\bar{C}_{pc} \cdot \varepsilon \, [T_{blade} - T_{c.in}]}$$

$$= \frac{(1 - \eta)q'}{\bar{C}_{pc} \cdot \varepsilon \, [T_{blade} - T_{c.in}]}$$

$$= \frac{(1 - \eta)\ 2.48\sigma\ St \cdot \rho \cdot U \cdot \bar{C}p_q \cdot K_1 \, (T_g - T_b)K_1}{\bar{C}p_c \cdot \varepsilon \, [T_{blade} - T_{c.in}]}$$

where St - blade mean Stanton number

$$\frac{\dot{m}_c}{\dot{m}_g} = \frac{(1 - \eta) \dfrac{A^*_{throat}}{A_{exit}} (2.48)\sigma \cdot St \cdot Cp_g \cdot K_1 (T_g - T_b)}{\bar{C}p_c \cdot \varepsilon [T_b - T_{c \cdot in}] \cos \beta} \qquad (5.9)$$

where K_1 - is the coefficient that takes into account the effect of blade rotation. Using experimental correlation of references (12), (13), and (14), K_1 is taken to be 1.5.

β - exit angle at the throat.

$$\left[\frac{\dot{m}_c}{\dot{m}_g}\right]_{\substack{film \\ cooling}} = K_2 \left[\frac{\dot{m}_c}{\dot{m}_g}\right]_{\substack{internal \\ cooling}}$$

where K_2 - is the fraction of internal cooling being used for film cooling and taken to be 1 in this analysis.

Equations 5.3 and 5.9 are coupled and solved simultaneously.

$$\frac{\dot{m}_c}{mg} = 1.2247\eta^{4.17}\, m^{-0.35}\, \theta^{-0.68}\, (s/c \cos \beta)^{-1} \qquad (5.10)$$

$$\frac{\dot{m}_c}{\dot{m}_g} = \frac{(1 - \eta)\ (2.1328)\sigma \cdot St \cdot Cp_g \cdot K_1 [T_g - T_b]}{\bar{C}p_c \cdot \varepsilon \cdot [T_b - T_{c.in}] \cos \beta} \qquad (5.11)$$

$$\theta = \frac{T_{c.exit}}{T_g} = \left[\frac{\varepsilon (T_b - T_{c.in}) + T_{c.in}}{T_g}\right]$$

Internal cooling effectiveness ε . (ε = 0.5, 0.75 and 0.9) .

For the single high pressure ratio transonic turbine stage the coolant mass flow requirements for the rotor blade row alone is considered. The coolant mass flow requirement for the nozzle row is not included as the nozzle is considered as part of the combustion chamber.

The turbine inlet stagnation absolute temperature defined here is for the rotor inlet To_2^{ab} ($\approx 1800^{o}K$)

Blade Row: For the rotor blade row, equations 5.3 & 5.9 are solved simultaneously

$$\Theta = \frac{T_{c.exit}}{T_g} = \frac{[\,(T_b - T_{c.in}) + T_{c.in}]}{T_{02}^{rel}} \qquad (5.12)$$

$T_b = 1200^{o}k$ allowable blade temperature

$T_{c.in} = 750^{o}k$

$T_{02}^{rel} = 1575^{o}k$

$S/c \cos \beta = (0.7)(0.42) = 0.315$

$\sigma = c/s = ;.4286$

$St = 0.00187$

$k_1 = 1.5$ accounting for the effect of rotation

$T_g = T_{02}^{rel}$

Computations are carried out for $m = 0.5$, 1.0, & 1.5 while varying ϵ. ($\epsilon = 0.5$, 0.75 and 0.9)

a_1 is defined as the ratio of coolant to gas flow rate.

$$a_1 = \frac{\dot{m}_{cr}}{\dot{m}_g} = a_{\substack{transonic \\ stage}}$$

Two-Stage Subsonic Turbine

Equation 5.3 and 5.9 are solved simultaneously to determine the coolant to gas flow rate.

As in the transonic stage; the first nozzle is not included. This is regarded as part of the combustion chamber.

The coolant mass flow requirements for the rotor of the first stage, the nozzle and rotor of the second stage are estimated.

1^{st} Stage Rotor

θ is defined as in equation 5.12

$T_b = 1200^{\circ}K$ - allowable balde temperature

$T_{c.in} = 750^{\circ}K$

$T_{02}^{rel} = T_g = 1680^{\circ}K$

$(s/c \cos \beta) = (0.7)(0.554) = 0.3878$

$\sigma = c/s = 1.4286$

$S_t = 0.00194$

$k_1 = 1.5$ accounting for the effect of rotation. Computations carried out for $m = 0.5$, 1.0, and 1.5 and $\varepsilon = 0.5$, 0.75 and 0.9

a_1 is defined as the ratio of coolant to gas flow rate

$$a_1 = \frac{\dot{m}_{cr}}{\dot{m}_g}$$

2nd Stage Nozzle

The 2nd stage nozzle inlet temperature is computed using energy conservation.

$$\dot{m}_g \, Cp_c \, T_{02}^{ab} + \dot{m}_{c.r1} \, Cp_c \, T_{c\ exit}$$

$$= (\dot{m}_g + \dot{m}_{c.r1}) C'p_q T_{03}^{ab} + (\dot{m}_g + \dot{m}_{c.r1}) \bar{C}p . \Delta T_0 m_g Cp_g . T_{02}^{ab} + m_{c.r1} Cp_{c\ exit} T_{c.exit}$$

$$= (\dot{m}_g + \dot{m}_{c.r1}) (C'p_g \, T_{03}^{ab} + \bar{C}_p \, . \, \Delta T_0) \qquad (5.13)$$

where $\dot{m}g$ is the **main** (hot) gas mass flow entering the first rotor,

$\dot{m}_{c.r1}$ - coolant mass flow for rotor blades of Stage 1

$(\dot{m}_g + \dot{m}c.r1)$ - mass flow leaving the rotor stage

ΔT_0 - stagnation temperature drop across the first stage.

Equation 5.14 then reduces to:

$$T_{03}^{ab} = \frac{\left[\frac{Cp_g}{C'p_g} \, T_{02}^{ab} + a_1 \frac{Cp_{c.exit}}{C'p_g} \, T'_{c.exit}\right]}{(1 + a_1)} \qquad (5.14)$$

$$T_{03}^{ab} = \frac{\frac{Cp_g}{C'p_g} \, T_{02}^{ab} + a_1 \frac{Cp_{c.exit}}{C'pg} \left[(Tg - T_{c.in}\right]}{(1 + a_1)} - \frac{\bar{C}_p}{C'p_g} \Delta T_{01} \qquad (5.15)$$

knowing T_{03}^{ab}, θ can be calculated.

$$\theta = \frac{T_{c.exit}}{T_g} = \frac{\left[(T_b - T_{c.in})^{\gamma} + T_{c.in}\right]}{T_{03}^{ab}}$$

$k_1 = 1$, - stationary row

$s/c \cos \beta = (0.8) (0.5812) = 0.4649$

σ = c/s = 1.4286

St = 0. 00194

$T_g = T_{03}^{ab}$ expressed by equation 6.2.14

T_b = 1200°K

$T_{c.in}$ = 600°K

The equations are solved again for $\dot{m}$ = 1.0 and 1.5 and = 0.5, 0.75 and 0.9.

a_2 is defined as the ratio of the coolant to gas flow rate for the 2nd stage nozzle

$$a_2 = \frac{\dot{m}_{c.n2}}{\dot{m}_g + \dot{m}_{c_{rl}}}$$

2nd Stage Rotor

Equations 5.3 and 5.9 are solved simultaneously to determine coolant mass flow.

The mean absolute stagnation temperature T_{04}^{ab} at 2nd rotor inlet is found using conservation of energy.

$$(\dot{m}_g + \dot{m}_{c.rl})T_{03} + m_{c.n2}\, Cp_c\, T_{c.exit} \approx (m_g + m_{c.rl} + m_{c.n2})\text{-}Cp_4 . T_{04}^{ab} \qquad (5.17)$$

$$T_{04}^{ab} = \frac{\frac{Cp_3}{Cp_4} . T_{03}^{ab} + a_2 \frac{Cp_c}{Cp_4} . [T_{c.exit}]}{(1 + a_2)} \qquad (5.18)$$

$$T_{04}^{ab} = \frac{\frac{Cp_3}{Cp_4} . T_{03}^{ab} + a_2 \frac{Cp_c}{Cp_4} . [(T_b - T_{c.in}) + T_{c.in}]}{(1 + a_2)}$$

$$T_{04}^{rel} = T_{04}^{ab} - \frac{(C_y^2 - W_4^2)}{2\overline{Cp}} \qquad (5.19)$$

where C_4 and W_4 - are the absolute and relative velocities (taken from the velocity triangle)

$$\Theta = \frac{T_{c.exit}}{T_{04}^{rel}}$$

$$\Theta = \frac{[\ (T_b - T_{c.in}) + T_{c.in}]}{T_{04}^{ab} - \frac{(C_4^2 - W_4^2)}{2Cp}} \qquad (5.20)$$

$k_1 = 1.5$

$s/c \cos \beta = (o.7) \times (0.5812) = 0.4068$

$\sigma = c/s = 1.4286$

$St = 0.00191$

$T_g = T_{04}^{rel}$ compressed as in equation 5.19

$T_{c.in} = 600°K$

The equations are solved for m = 0.5, 1.0 and 1.5 and ε = 0.5, 0.75 and 0.9.

a_3 is defined as $\dfrac{\dot{m}_{c.r2}}{\dot{m}_g + \dot{m}_{c.r1} + \dot{m}_{c.n2}}$

and a

$$\text{subsonic} = \frac{\dot{m}_{c.r1} + \dot{m}_{c.n2} + \dot{m}_{c.r2}}{\dot{m}_g + \dot{m}_{c.r1} + \dot{m}_{c.n2} + \dot{m}_{c.r2}}$$

The analysis yields the total coolant mass flows for both the subsonic and transonic turbines. The savings in coolant mass flow may then be computed.

Limitations of the Anlaysis

The major limitations of the anlysis lie with the data used. For example, the film-cooling correlation used here is one which was obtained for film cooling on a flat plate. Thus the effects of curvature, the effects of the coolant from the preceeding line of holes and the effect of secondary flows on cooling in a 3D machine are not taken into account. Also many other considerations such as the losses due to coolant flow injection and a detailed heat transfer and structural analysis must be carried out before final design criteria can be set.

5.3 Comparison of Required Heat Removal:

Without specifying any cooling technique to be used a general approach to determine the desirability of using transonic turbine to replace subsonic turbine can be roughly estimated by considering the ratio of the amount of heat that has to be removed from the stage to the work output from the stage.

5.3.1 Transonic Stage

It is assumed that both the transonic and subsonic turbine have the same turbine inlet total temperature and total pressure; operate with the same mass flow, axial velocity and tip speed. And we are considering the case, where the highly loaded transonic stage $\frac{Po1}{Po3} = 4$ is used to replace, two stages, say moderately $\frac{Po1}{Po3} = 2$

subsonic stages. For the Single Transonic Stage,

$$d_{transonic} = \frac{\Sigma q_{transonic}}{\dot{m}(C_p \Delta T_0)_{transonic}}$$

where $\Sigma q_{transonic} = q_{nozzel} + q_{\substack{rotor \\ blade}} + q_{disc} + q_{casing}$

= sum of all the heat that has to be removed from the turbine components.

For simplicity, let us consider only the nozzle and blade rows.

Using the example we are dealing with here, let us first compare the highly loaded single stage transonic turbine with the moderately loaded subsonic one.

5.3.1 Transonic Stage:

For the Transonic Stage with a pressure ratio of 4, turbine inlet temperature of 1800°K we have:

$$d = \frac{q_{nozzle} + q_{rotor}}{\dot{m}\bar{C}p\ \Delta T_0}$$

$$= \frac{\dfrac{q_{nozzle}}{\dot{m}\bar{C}p} + \dfrac{q_{rotor}}{\dot{m}\bar{C}p}}{\Delta T_0}$$

$$= \frac{\left[\dfrac{2.48\sigma St.[\rho U_1 Cp(T_u - T_g]}{\rho U_1\ g\ \cos\beta\ \bar{C}p}\right] + \left[\dfrac{2.48\sigma St.K.[\rho U_3 \bar{C}_p (T_{02}^{rel} - T_b)g]}{\rho U_3\ g\ \cos\beta\ \bar{C}p}\right]}{\Delta T_0}$$

$$= \frac{\dfrac{(2.48)(1.33)(0.000188)(600)}{0.423} + \dfrac{(1.5)(2.48)(1.333)(0.00188)(1575-1200)}{0.423}}{450}$$

$$= 0.367$$

5.3.2 Subsonic Stage

For the subsonic stage, let us consider the first stage of the two-stage turbine.

$$d = \frac{\dfrac{2.48\sigma\ St(T_{01}-T_b)}{\cos\beta} + \dfrac{2.4\sigma\ St.K_1(T_{02}^{rel} - T_b)g}{\cos\beta}}{\Delta T_{0I}}$$

$$= 0.0602$$

Second Subsonic Stage

With pressure ratio of two, with turbine inlet temperature of 1560°K

$$d_{\text{subsonic II}} = \frac{3.7659 + 2.6727}{210^\circ}$$

$$= 0.0307$$

For the Multistage Subsonic Turbine

$$d_{\substack{\text{multistage}\\ \text{subs.}}} = \frac{q_{\substack{\text{nozzle}\\ \text{stage 1}}} + q_{\substack{\text{rotor}\\ \text{stage 1}}} + q_{\substack{\text{nozzle}\\ \text{stage 2}}} + q_{\substack{\text{rotor}\\ \text{stage 2}}}}{\dot{m}\bar{C}_p\ \Delta T_{0I} + \dot{m}\bar{C}p\ \Delta T_{0II}}$$

$$= \frac{\frac{q_{\text{nozzle I}}}{\dot{m}\bar{C}p} + \frac{q_{\text{rotor}}}{\dot{m}\bar{C}p} + \frac{q_{\text{nozzle II}}}{\dot{m}\bar{C}p} + \frac{q_{\text{rotor II}}}{\dot{m}\bar{C}p}}{(\Delta T_{01} + \Delta T_{02})}$$

$$= \frac{6.5681 + 7.8817 + 3.7659 + 2.6727}{450}$$

$$= 0.0464$$

$$D = \frac{d_{\text{multistage}} - d_{\text{transonic}}}{d_{\text{multistage}}}$$

$$= \frac{0.0464 - 0.0367}{0.0464} = 20.95\%$$

i.e. by replacing two subsonic stages with a single highly loaded transonic stage to produce the same work output, the amount of heat that has to be removed from the turbine stage has been decreased by as musch as 21%.

It also is worth mentioning that for a fixed rotor blade temperature, the turbine nozzle inlet temperature can be raised for the transonic case since the blade relative stagnation temperature is generally lower in transonic turbine than in subsonic ones.

And when this increased temperature is matched with a corresponding increase in compressor pressure ratio, the overall cycle - efficiency will improve.

The analysis thus shows the potential for gains in the work output per unit of cooled blade surface for high performance transonic turbines.

VI. CONCLUSIONS

The most significant results of the study may be summarized in the following conclusions:

(a) Since the pressure distribution obtained in the cascade blowdown facility is the same as that obtained in the conventional wind tunnel at the Von Karman Institute, then the blowdown facility is a bonafide and practical method of aeordynamic testing. It is also a flexible means of solving rather complicated heat-transfer problems while providing a fairly rigorous modeling of the aerodynamic flow and temperature fields to simulate turbine operating conditions.

(b) A comparison of the isotropic Mach number distribution obtained in VKI with that obtained in the MIT cascade facility shows that the level of turbulence in the mainstream has a marked effect on the transition to turbulence in the boundary layer.

(c) The losses measured for transonic cascades are of the same order of magnitude as for subsonic cascades which seems to suggest that the effectiveness of both turbines are comparable. However, this will have to be modified by an evaluation of the effect of coolant flow on these efficiencies.

(d) A comparison of the loss curves for the four blade profiles shows that each profile has a superior performance in a different Mach number range. Thus the reference blade with the thin trailing edge is superior up to the design point and then the plug nozzle as well as the blade with a convergent-divergent nozzle are superior in the higher Mach number range. The comparison also shows that the thickness of the trailing edge has a marked effect on losses.

(e) The Nusselt number distribution predicted from a NASA computer agrees well with the measurement except in the regions where shock waves interact with boundary layers. This serves to confirm its validity. The distribution of Nusselt numbers also shows a very high heat transfer rate at the trailing edge.

(f) The comparison of the results obtained with those of Turner [15] seem to suggest that the level of turbulence may be a key variable in determining heat transfer.

(g) Lastly, comparative studies between subsonic and transonic turbines show that there is 21% less heat to be taken out by internal cooling in the case of transonic turbines, and that less coolant flow is required to cool a single stage transonic turbine with a pressure ratio of 4 used to replace a subsonic turbine with two stages with pressure ratios of 2 per stage. All these point to the great potential of transonic turbines. But before this potential is realised further investigations are necessary such as the effect of coolant flow injection on the efficiency of transonic turbines.

REFERENCES

[1] McNally, W. D. (1970), "Fortran Program for Calculating Compressible Laminar and Turbulent Boundary Layers in Arbitrary Pressure Gradients," NASA TN D-5681

[2] Kestin, J. and R.t. Wood (1971), "The Influence of Turbulence on Mass Transfer from Cylinders," ASME Journal of Heat Transfer, November.

[3] Dyban, V.P. and Ye. R. Yertik, (1974), "Heat Transfer in Laminar Boundary Layer with Increased Turbulence of the Outer Flow," Heat Transfer--Soviet Research, 6 No. 3, May-June.

[4] Zysina-Molozhen, L.M. and V.D. Kurosh (1971), "The Effect of Turbulence of Transition in the Boundary Layer of Gas Turbine Blades," Teploenergetika, 18, No. 12.

[5] Kurosh, V.D. and E. Ya. Epik (1970), "The Effect of Turbulence on Heat Transfer in Turbomachinery Flow Passages," Heat Transfer--Soviet Research, 2, No. 1, January.

[6] Launder, B.E., (1964), "Laminarization of the Turbulent Boundary Layer by Acceleration," MIT Gas Turbine Laboratory Report No. 77, November.

[7] Jones, W.P. and B.E. Launder (1972), "The Prediction of Laminarization with a Two-equation Model of Turbulence," International Journal of Heat Transfer, 15, pp. 301-314.

[8] Dyban, Ye.P., E.Ya. Epik and L.G. Kozlova, (1973), "Heat Transfer in the Vicinity of the Front Stagnation Point of a Cylinder in Traverse Flow," Teplofizika i Teplotekhnika, 24, pp. 57-60, (kiev).:

[9] Smith, M.C. and A.M. Kuethe, (1966), "Effect of Turbulence on Laminar Skin Friction and Heat Transfer," Physics Fluids, 9, No. 12, p. 2337.

[10] Mujumdar, A.S. and W.J.M. Douglas (1970), "Some Effects of Turbulence and Wake-Induced Periodicity on Heat Trasnfer from Cylinders," Paper presented at the 20th Canadian Chemical Engineering Conference, Sarnia, Onrario, Canada, October.

[11] Demuren, H. O., (1976) "Aerodynamic Performance and Heat Transfer Characteristics of High Pressure Ratio Transonic Turbines," Doctor of Science Thesis, Department of Aeronautics and Astronautics, MIT, Cambridge, Mass.

[12] Lokai, Ivanov, V.L.; "High Temperature Cooled Gas Turbines" (in Russian), Mashinostroenie Moscow 1971

[13] Zhiritski, I.S., et al; "Gas Turbine Engines for Flight Vehicles" (in Russian), Mashinostroenie Moscow 1971.

[14] Kopelev C.Z., Tihonov, H.D.; "Design of Turbines for Aircraft Engines" (in Russian), Mashinostroenie Moscow 1974.

[15] Turner, A.B.; "Local Heat Transfer Measurements on a Gas Turbine Blade", Journal Of Mechanical Science, Vol. 13, No. 1, 1971.

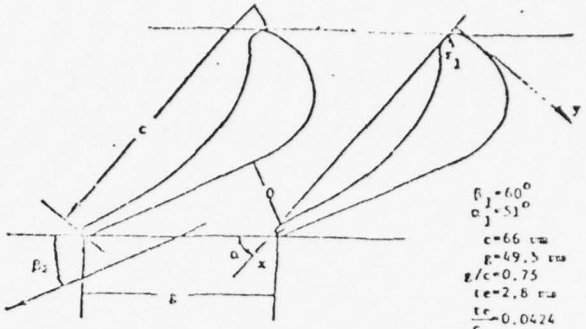

(a) Convergent Reference Blade with Straight Suction Back and Thick Trailing Edge

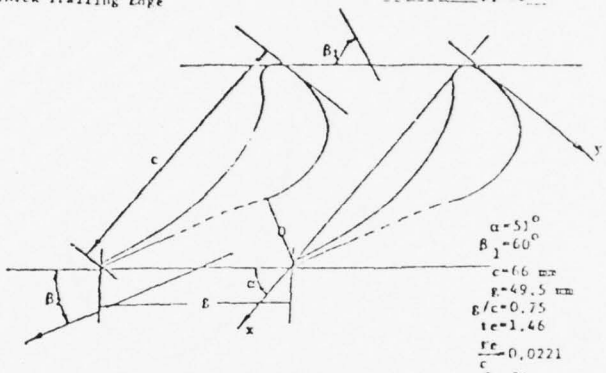

(b) Blade Profile with Unguided Expansion on the Suction Side

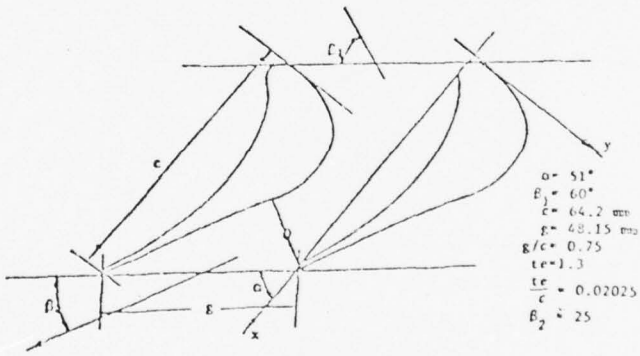

(c) Convergent Blade with Straight Suction Back but Thin Trailing Edge

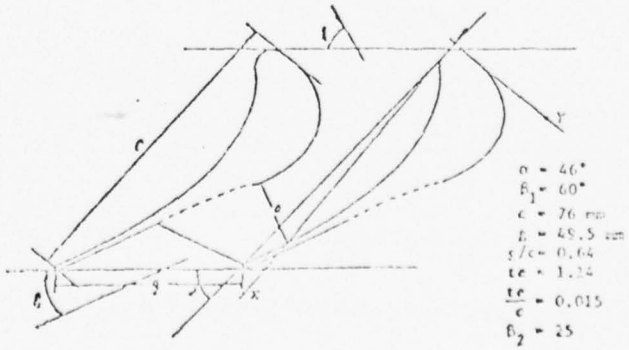

(d) Convergent-Divergent Blade

Figure 1 Transonic Reaction Blade Profiles

BLADE MACH NUMBER DISTRIBUTION

BLADE WITH STRAIGHT SUCTION BACK

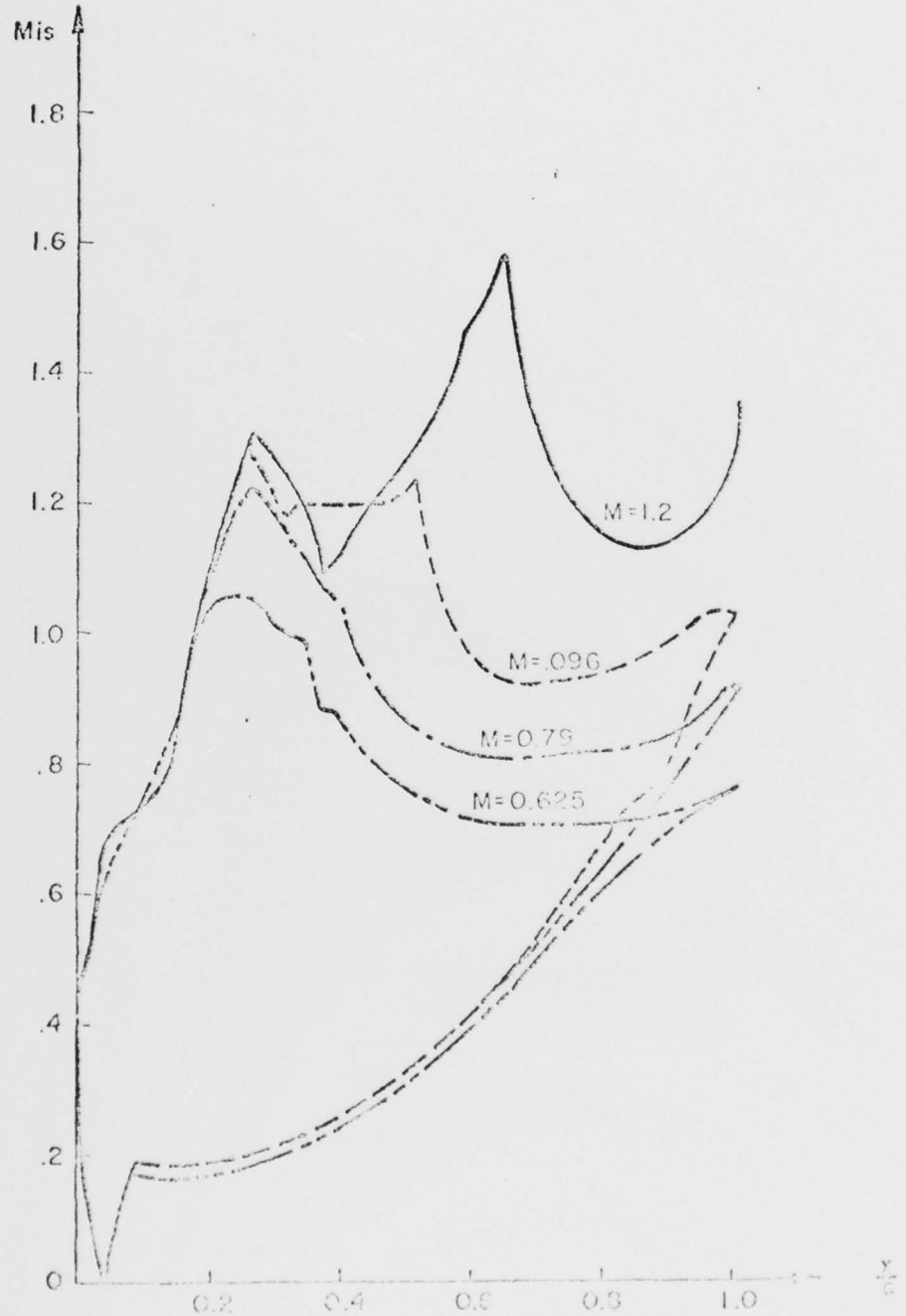

Figure 2 - Blade 1 Surface Mach Number Distribution $g/c = 0.75$

BLADE MACH NUMBER DISTRIBUTION

BLADE WITH STRAIGHT SUCTION BACK WITH THIN TRAILING EDGE

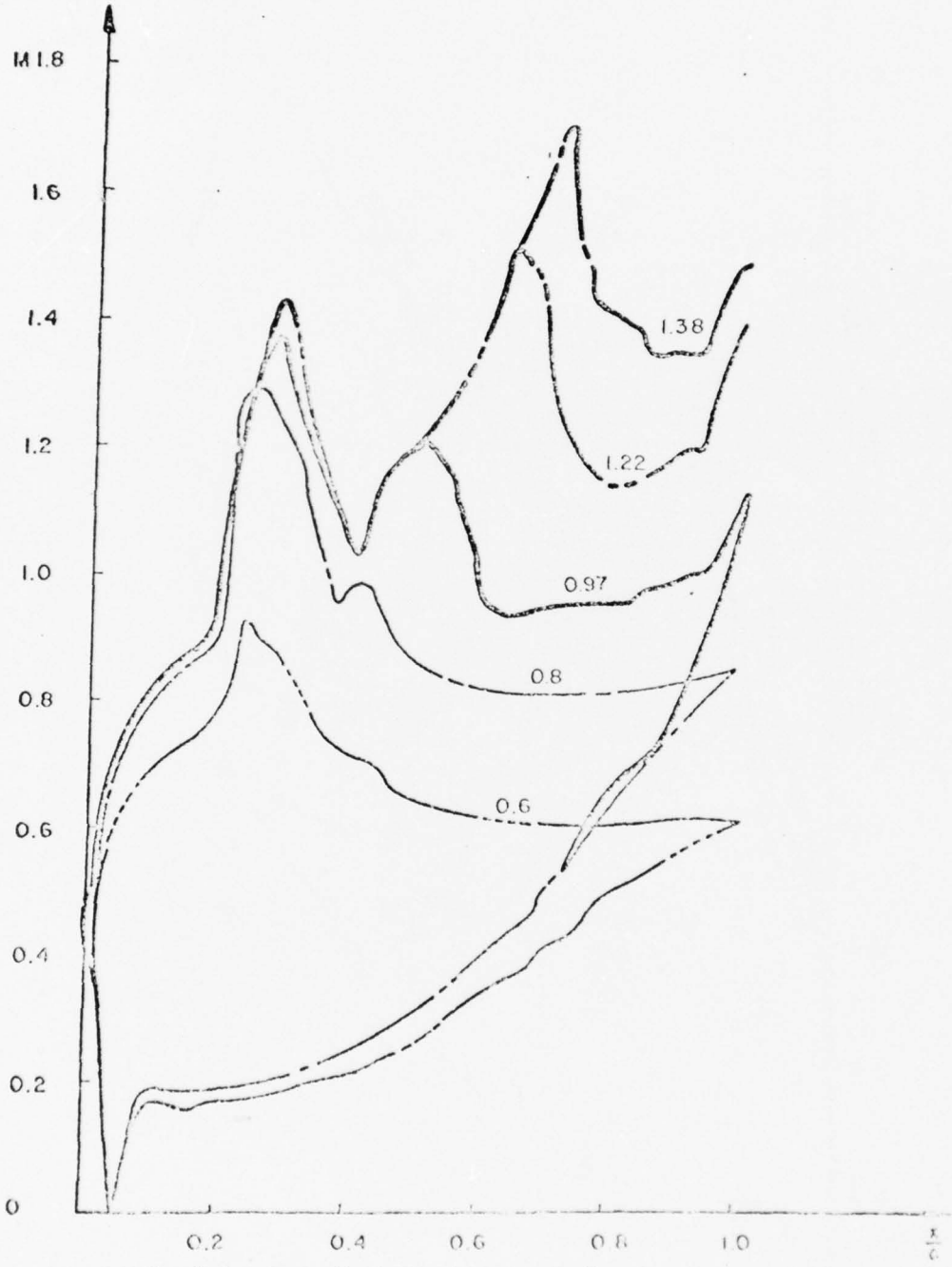

Figure 3 Blade 2 Surface Mach Number Distribution $\gamma/s = 0.75$

BLADE MACH NUMBER DISTRIBUTION

BLADE WITH EXPANSION ON SUCTION SIDE

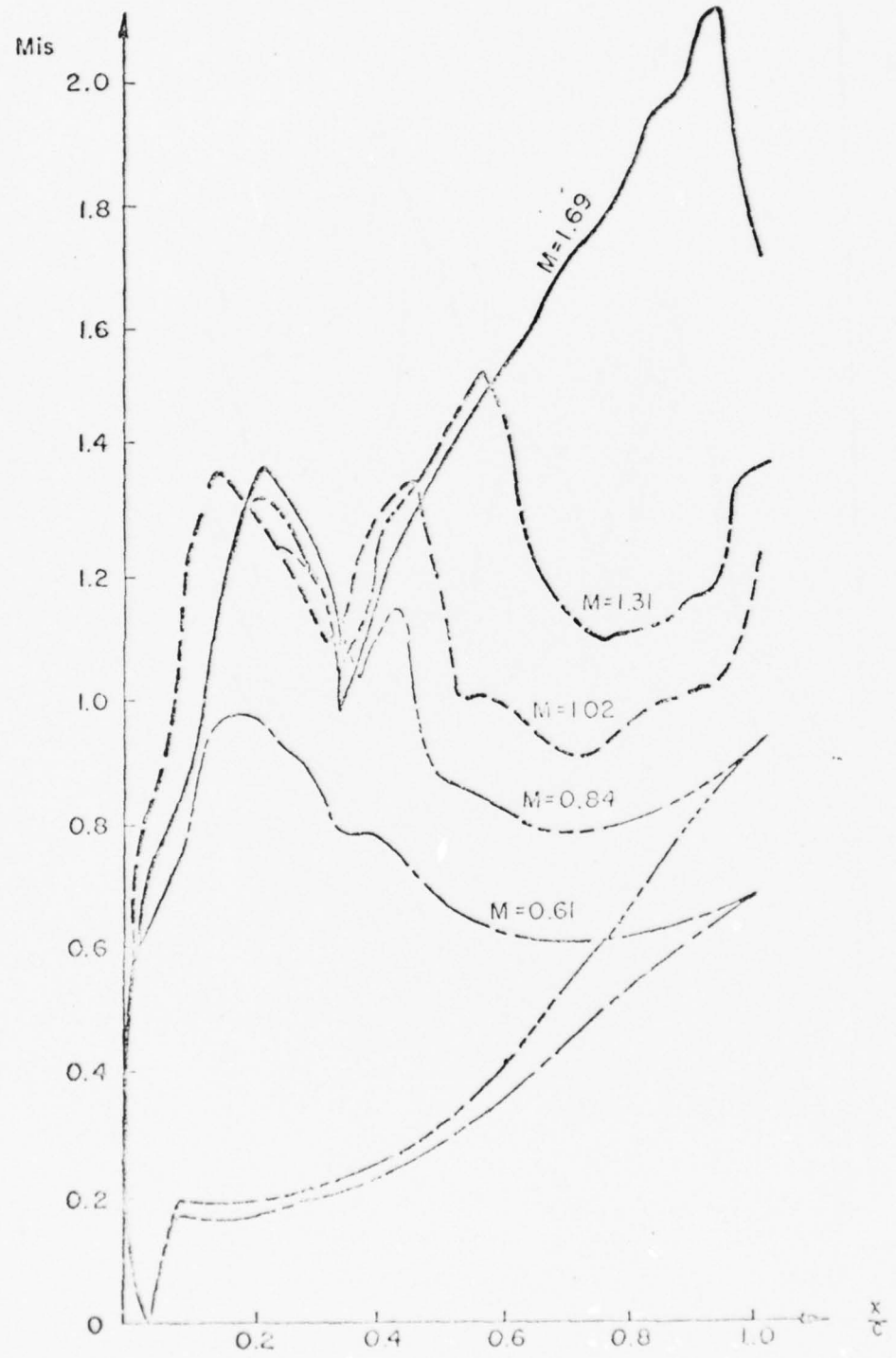

Figure 4 Blade 3 Surface Mach Number Distribution $g/c = 0.75$

BLADE MACH NUMBER DISTRIBUTION

CONVERGENT-DIVERGENT BLADE

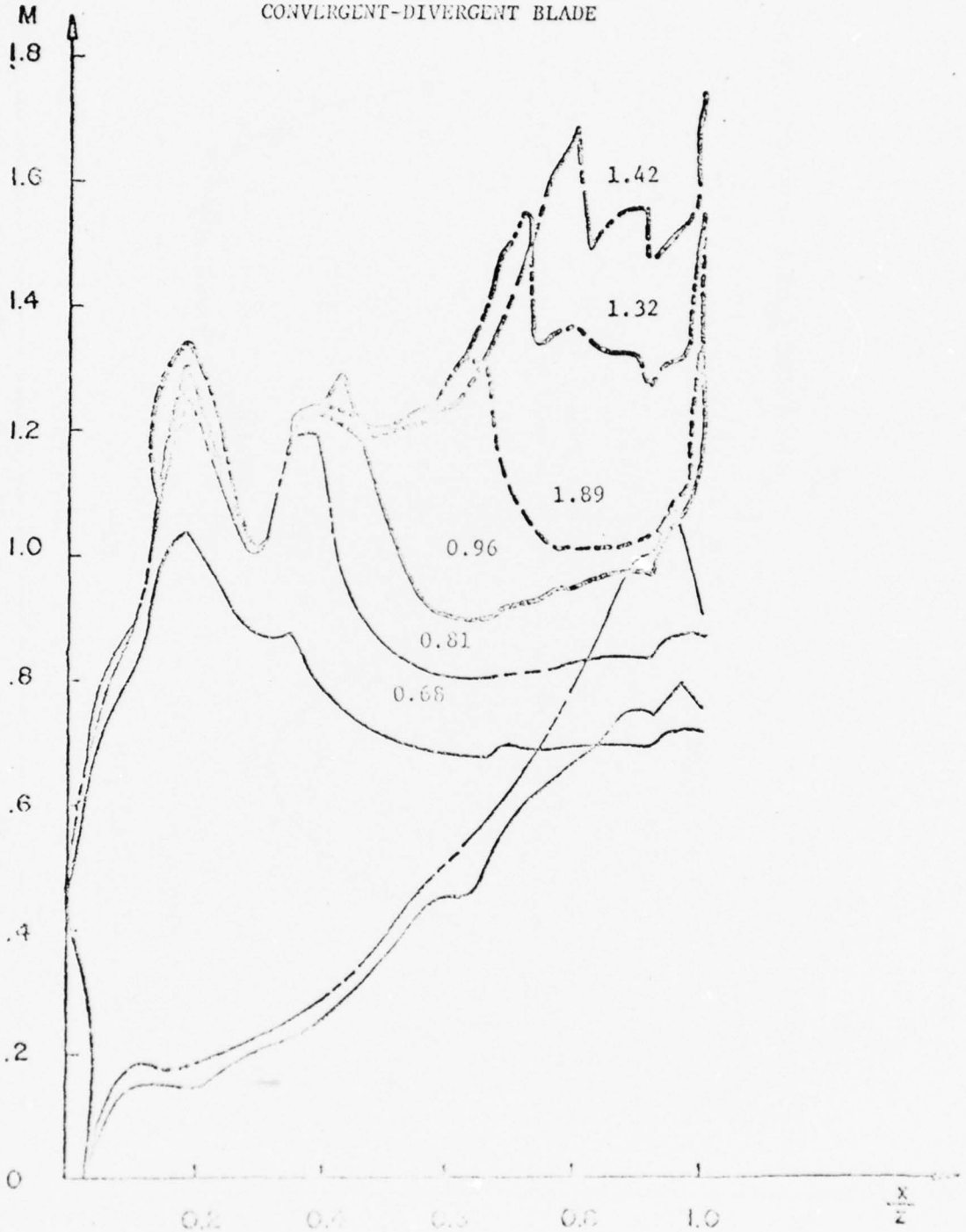

Figure 5 Blade A Surface Mach Number Distribution $g/c = 0.75$

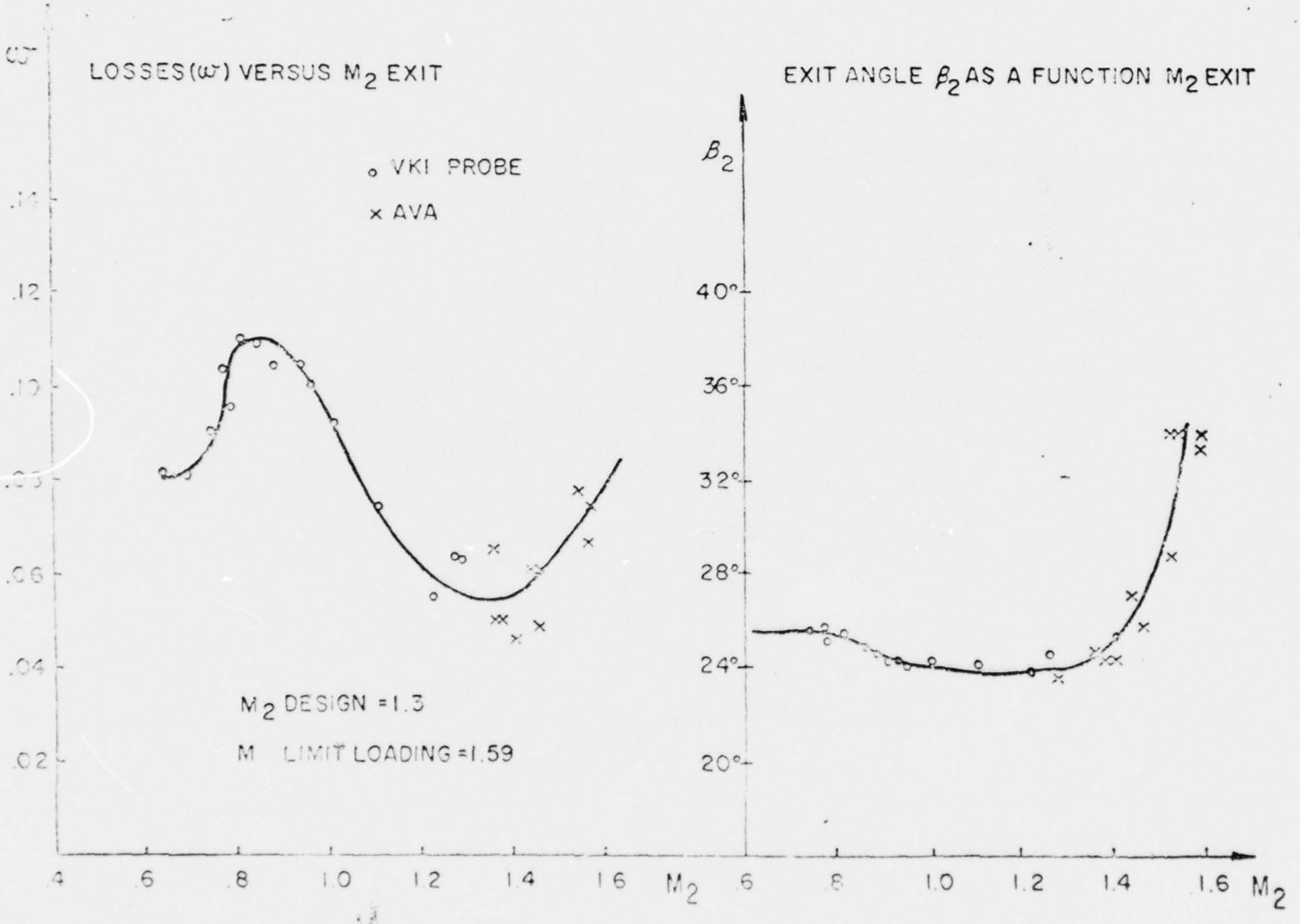

Figure 6 Performance Curve-Blade with Straight Suction Back

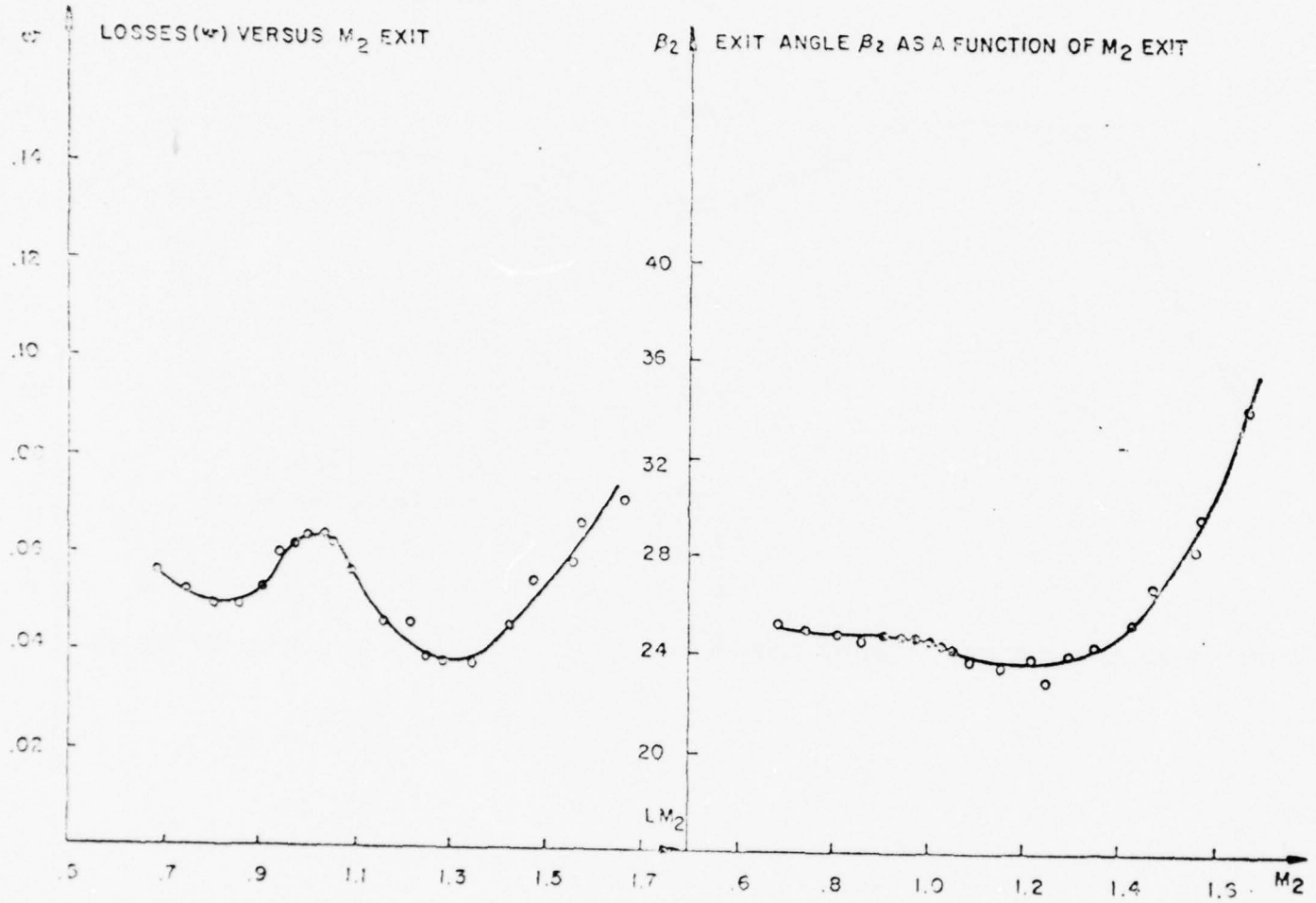

Figure 7 Performance Curve, Convergent Blade, Straight Suction Back with Thin Trailing Edge

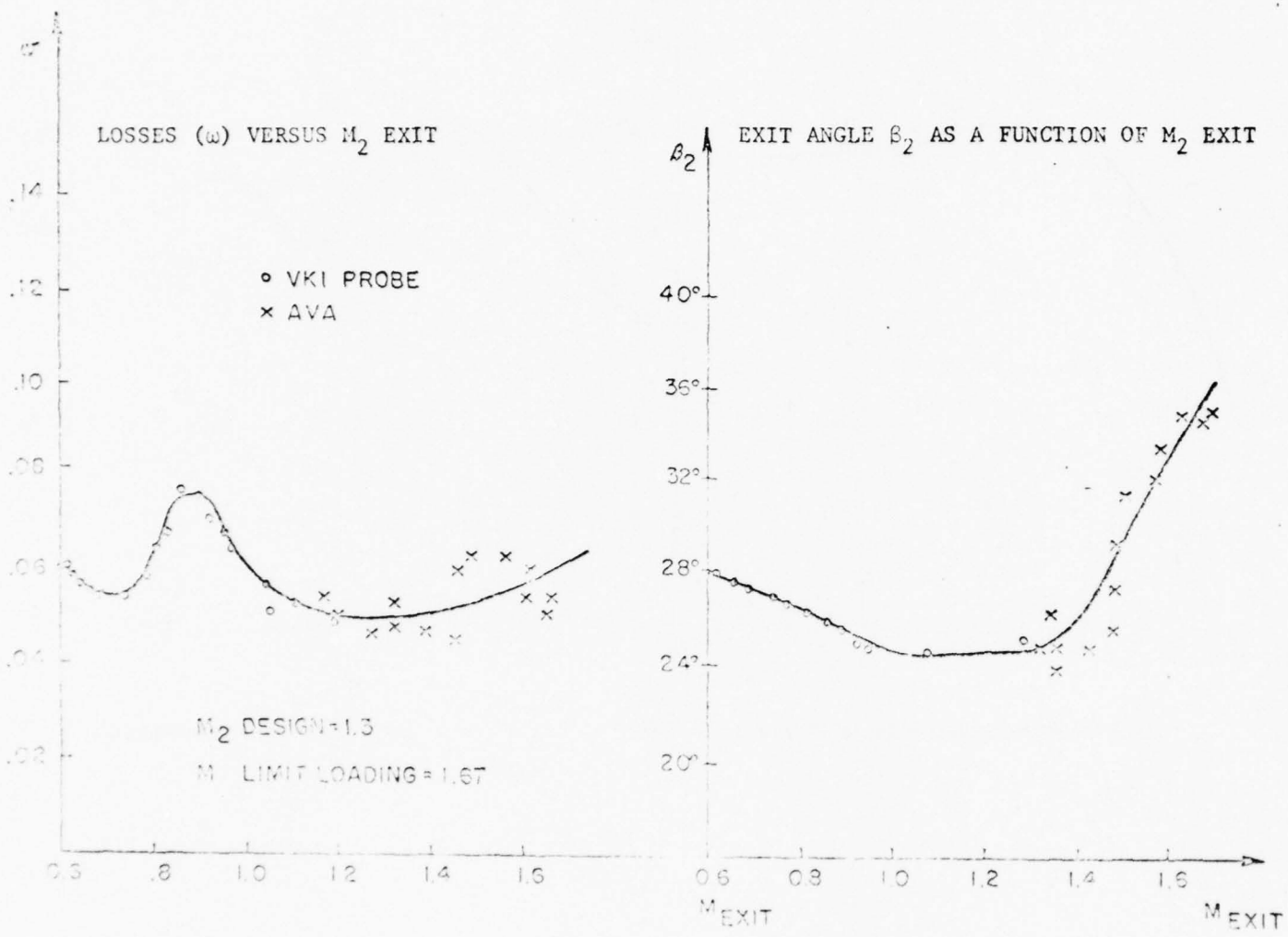

Figure 8 Performance Curve, Blade with Expansion on Suction Side (Plug)

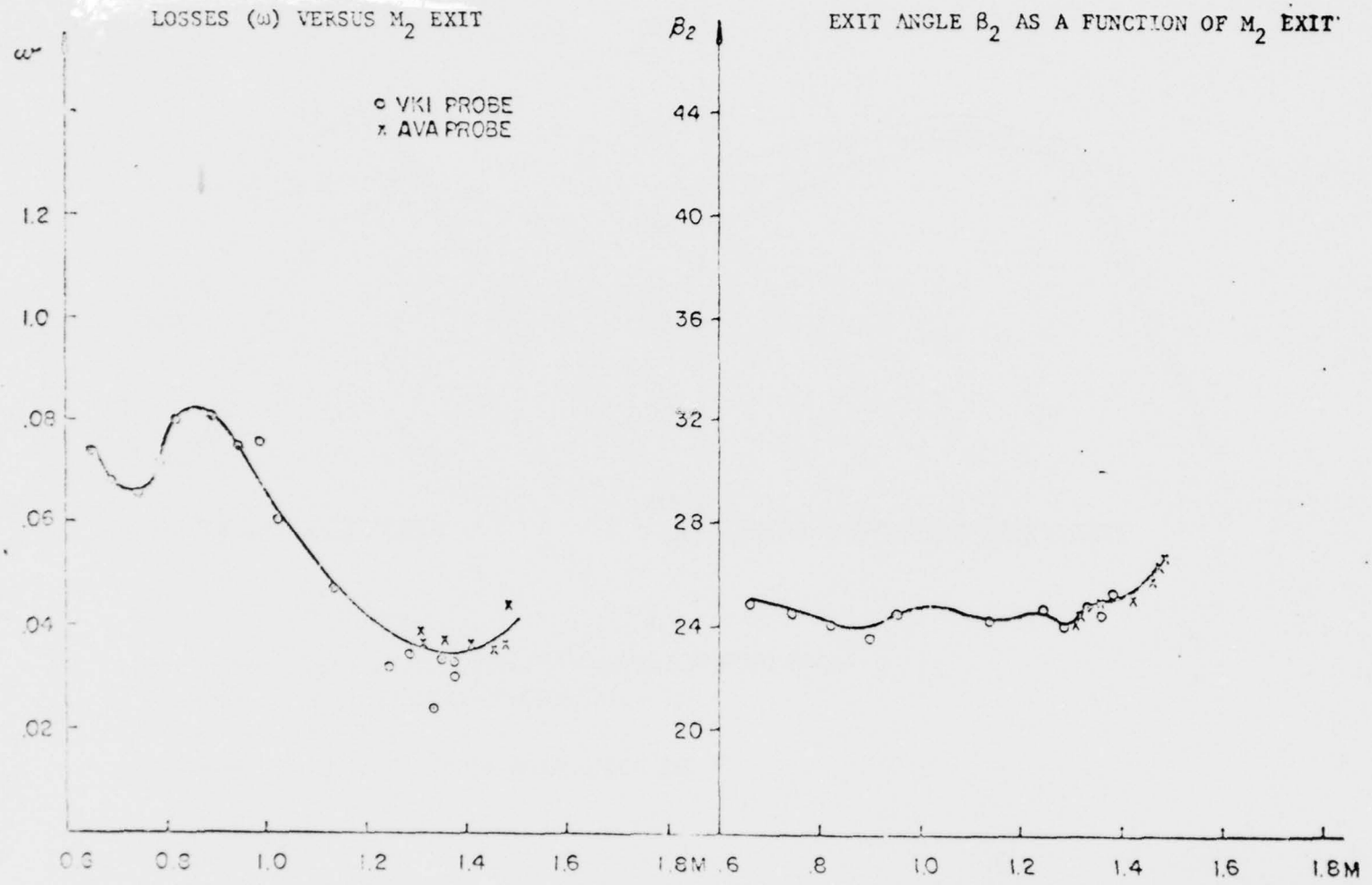

Figure 9 Performance Curve, Convergent-Divergent Blade

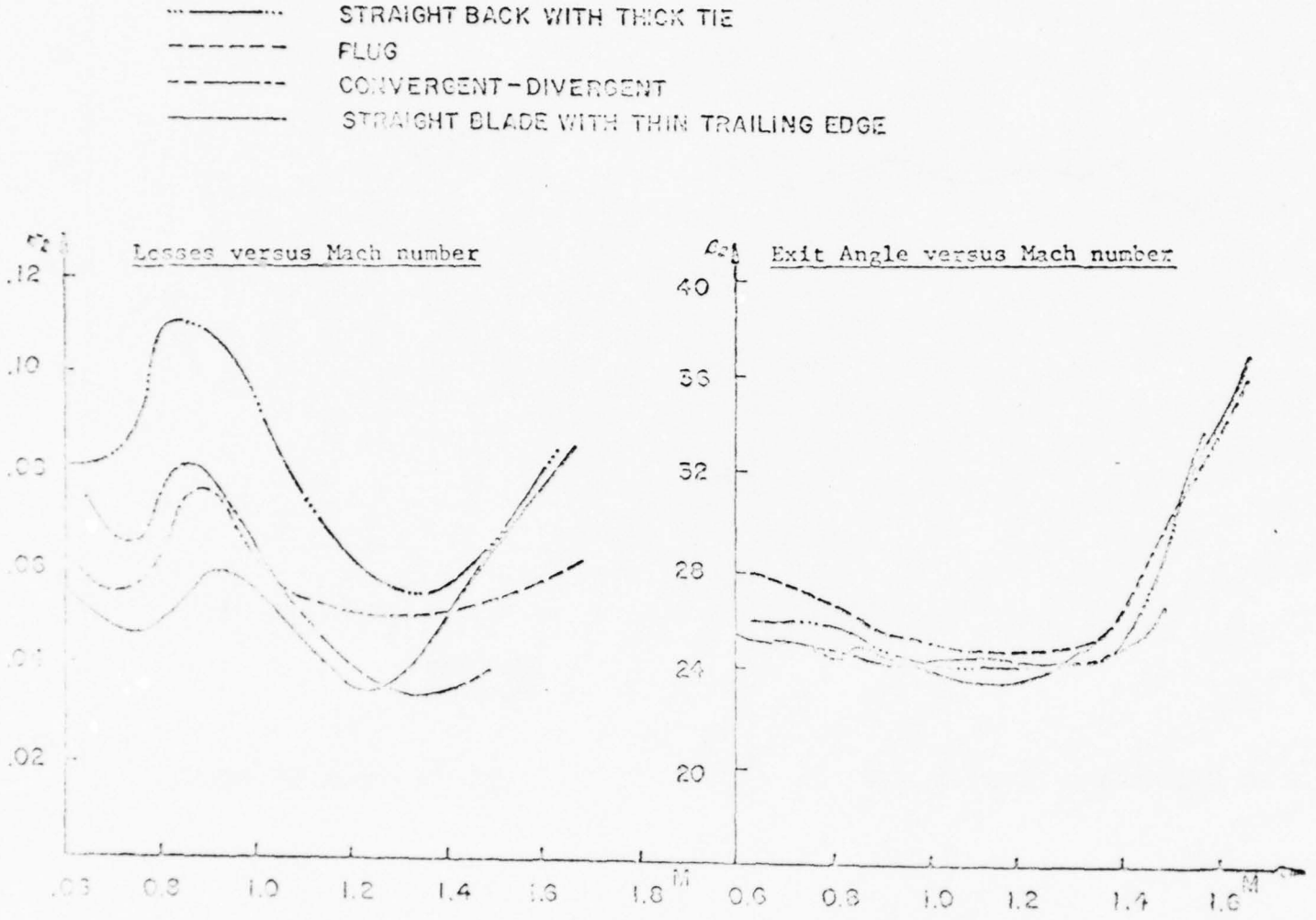

Figure 10 Comparison of Aerodynamic Performance of Different Transonic Turbine Blade Profiles

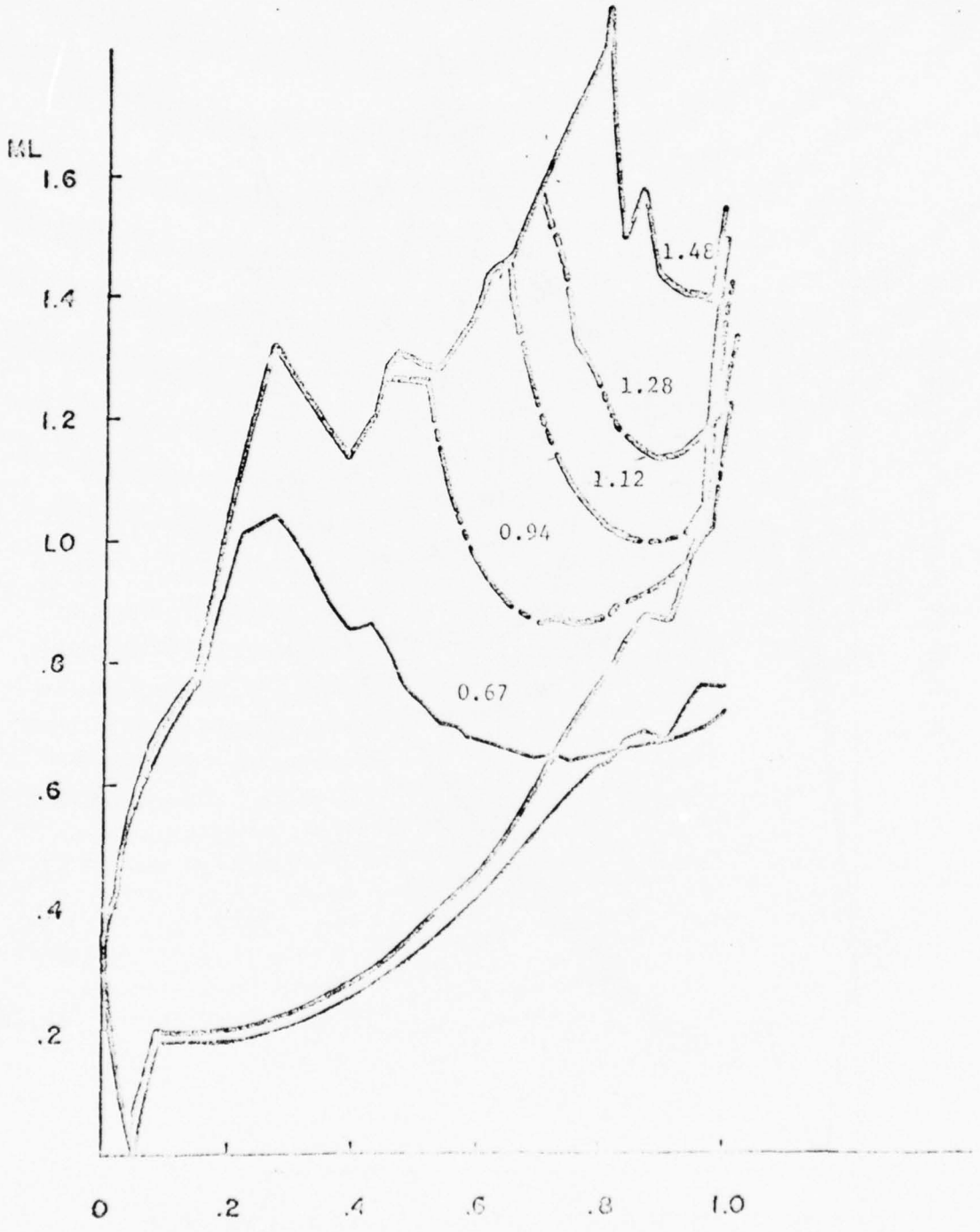

Figure 11 Blade 3 Mach Number Distribution g/c = 0.695

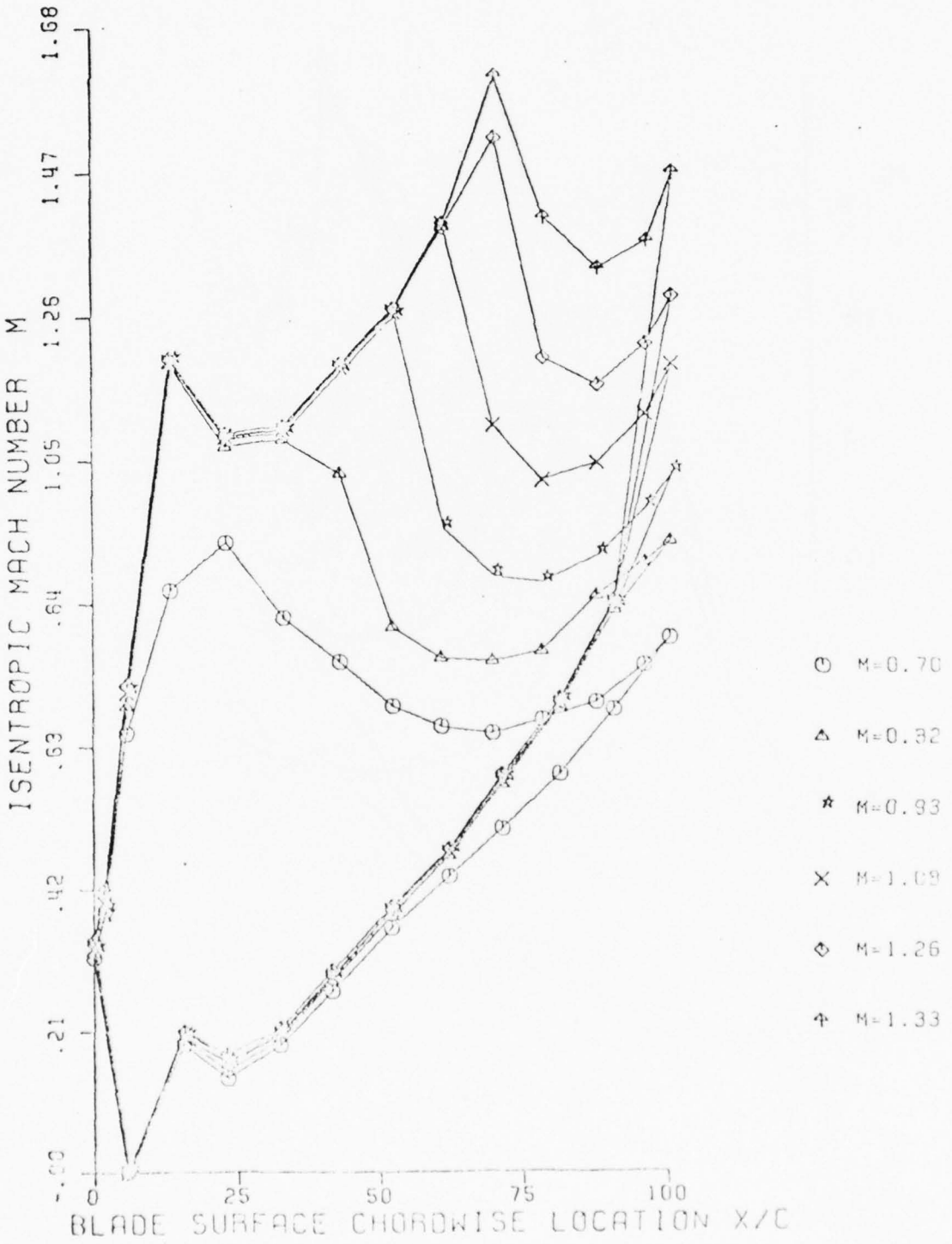

Figure 12. Blade 3 Mach Number Distribution $g/c = 0.695$
(Test conducted in hot blowdown cascade facility)

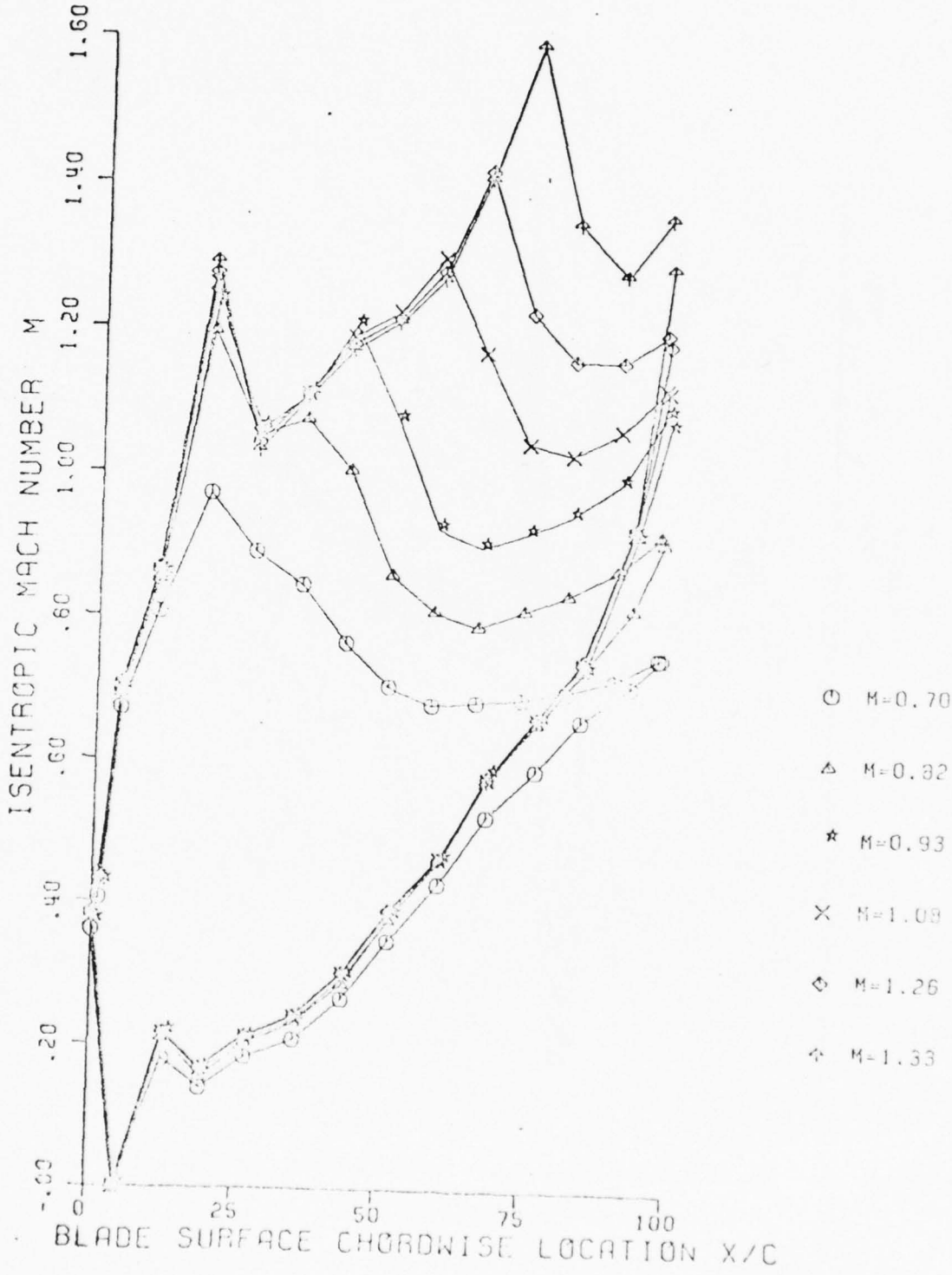

Figure 13 Blade 4 Mach Number Distribution $g/c = 0.695$
(Test conducted in hot blowdown cascade facility)

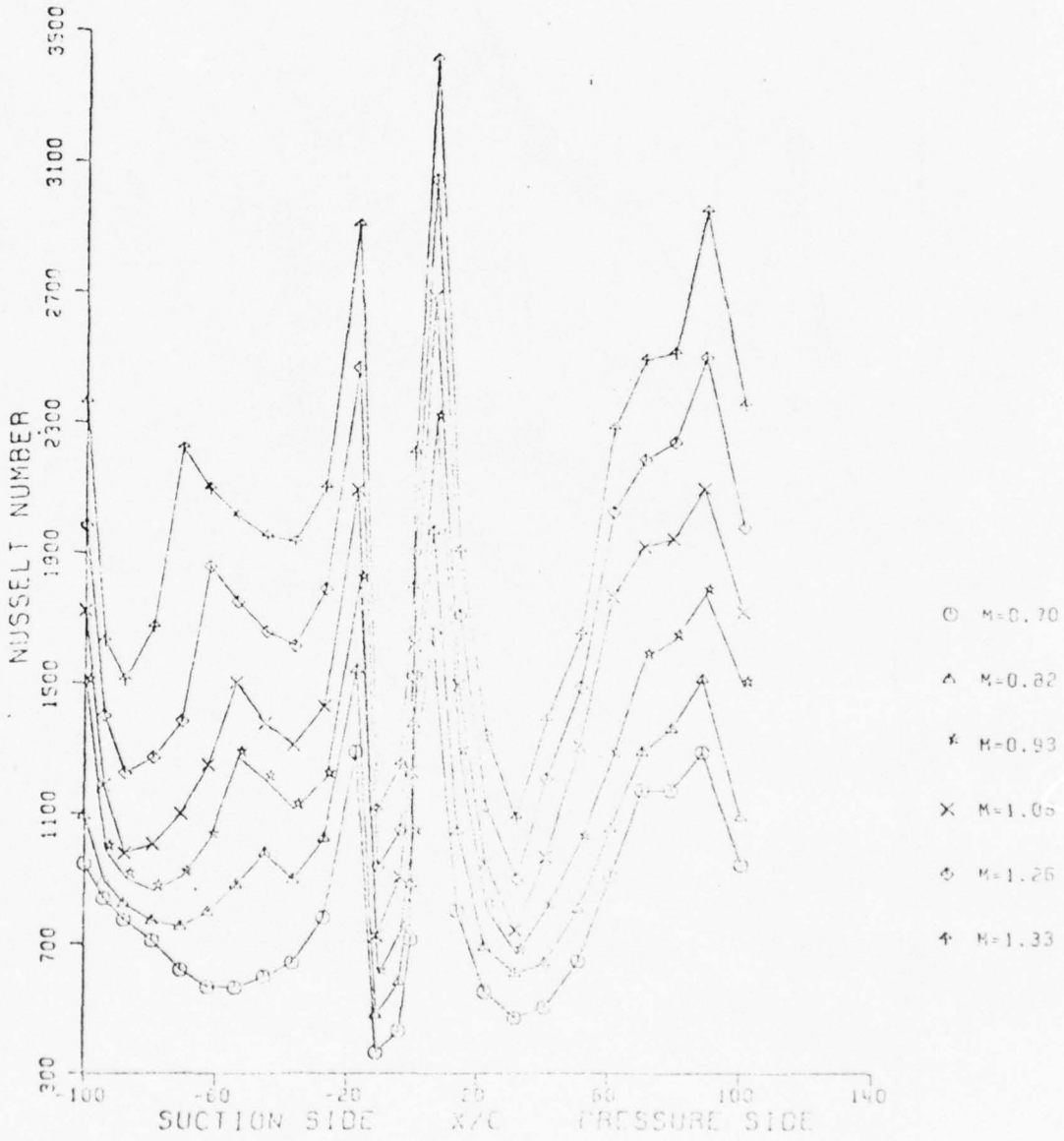

Figure 14 Blade 1 Nusselt number variation over the blade surface for different exit Mach Numbers.

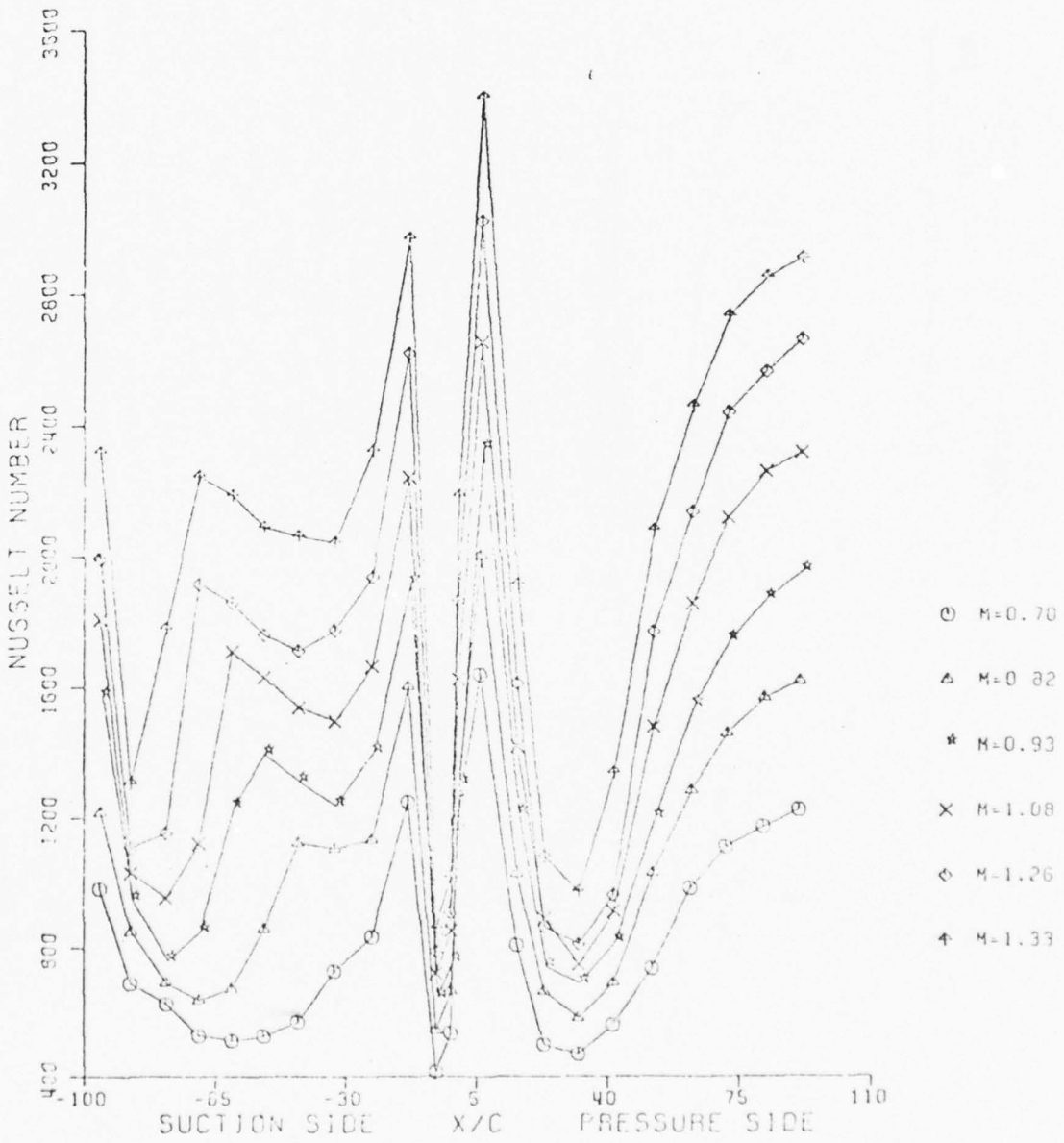

Figure 15 Blade 3 Nusselt number variation over the blade surface for different exit Mach Number.

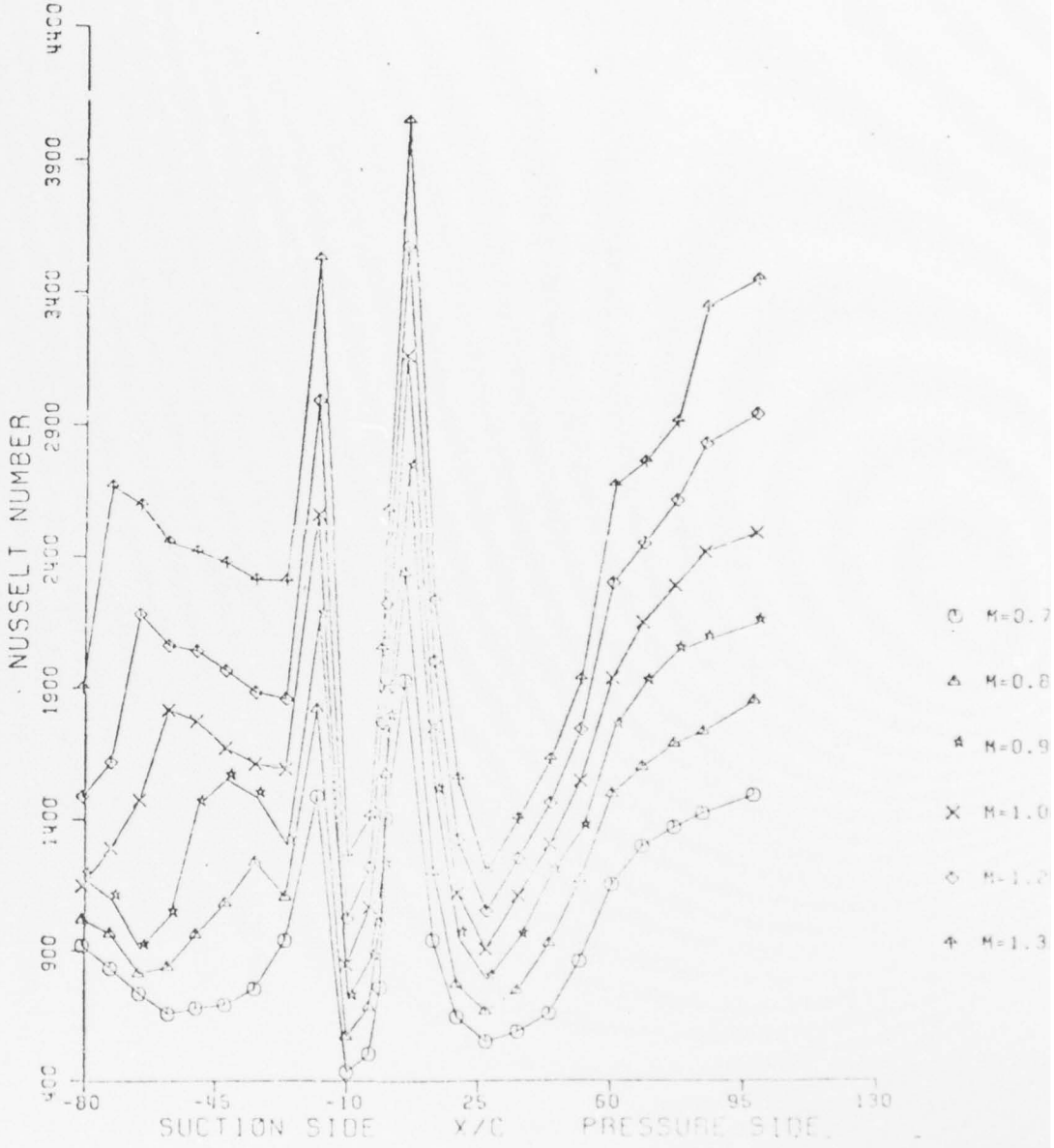

Figure 16 Blade A Nusselt number variation over the blade surface for different exit Mach Number.

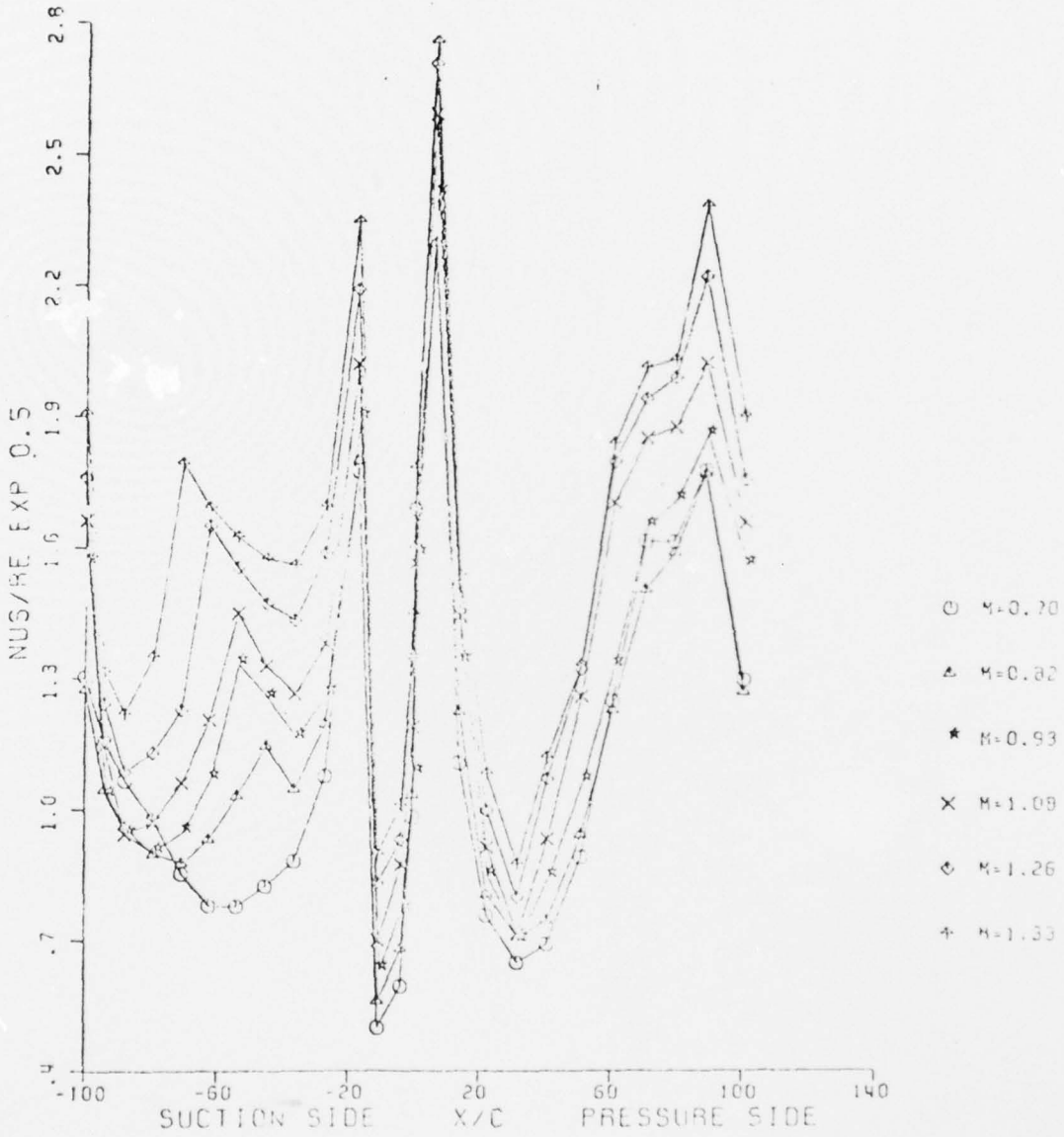

Figure 17 Blade 1 Distribution of $Nu/Re^{0.5}$ Over the Blade Surface

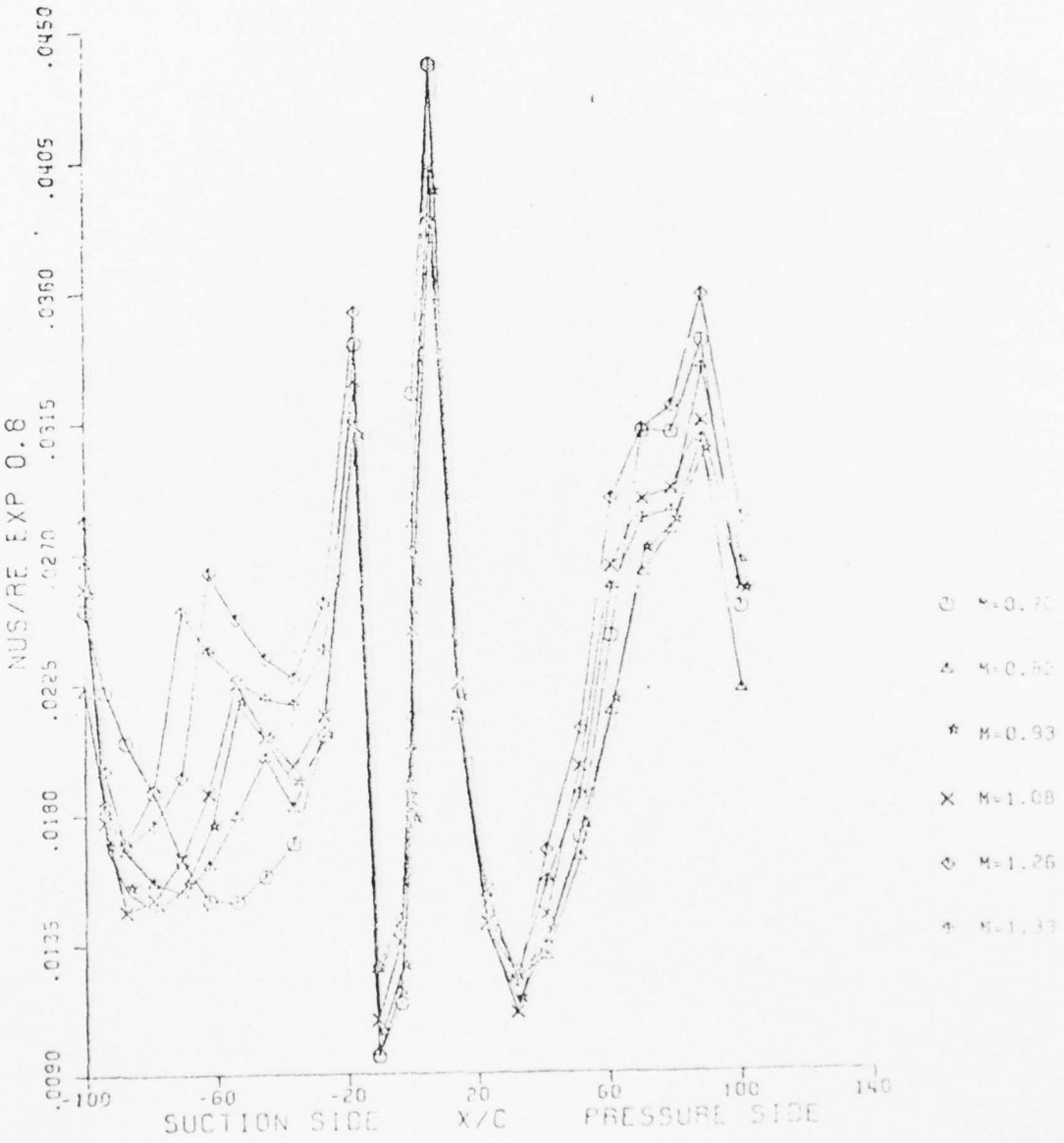

Figure 13 Blade 1 Distribution of $Nu/Re^{0.8}$ Over the Blade Surface

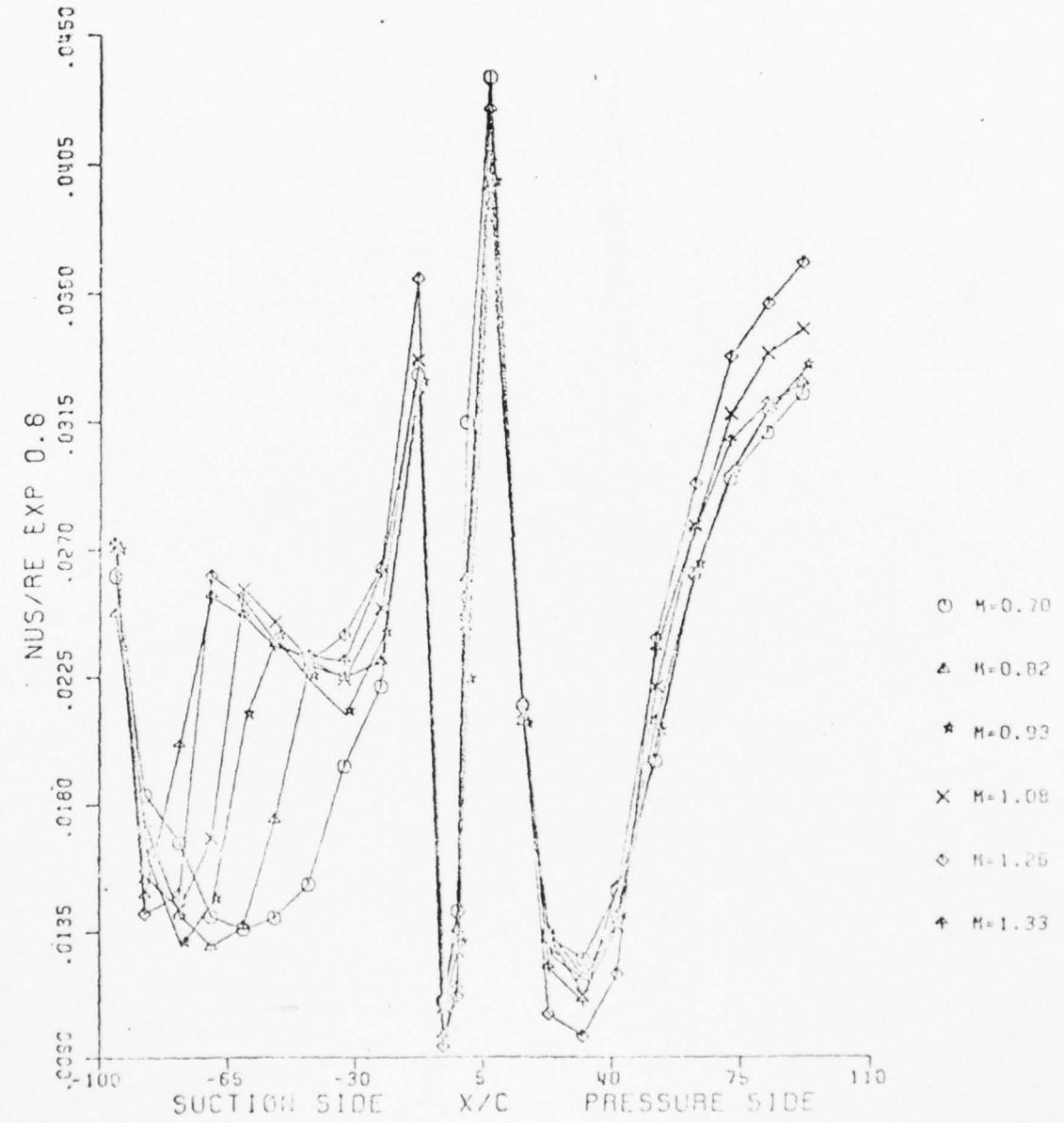

Figure 19 Blade 3 Distribution of $Nu/Re^{0.6}$ Over the Blade Surface

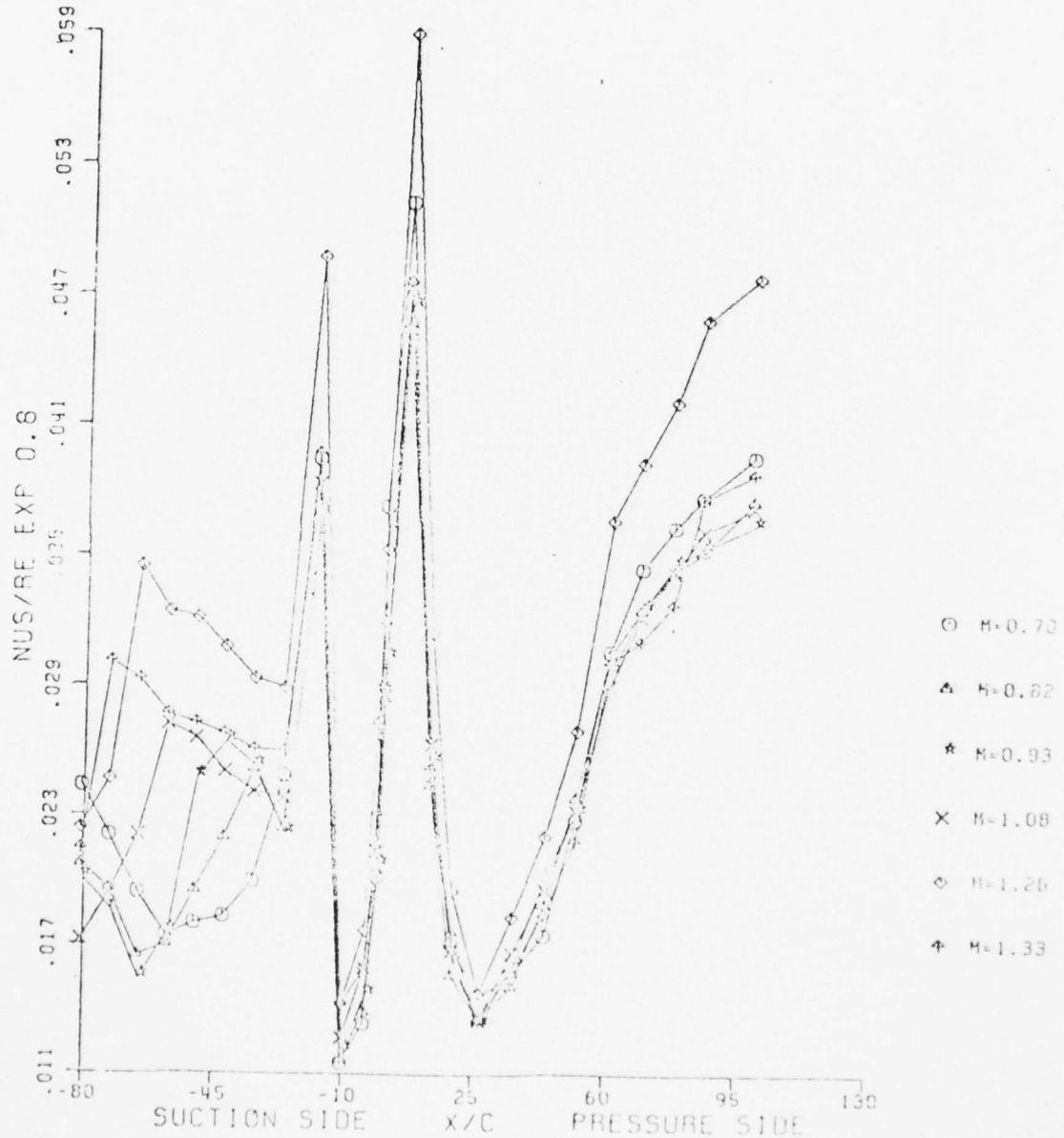

Figure 20 Blade 4 Distribution of $Nu/Re^{0.8}$ over the blade surface.

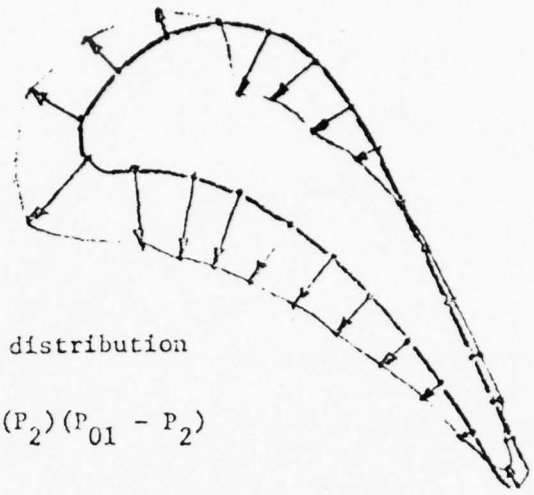

Blade 1 Static Pressure distribution
M = 0.7

$$\bar{P} = (P - (P_2)(P_{01} - P_2)$$

1 cm = 1 $\bar{P}$

Blade 1 Nusselt number distribution M = 0.7

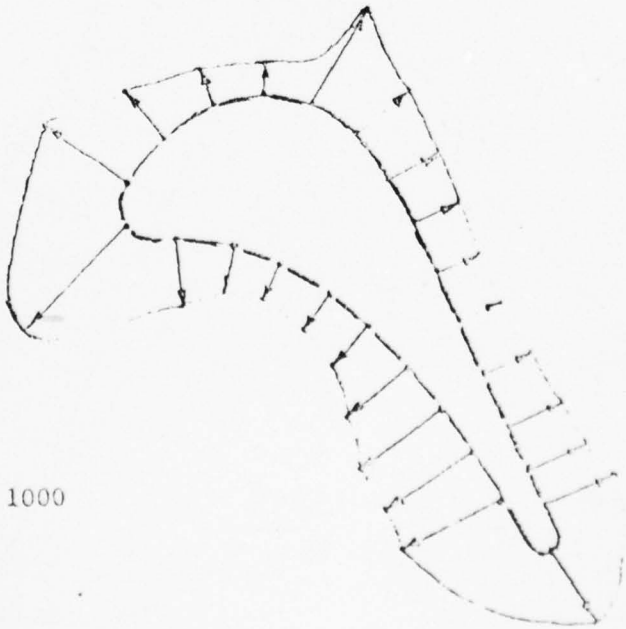

1 cm = Nu no. of 1000

Figure 21 Blade 1 Pressure and Mach Number Distributions $M_2 = 0.7$

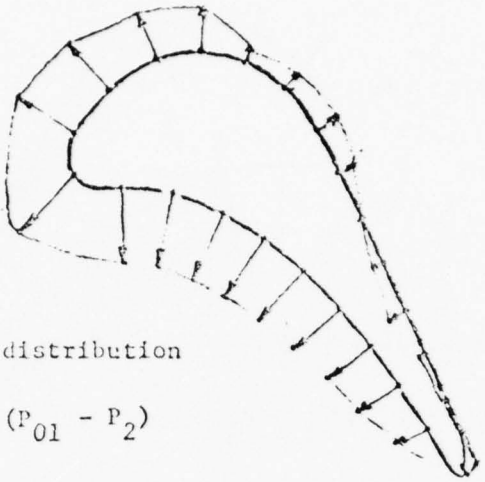

Blade 1 Static Pressure distribution

$M = 1.33$

$\bar{P} = (P-P_2)(P_{01} - P_2)$

1 cm = 1 $\bar{P}$

Blade 1 Mach number distribution M = 1.33

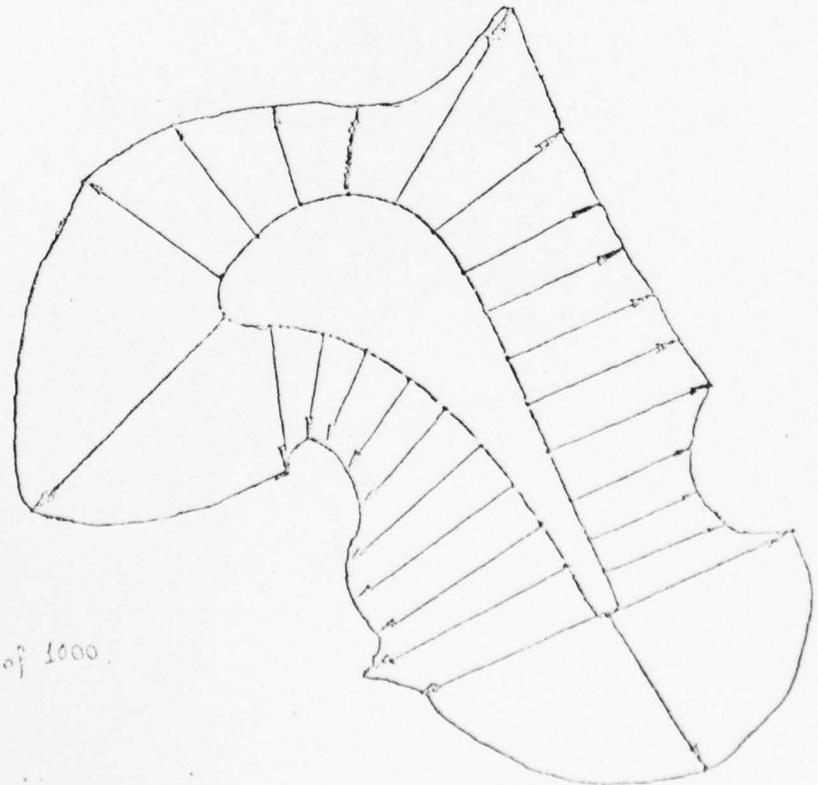

1 cm = Mach no. of 1000.

Figure 22 Blade 1 Pressure and Mach Number Distributions $M_2 = 1.33$

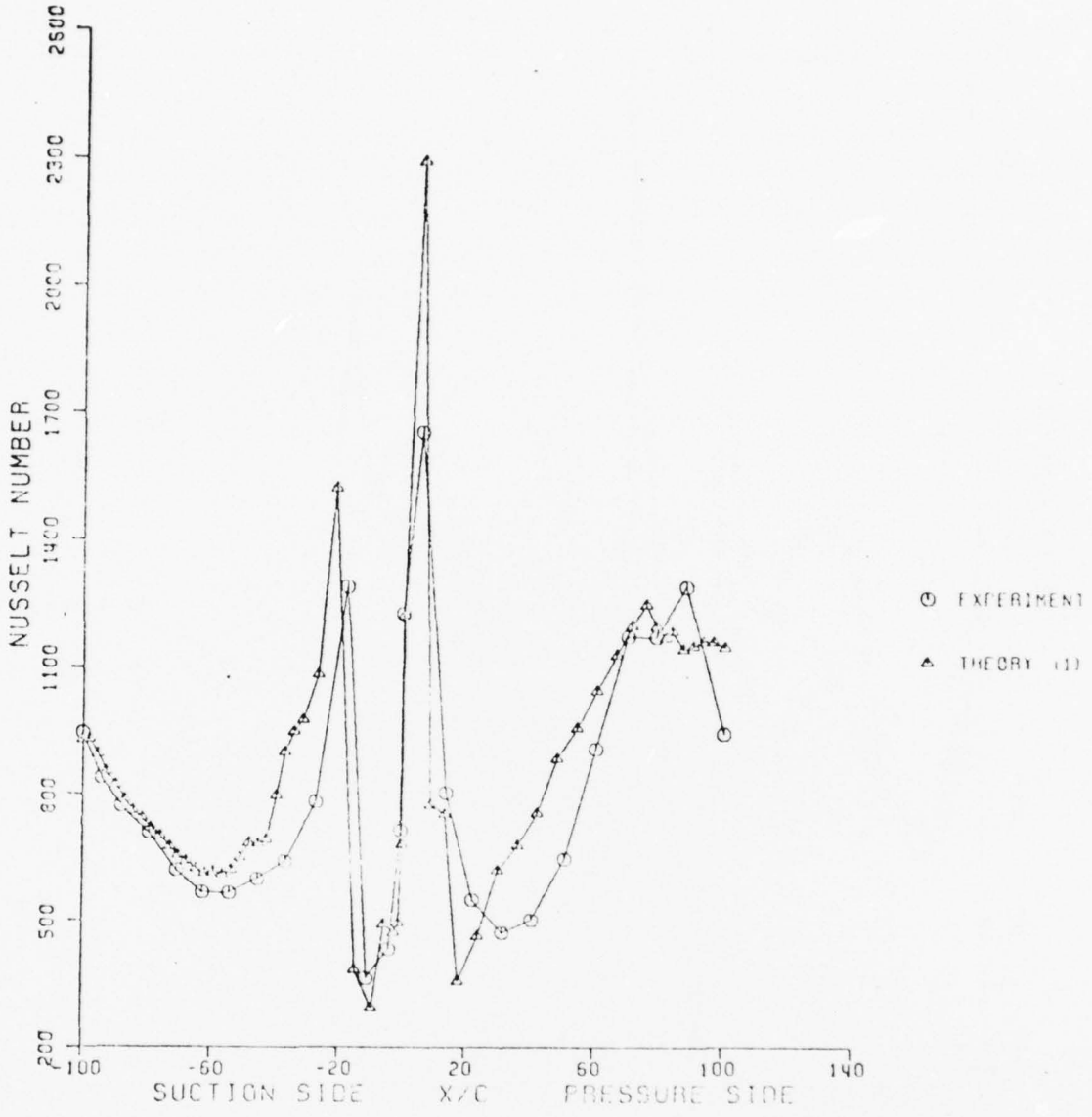

Figure 23 Comparison between $Nu_{experimental}$ and $Nu_{theoretical\ prediction}$ for Blade 1 at M = 0.7 (using hot flow high turbulence level (10%) experimental pressure distribution)

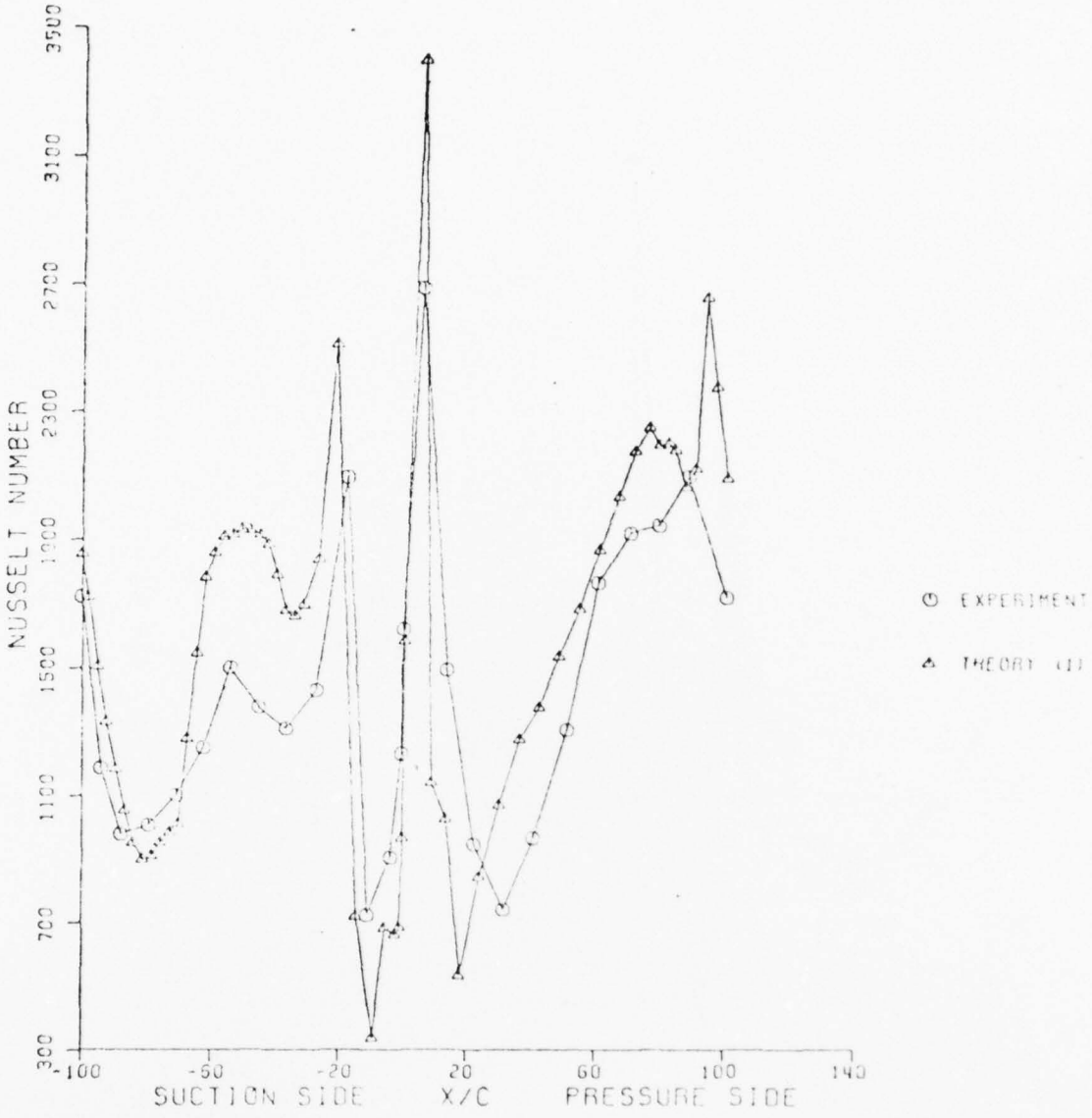

Figure 24 Comparison between Nu_{exp} and $Nu_{theor.\ pre}$ for Blade 1 at M = 1.08 (using hot flow high turbulence level (10%) experimental pressure distribution)

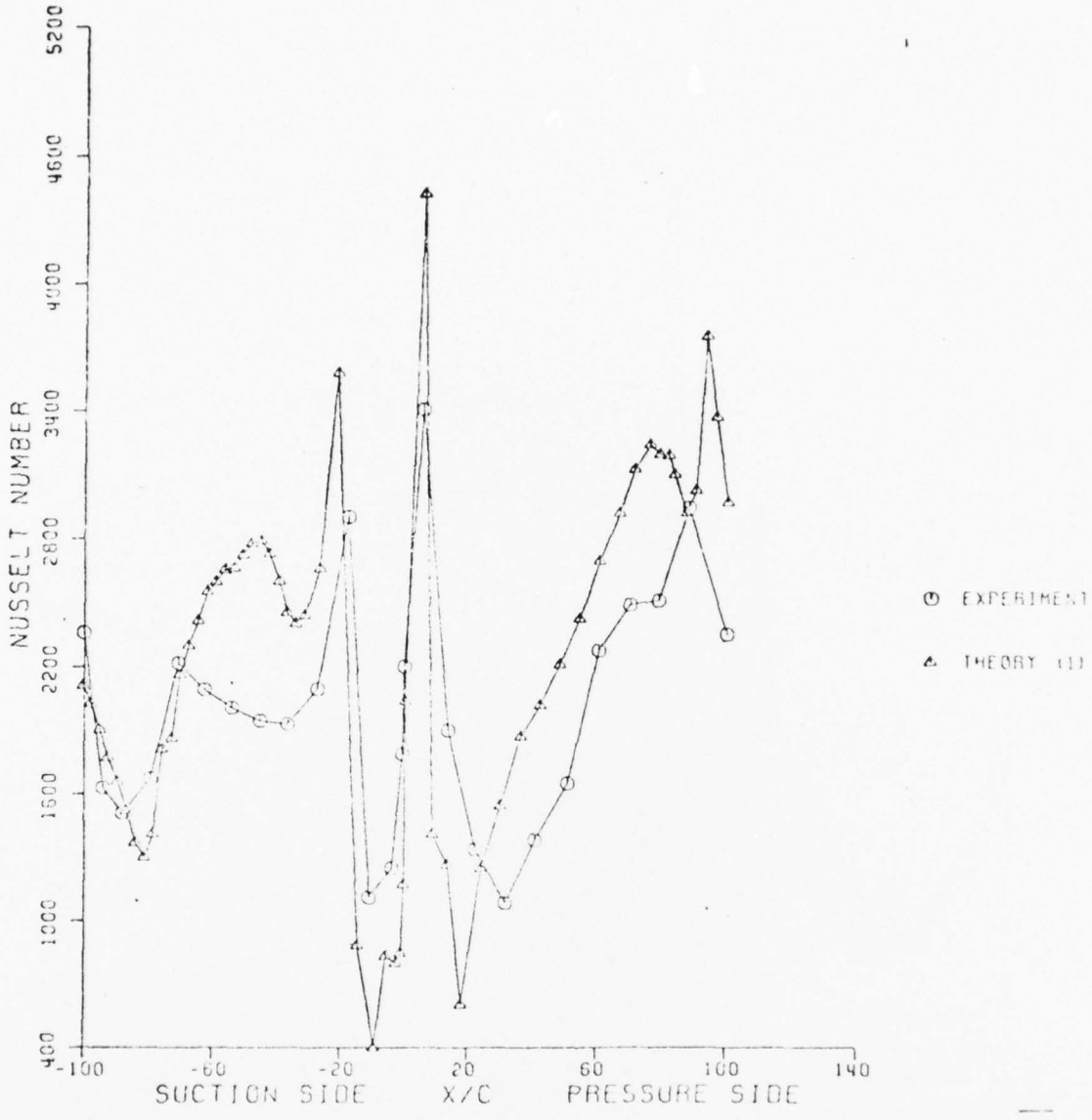

Figure 25 Comparison between Nu_{exp} and $Nu_{theor.\ pre}$ for Blade 1 at M = 1.33 (using hot flow high turbulence level (10%) experimental pressure distribution)

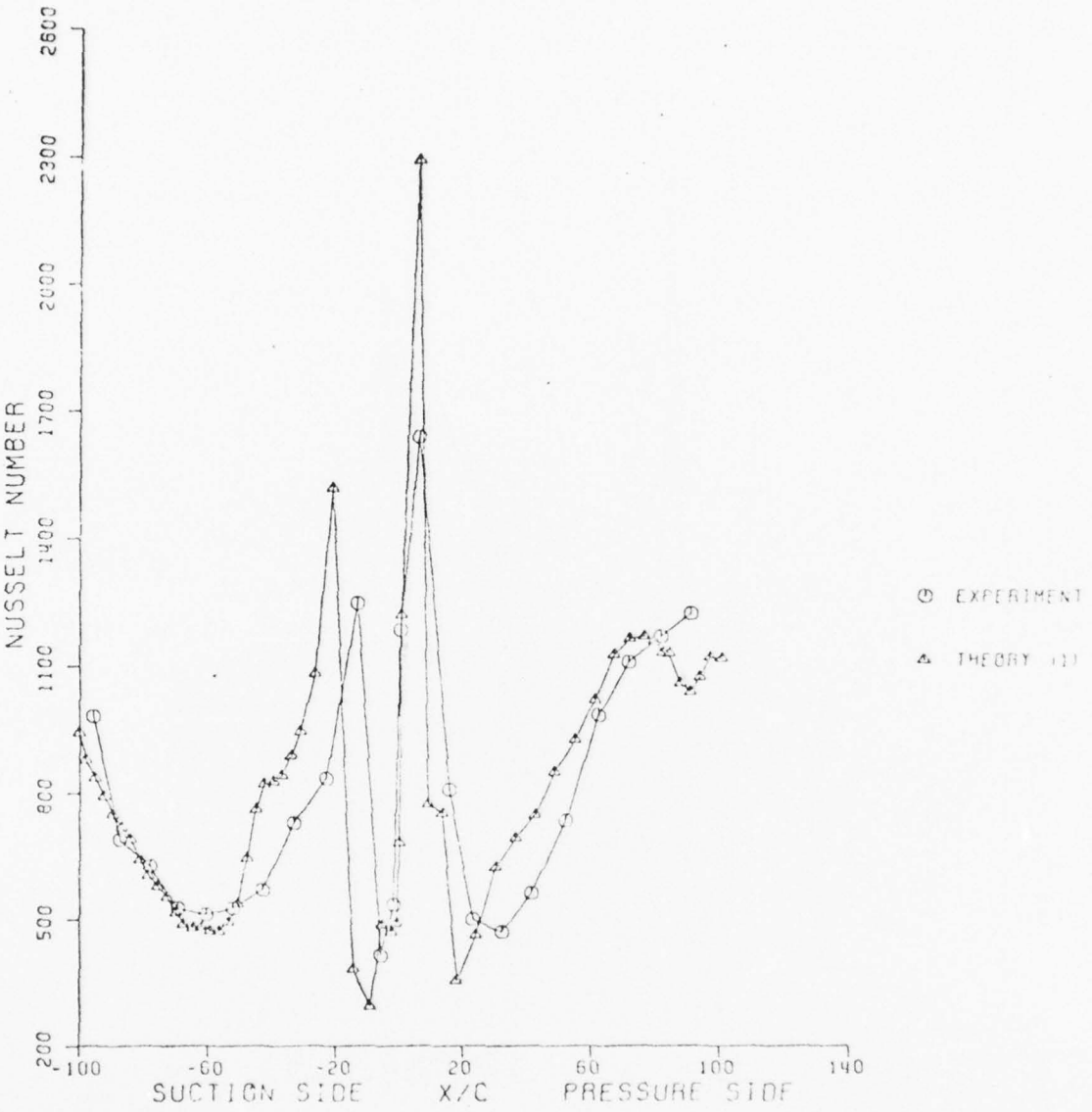

Figure 26 Comparison between Nu_{exp} and $Nu_{theor.\ pre}$ for Blade 3, $M_{exit} = 0.7$ (using hot flow high turbulence level (30%) experimental pressure distribution)

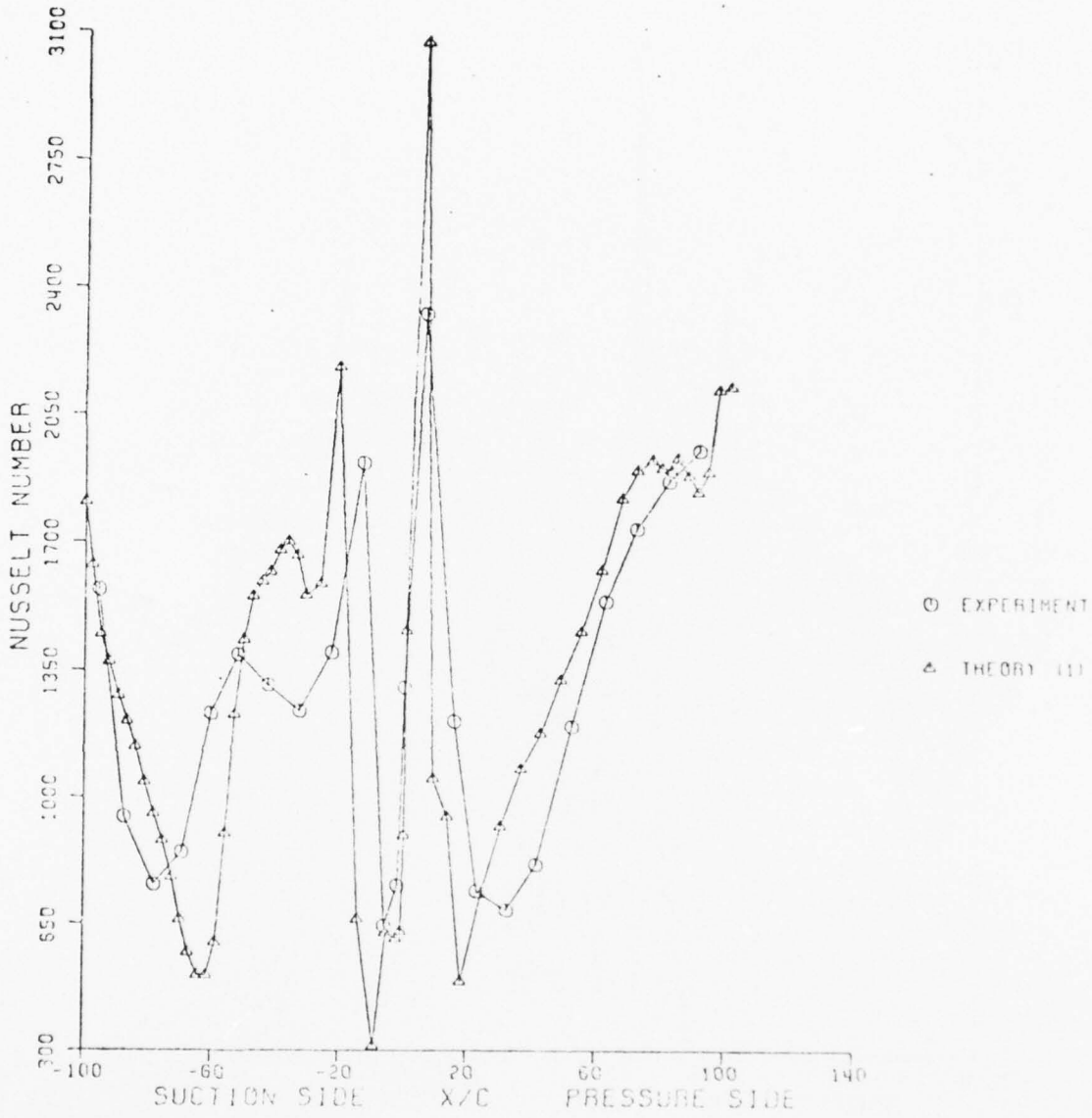

Figure 27 Comparison between Nu_{exp} and $Nu_{theor.\ prc}$ for Blade 3, $M_{exit} = 0.93$ (using hot flow high turbulence level (10%) experimental pressure distribution)

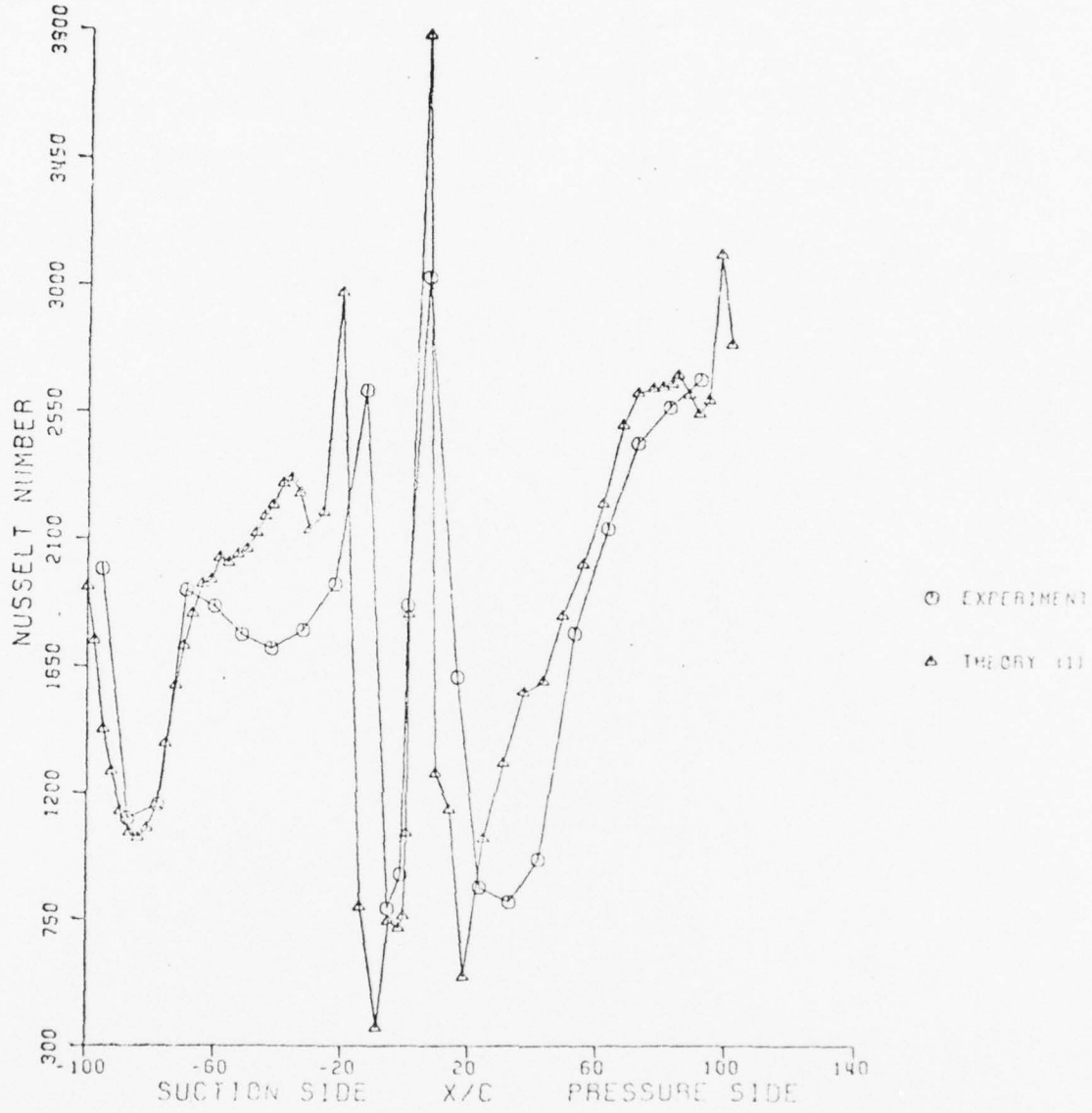

Figure 28 Comparison between Nu_{exp} and $Nu_{theor.\ pre}$ for Blade 3, $M_{exit} = 1.26$ (using hot flow high turbulence level (10%) experimental pressure distribution)

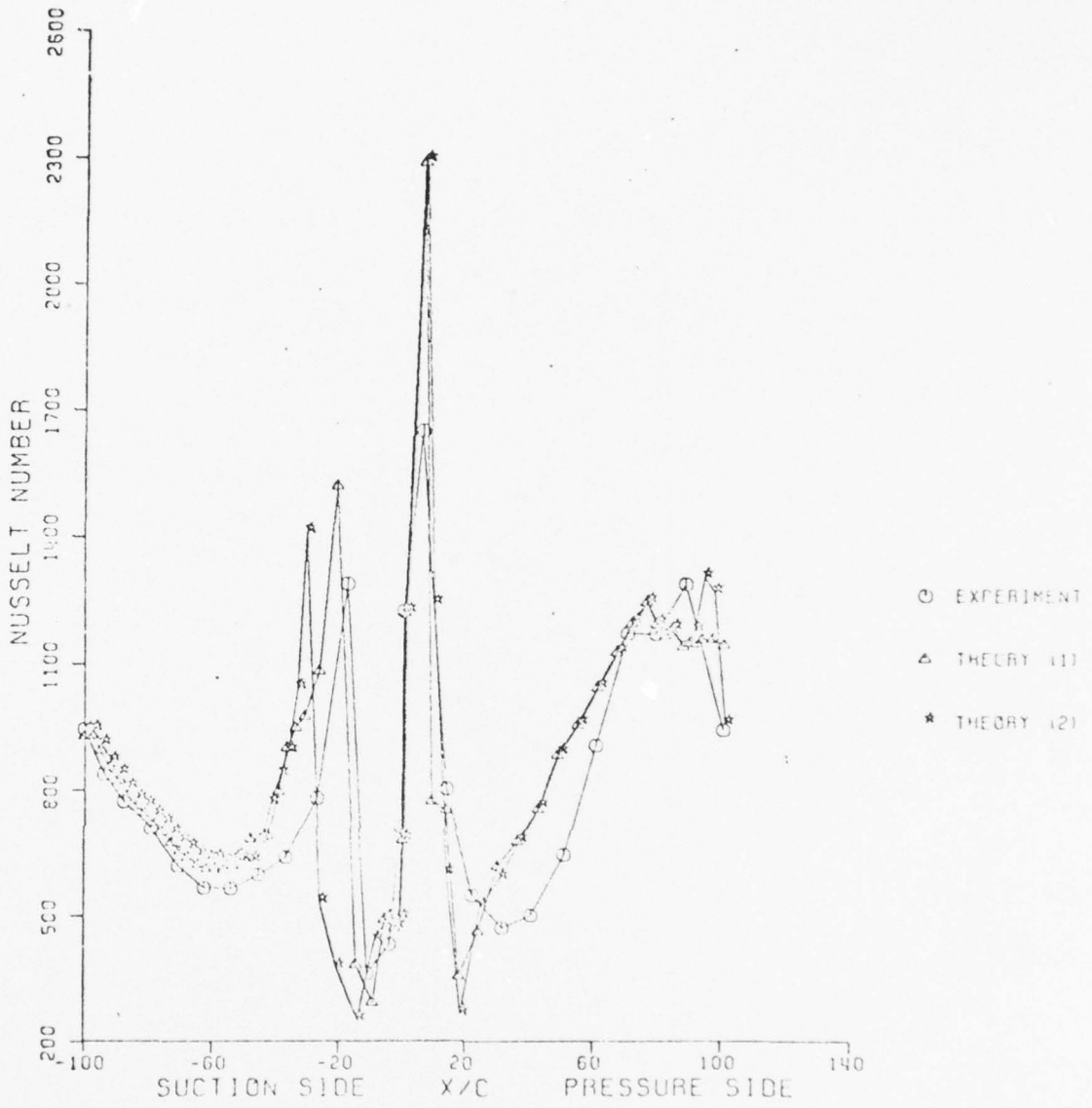

Figure 29 Comparison between Nu_{exp}, $Nu_{theor.pre.(1)}$ and $Nu_{theor.pre.(2)}$ for Blade 1 at M = 0.7. Theory (1) is based on hot flow high turbulence (10%) experimental pressure distribution. Theory (2) is based on cold flow low turbulence (0.7%) experimental pressure distribution.

AD-A036 402 MASSACHUSETTS INST OF TECH CAMBRIDGE GAS TURBINE LAB F/G 21/5
STUDIES ON TRANSONIC TURBINES WITH FILM-COOLED BLADES.(U)
JUN 76 H O DEMUREN, N ADAMS, F HAJJAR N00014-67-A-0204-0079
UNCLASSIFIED TR-76-1 NL

2 OF 2
ADA036402

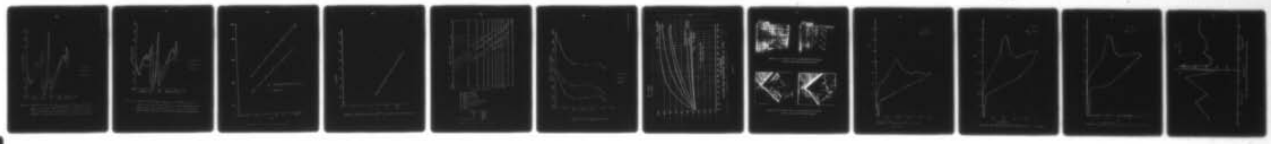

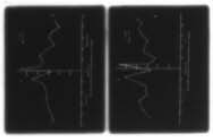

END

DATE
FILMED
3-77

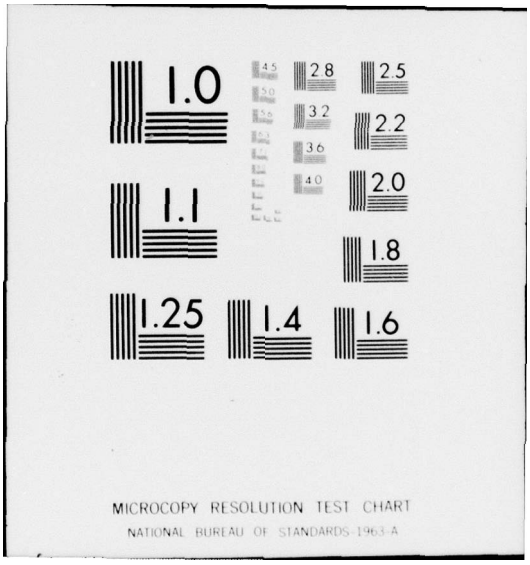
1.0
1.1
1.25
1.4
1.6
1.8
2.0
2.2
2.5
2.8
3.2
3.6
4.0
4.5
5.0
5.6
MICROCOPY RESOLUTION TEST CHART
NATIONAL BUREAU OF STANDARDS-1963-A

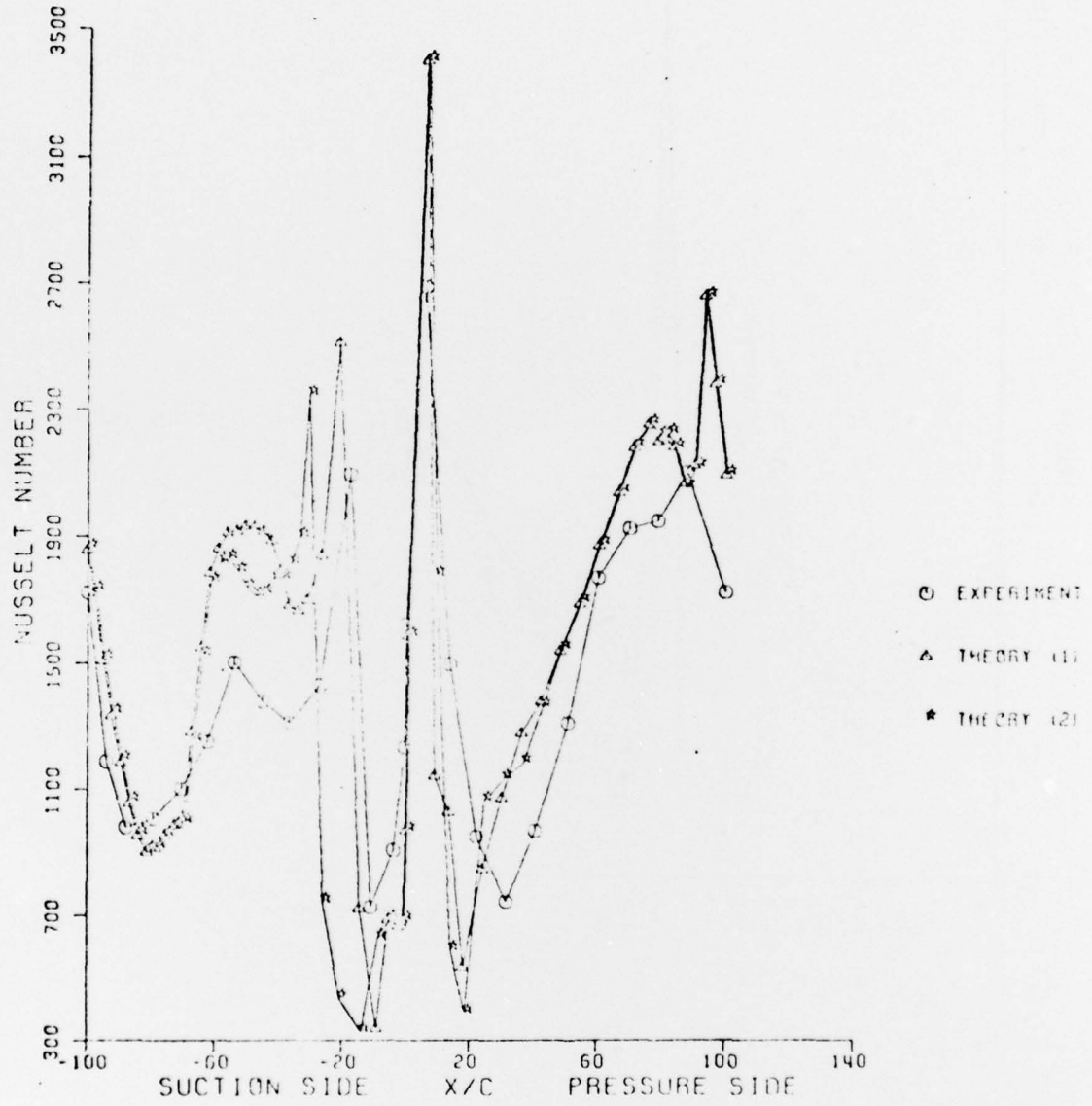

Figure 30 Comparison between Nu_{exp}, $Nu_{theor.pre.(1)}$ and $Nu_{theor.pre.(2)}$ for Blade 1 at M = 1.08. Theory (1) is based on hot flow high turbulence (10%) experimental pressure distribution. Theory (2) is based on cold flow low turbulence (0.7%) experimental pressure distribution.

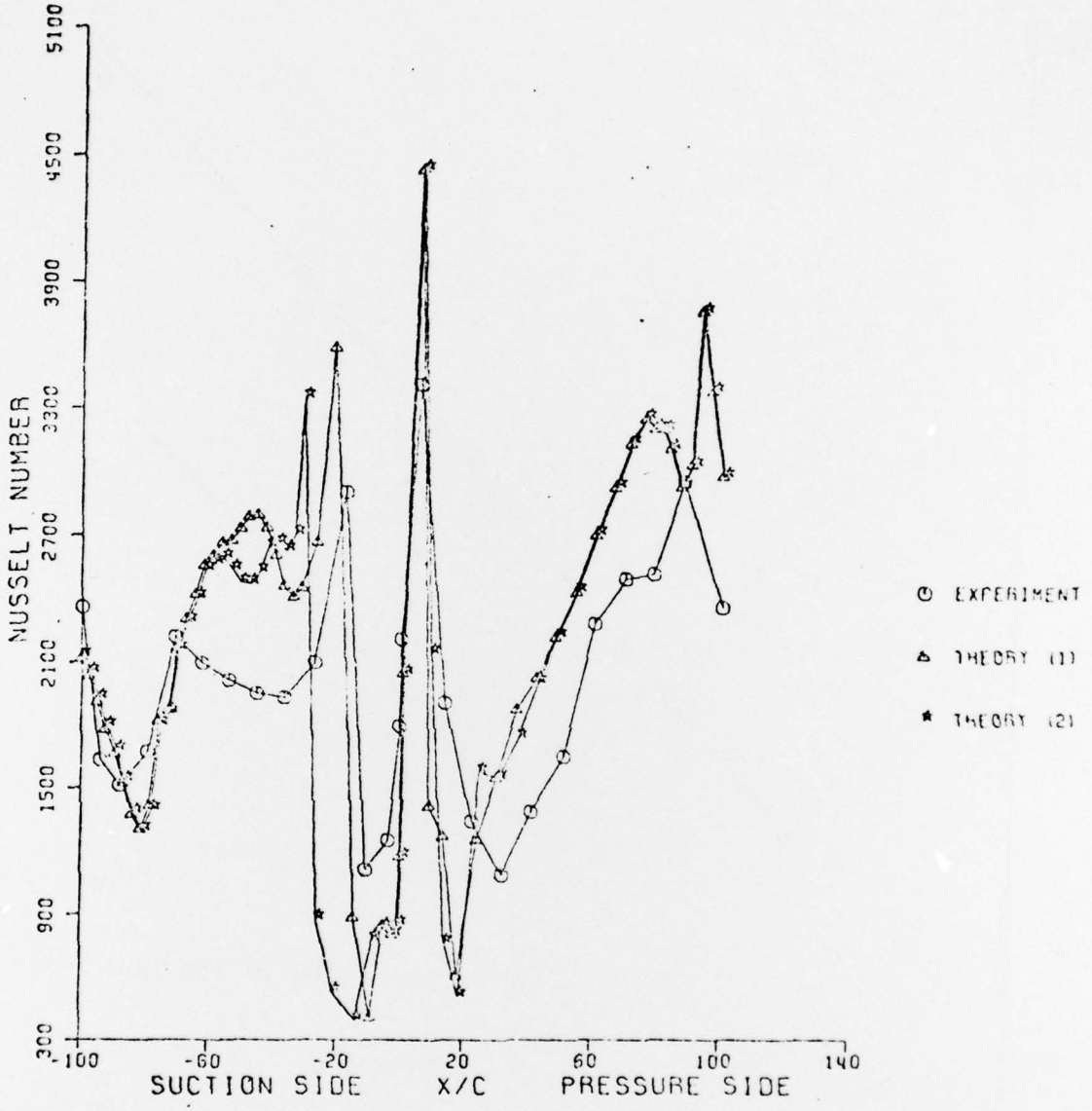

Figure 31 Comparison between Nu_{exp}, $Nu_{theor.pre.(1)}$ and $Nu_{theor.pre.(2)}$ for Blade 1 at M = 1.33. Theory (1) is based on hot flow high turbulence (10%) experimental pressure distribution. Theory (2) is based on cold flow low turbulence (0.7%) experimental pressure distribution.

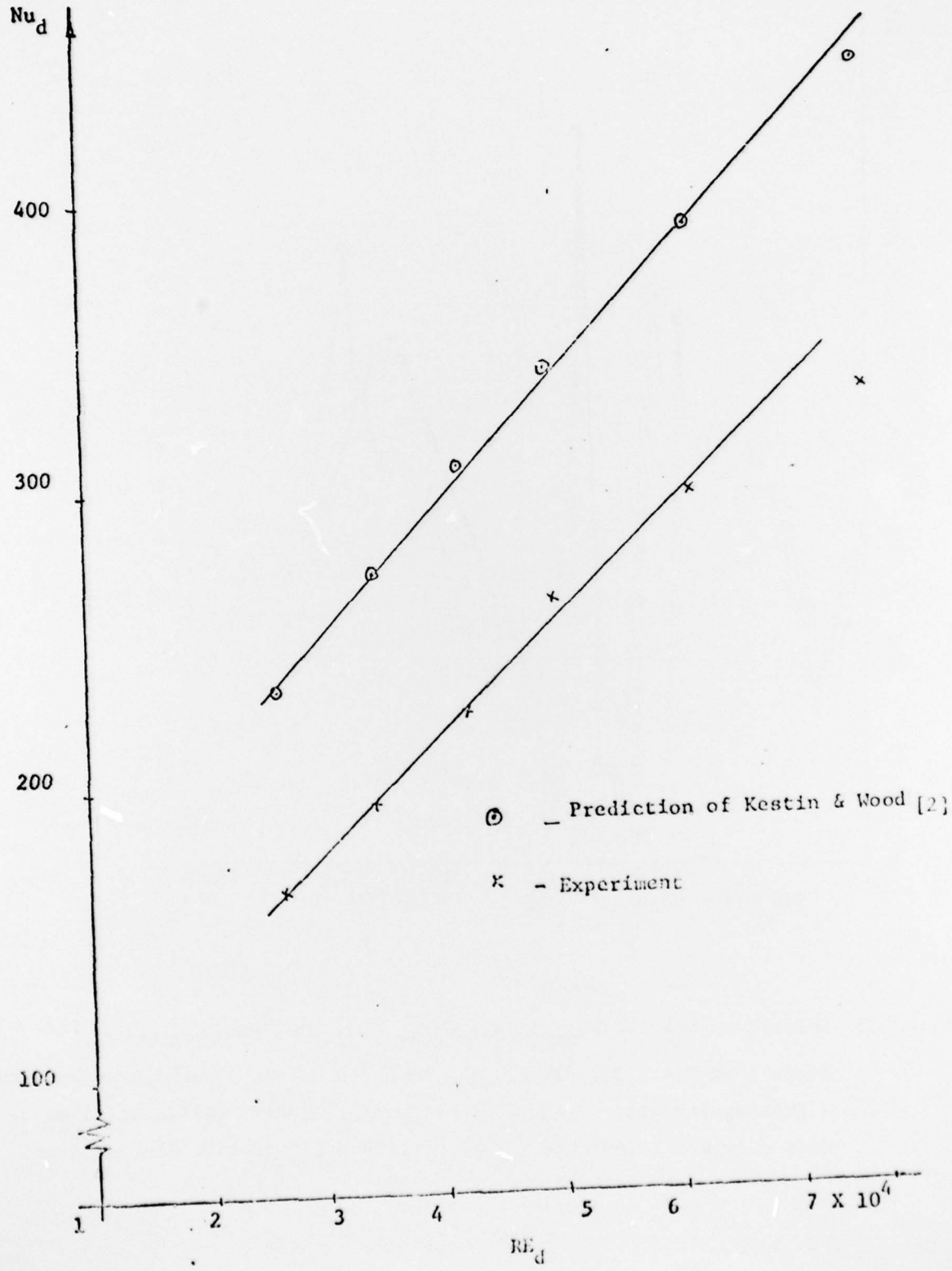

Figure 32 Heat Transfer at the Leading Zone

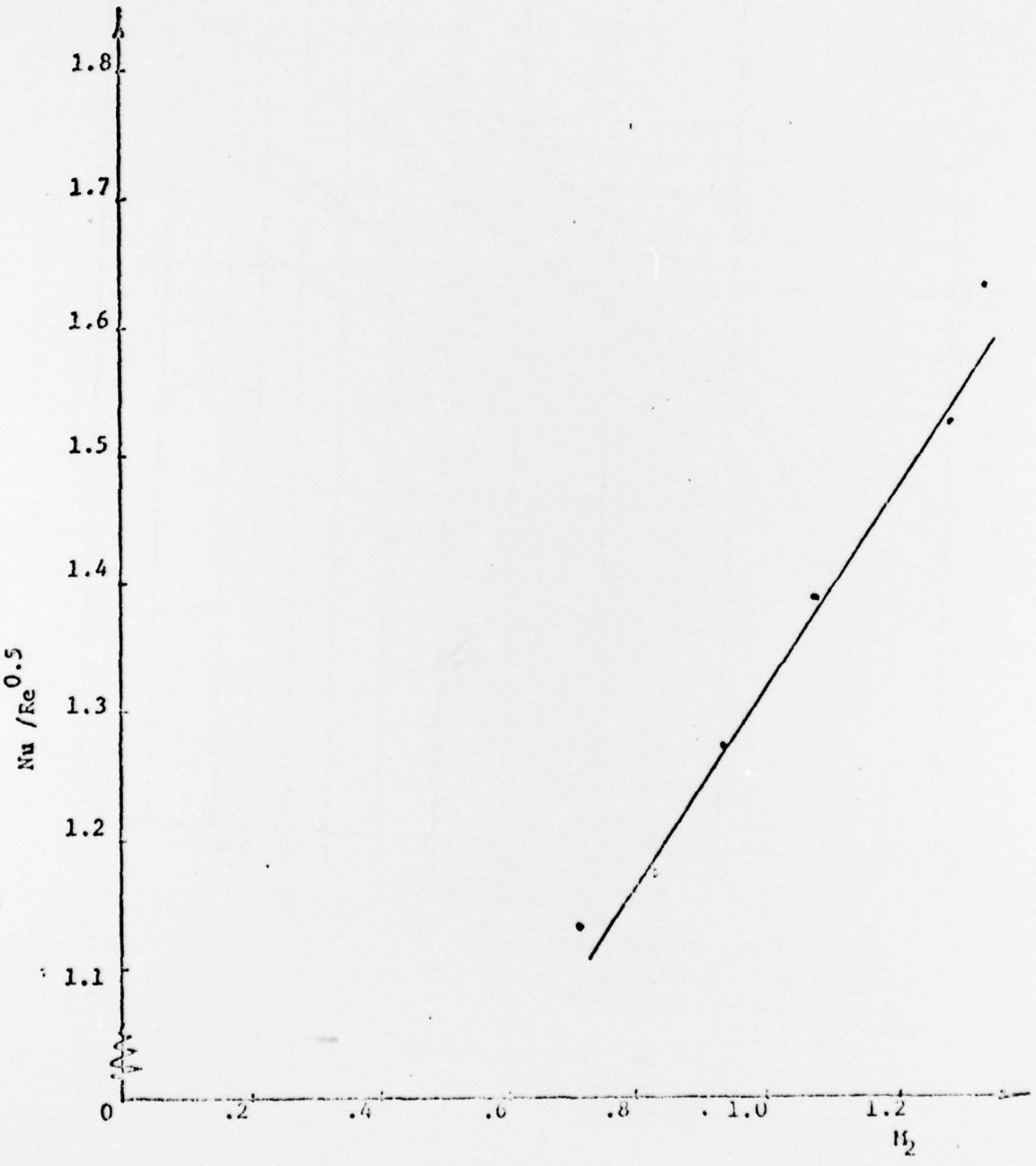

Figure 33 Distribution of mean $Nu/Re^{0.5}$ as a function of exit Mach numbera

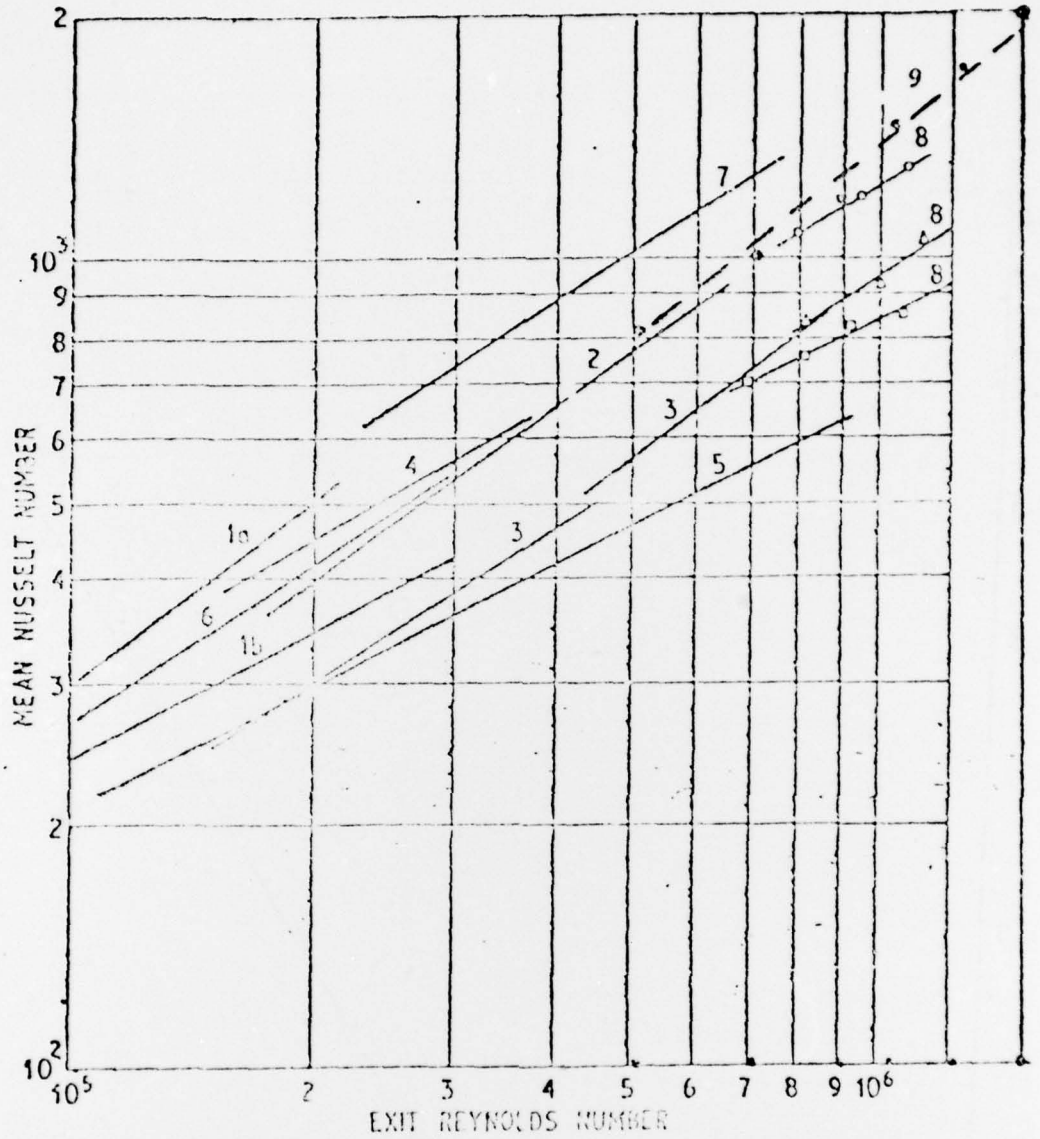

1*a* Ainley turbine
1*b* Ainley cascade
2 Wilson and Pope
3 Hodge
4 Bammert and Hahnemann
5 Andrews and Bradley
6 Fray and Barnes
7 Halls
8 Turner

Symbol	Turbulence
O	5·9%
Δ	2·2%
□	0·45%
◇	10%

9 Experiment

Figure 34 Mean Heat Transfer Results

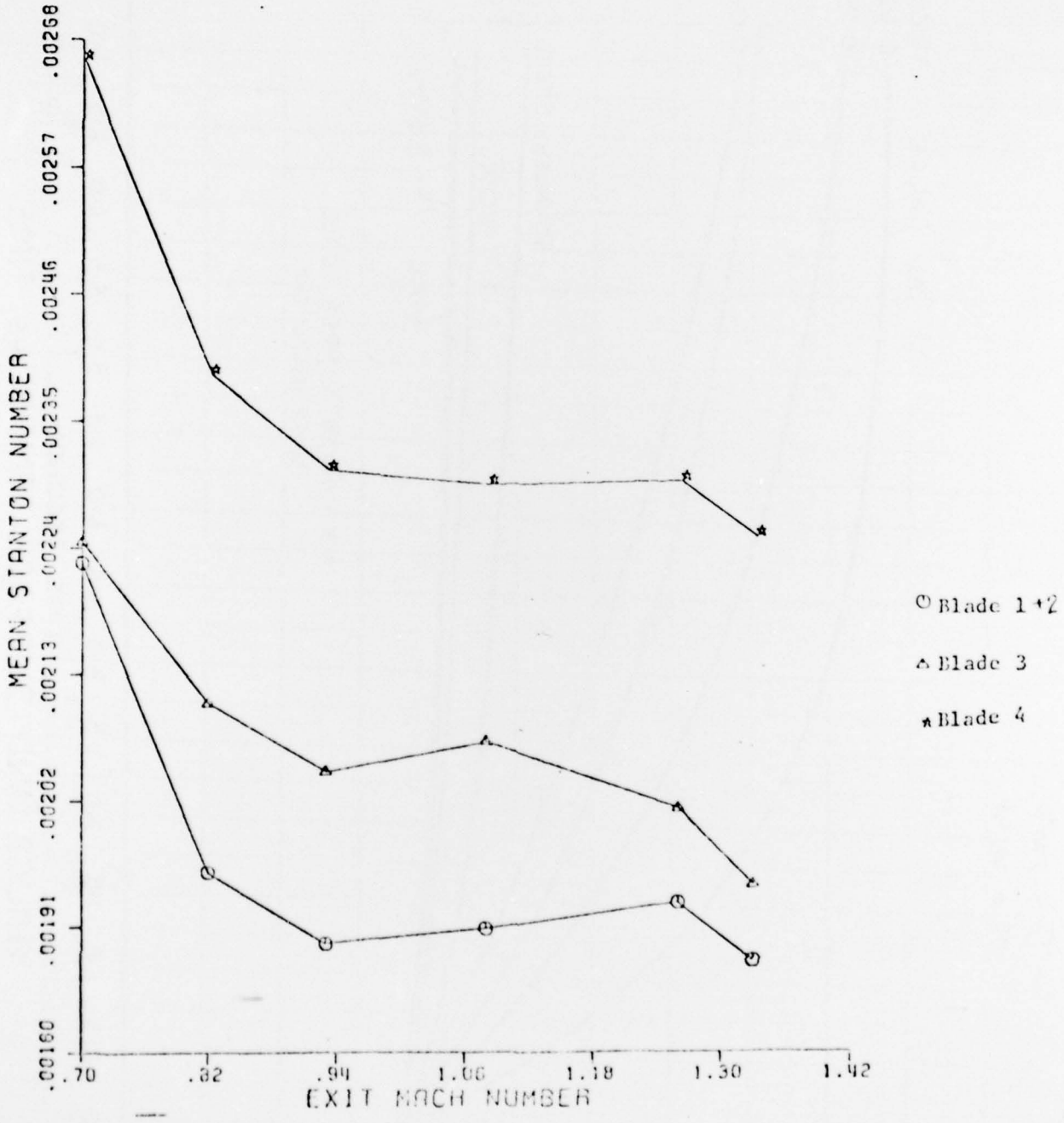

Figure 35 Blade average Stanton Number

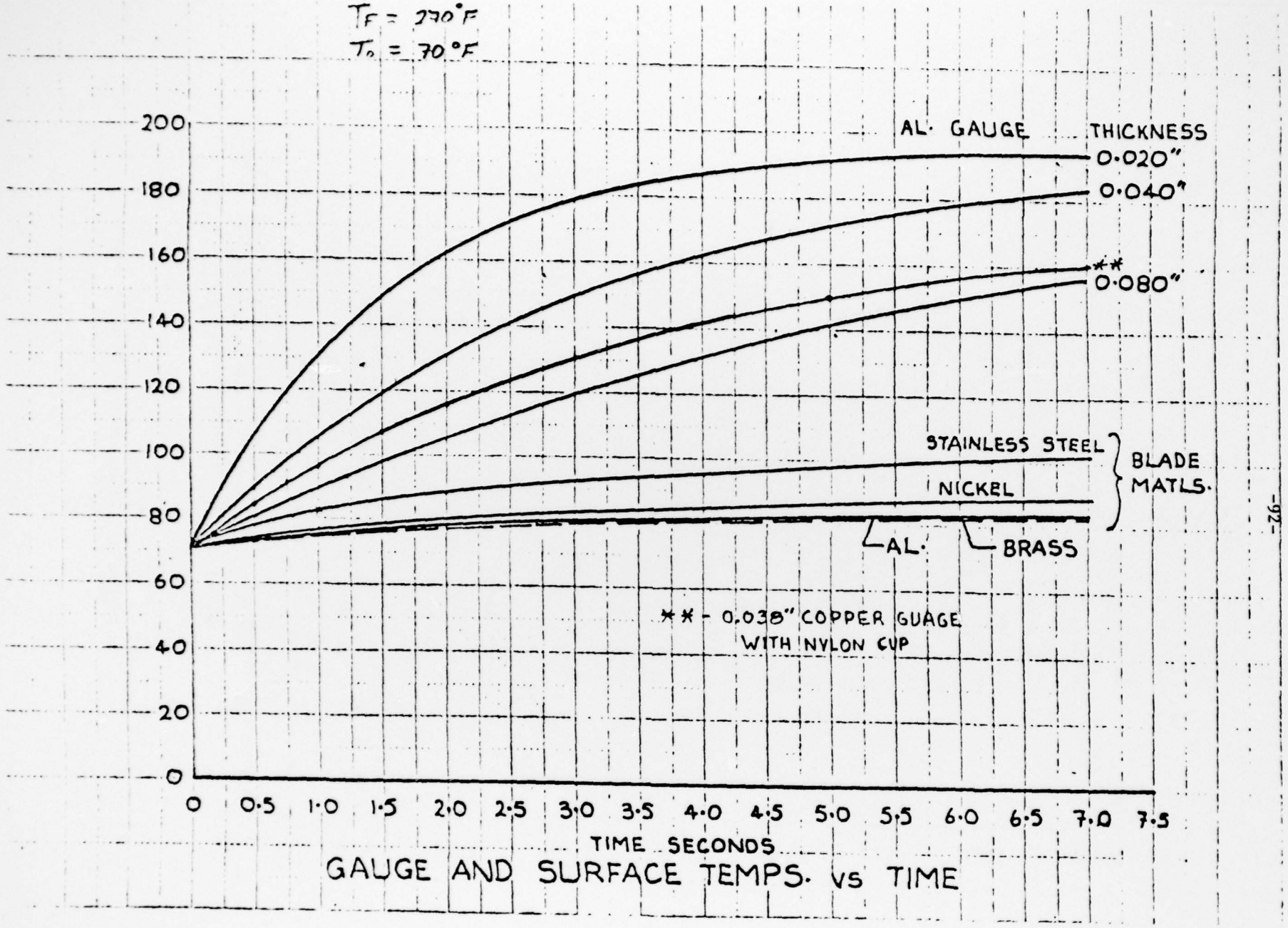
T_F = 270°F
T_o = 70°F
AL. GAUGE THICKNESS
0.020"
0.040"
**
0.080"
STAINLESS STEEL
NICKEL
AL.
BRASS
BLADE MATLS.
** - 0.038" COPPER GUAGE WITH NYLON CUP
200
180
160
140
120
100
80
60
40
20
0
0 0.5 1.0 1.5 2.0 2.5 3.0 3.5 4.0 4.5 5.0 5.5 6.0 6.5 7.0 7.5
TIME SECONDS
GAUGE AND SURFACE TEMPS. VS TIME

Figure 36

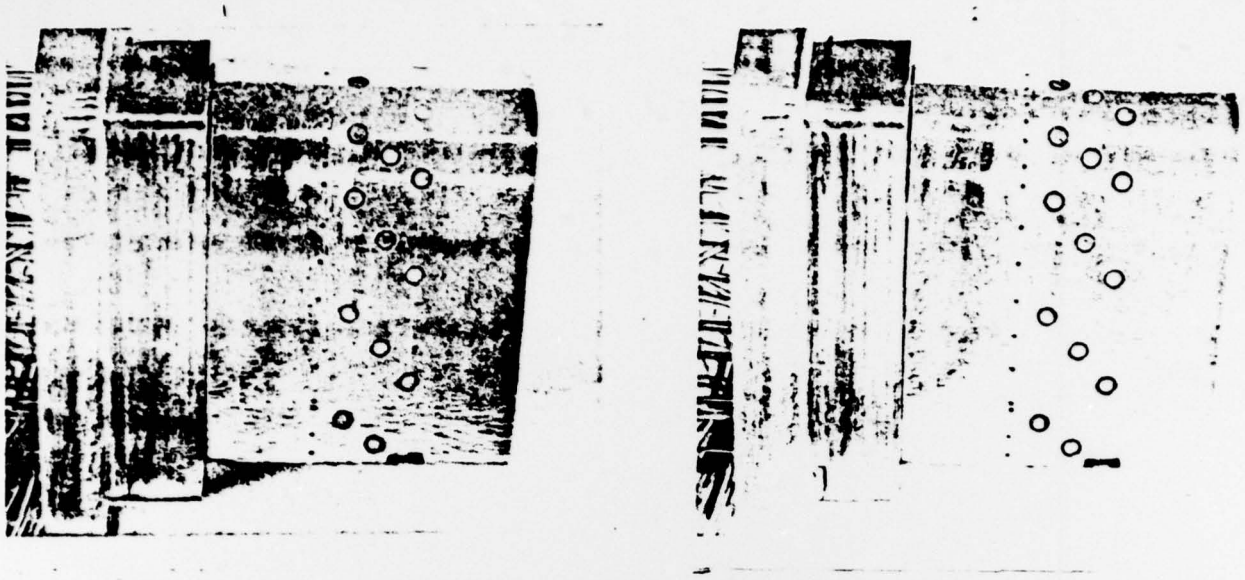

Figure 37 (a): Suction side of instrumented blade showing pressure taps and heat transfer gauges.

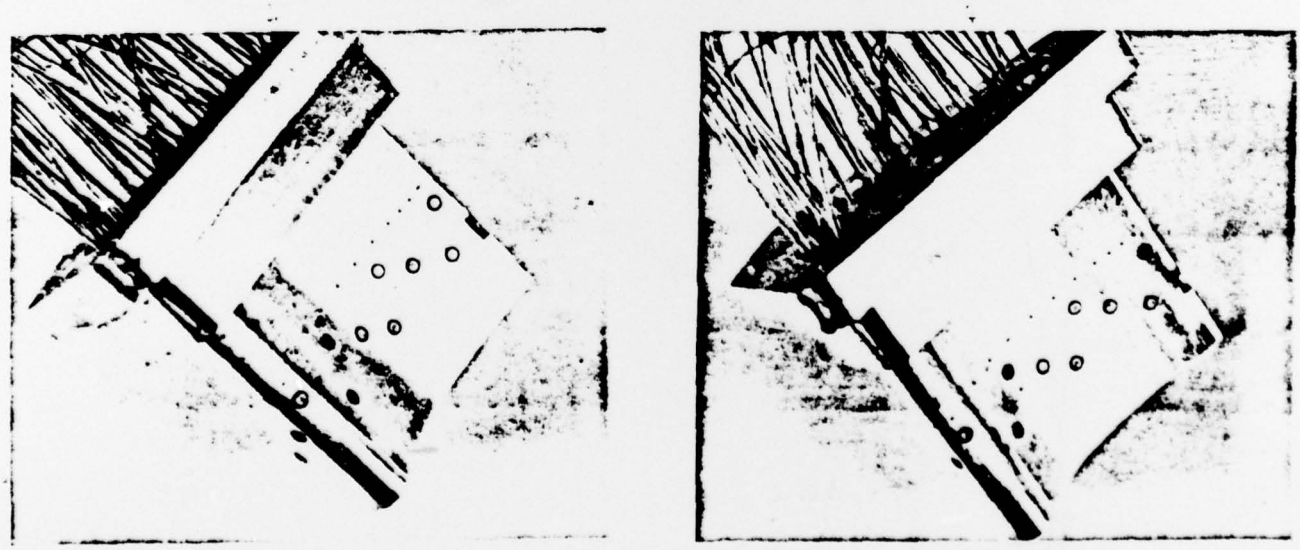

Figure 37 (b): Pressure side of instrumented blade showing pressure taps and heat transfer gauges.

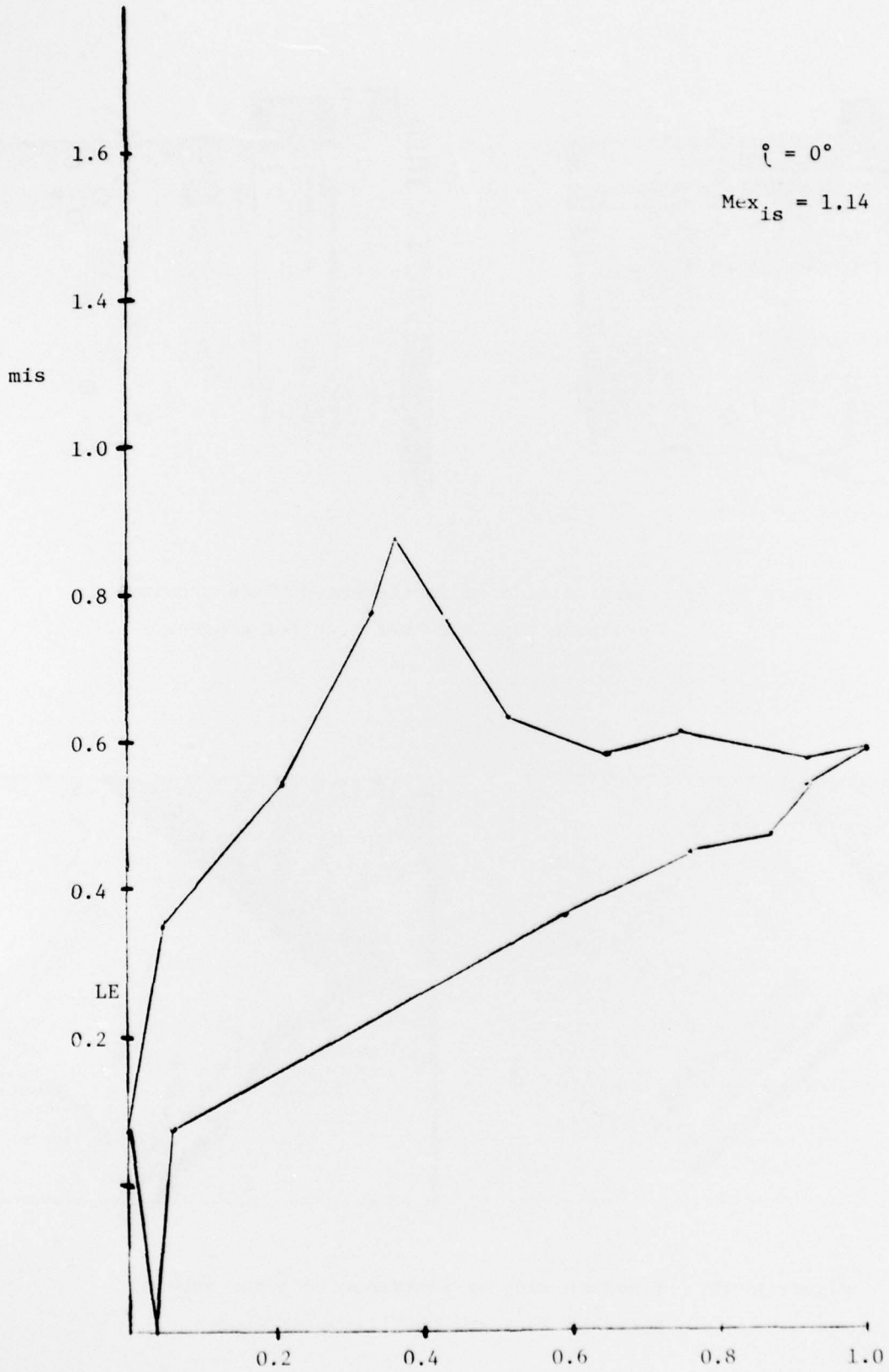

Isentropic number distribution for Reference blade at 0° incidence

Figure 38 (a)

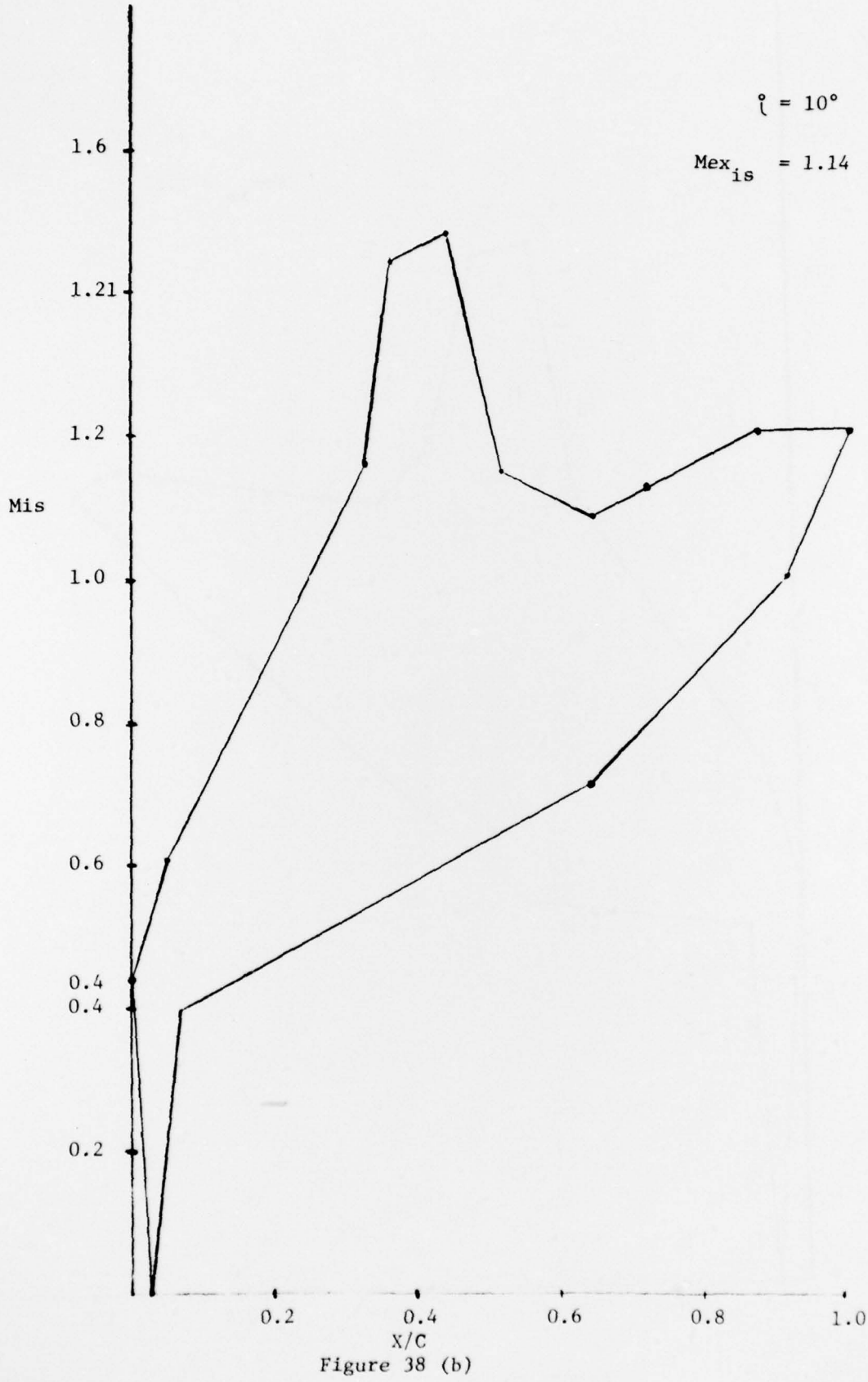

Figure 38 (b)

Isentropic Mach number distribution for Reference Blade at 10° incidence

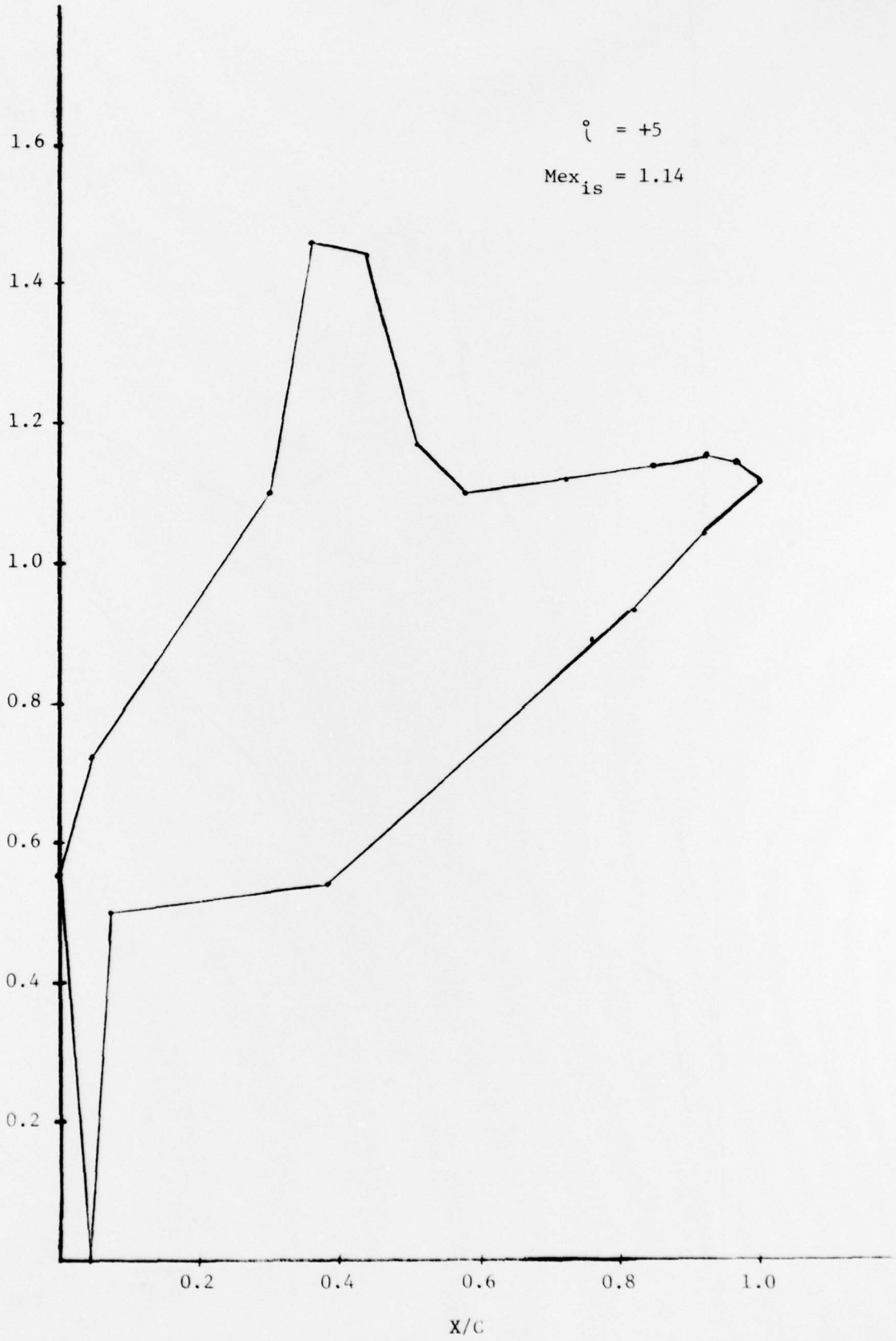

Figure 38 (c)
Isentropic Mach number distribution for Reference blade at 0° incidence

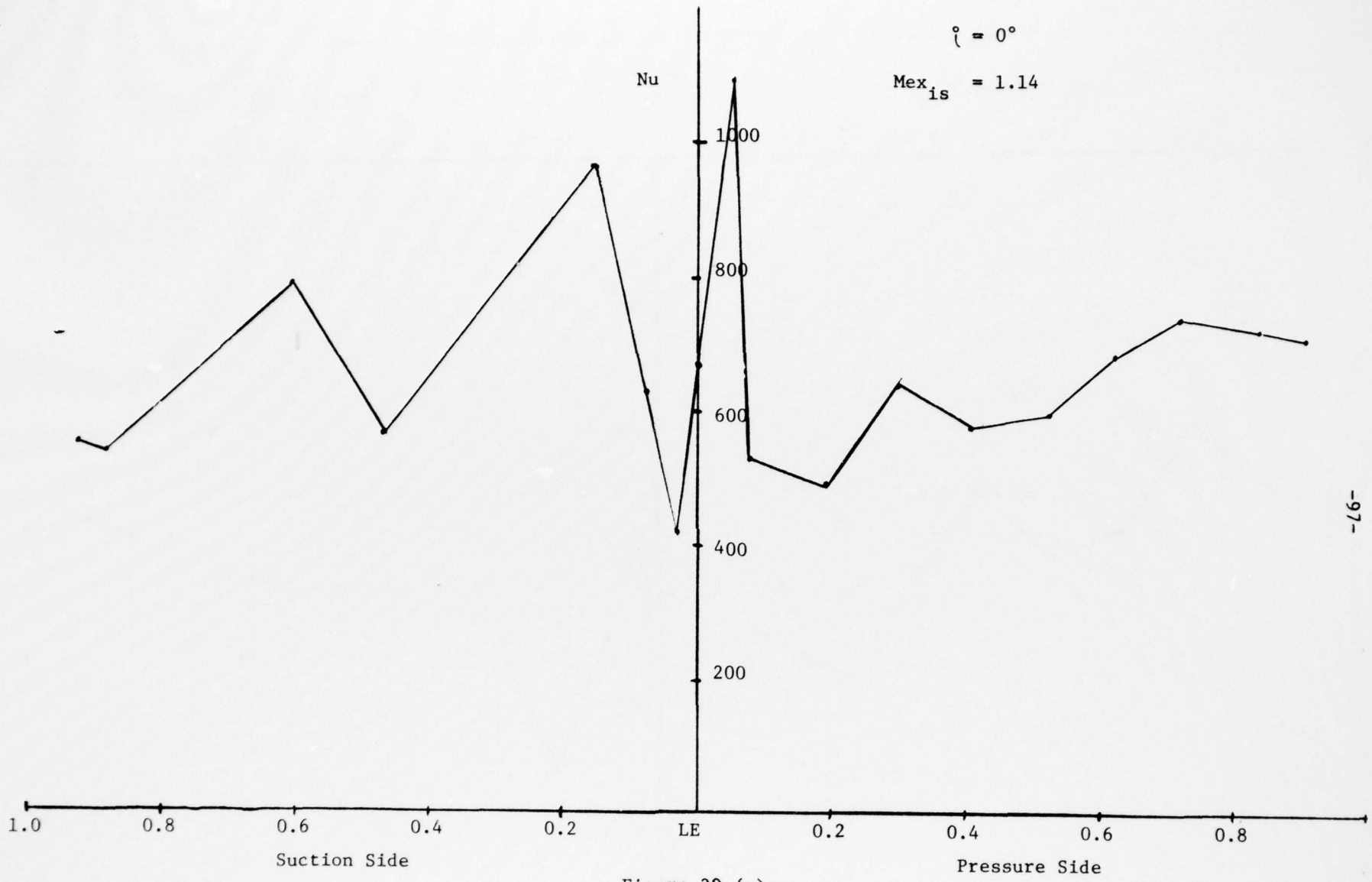

Figure 39 (a)

Nusselt Number distribution for Reference blade at 0° incidence

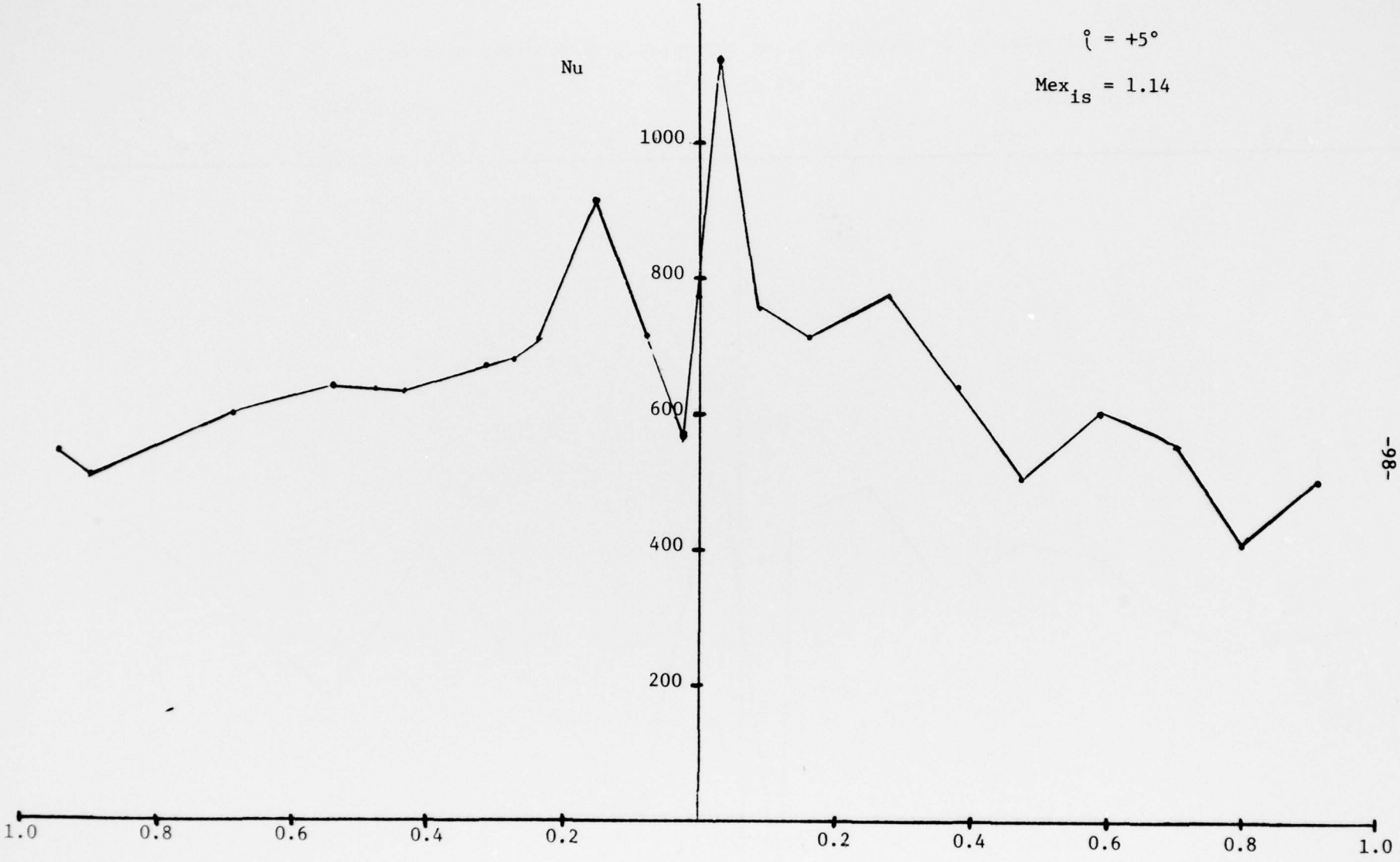

Figure 39 (b)

Nusselt Number distribution for Reference Blade at +5° incidence

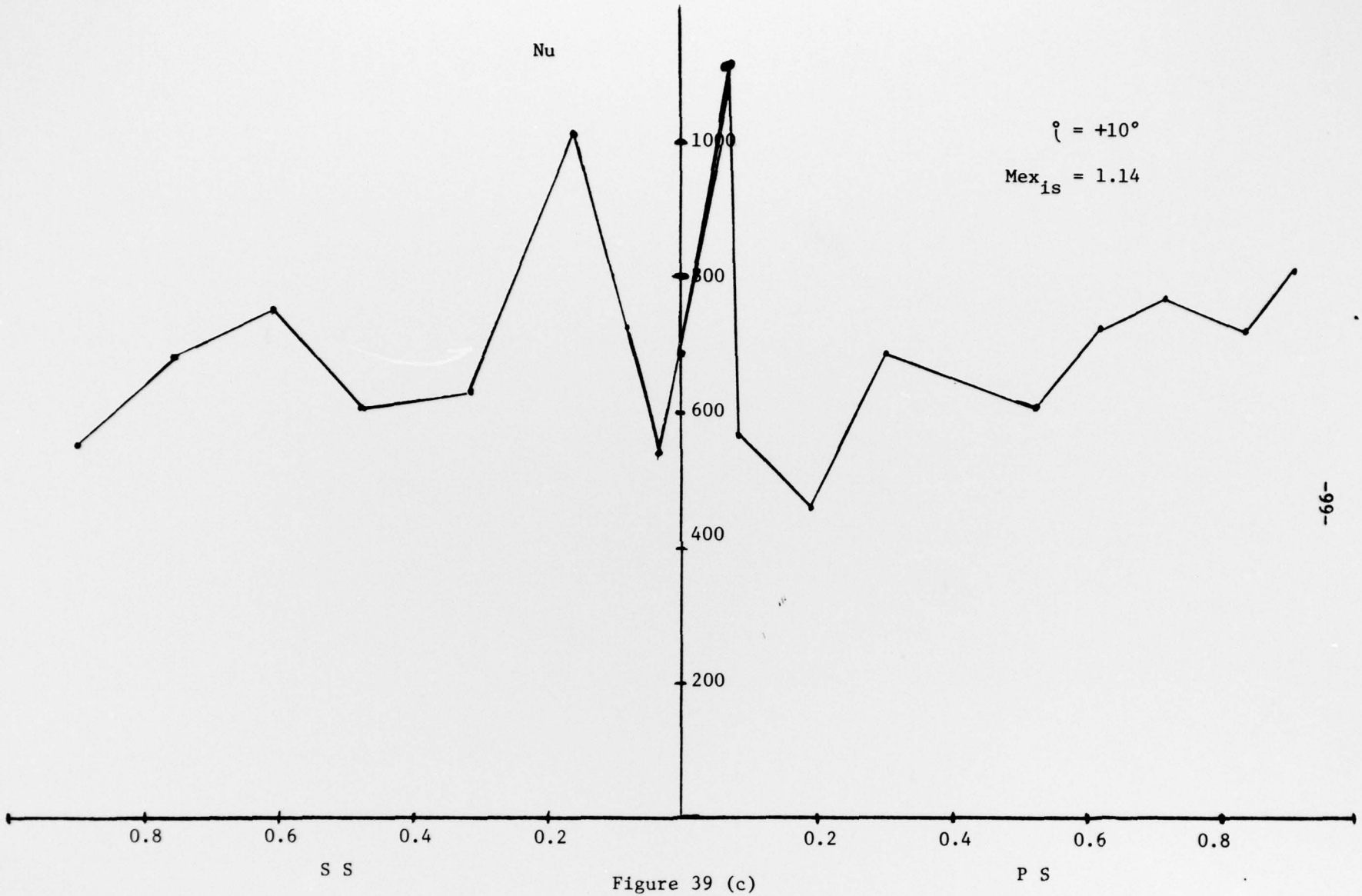

Figure 39 (c)

Nusselt Number distribution for Reference Blade at +10° incidence